Universidade do Minho
Escola de Ciências

Inês Paula Ribeiro

Heterologous expression of mammalian phospholipase D1 and D2 in the yeast model

dezembro de 2021

Heterologous expression of mammalian phospholipase D1 and D2 in the yeast model
Inês Paula Ribeiro

UMinho | 2021

Universidade do Minho
Escola de Ciências

Inês Paula Ribeiro

Heterologous expression of mammalian phospholipase D1 and D2 in the yeast model

Dissertação de Mestrado
Mestrado em Genética Molecular

Trabalho efetuado sob a orientação de
Doutora Sandra Cristina Almeida Paiva
e de
Doutor Tiago Gil Rodrigues Oliveira

dezembro de 2021

STATEMENT OF INTEGRITY

I hereby declare having conducted this academic work with integrity. I confirm that I have not used plagiarism or any form of undue use of information or falsification of results along the process leading to its elaboration.

I further declare that I have fully acknowledged the Code of Ethical Conduct of the University of Minho.

AGRADECIMENTOS

Aqueles que passam por nós, não vão sós, não nos deixam sós.
Deixam um pouco de si, levam um pouco de nós. - Antoine de Saint-Exupéry

Em primeiro lugar, um enorme obrigada à Professora Sandra Paiva e ao Professor Tiago Gil, meus orientadores, que me proporcionaram com todo o apoio, condições e meios necessários para realizar esta dissertação. Pela sabedoria, pelas sugestões, pelas oportunidades, pela constante valorização do trabalho desenvolvido. Pela calma que sempre me trasmitiram, e pelo exemplo de compreensão e espírito positivo.

À Rosana, minha mentora, por ser responsável por grande parte de tudo o que eu sei sobre investigação e trabalho laboratorial. Pela paciência, pela disponibilidade, pelas palavras de incentivo e motivação. Acima de tudo, por ser um exemplo de trabalho e dedicação.

À Cidália e ao Félix, meus amigos e colegas de mestrado, e à Adília, à Sónia e à Natacha, minhas amigas, pelo carinho, pela ajuda, pelas gargalhadas, pelas conversas sobre ciência e pelas que nada têm a ver com ciência, pelas cartadas, por me manterem com os pés no chão.

Aos meus colegas de laboratório, à Cláudia, à Tatiana, à Alexandra, ao Paulo e ao Humberto, um agradecimento especial por todos os conselhos, esclarecimentos e ajuda. Por criarem, no LGM um ambiente acolhedor e de entreajuda.

À Rafaela, pela disponibilidade constante, por todo o tempo e ajuda na aquisição de fotos de microscopia confocal.

Ao Professor Rui Oliveira, por toda a ajuda e conhecimento no cruzamento de leveduras e separação de tétradas.

Por último, o maior agradecimento à minha família, os meus alicerces. Pelo apoio e carinho constantes. Ao meu pai, e à minha mãe que sempre fizeram tudo para que eu tivesse as ferramentas e condições para estar aqui hoje e cujo orgulho é a minha maior motivação. À Gabi, minha irmã, pelo companheirismo, pela cumplicidade e pelas gargalhadas.

RESUMO

Lipídos são moléculas com funções biológicas extremamente diversas, desde fontes de energia armazenada, a cofatores de enzimas e mensageiros intracelulares. Os glicerofosfolipídos, ou simplesmente fosfolipídos, são uma categoria de lipídos tipicamente conhecida como sendo componentes maioritários das membranas celulares. Quando fosfolipídos são hidrolisados por fosfolipases, os compostos resultantes podem atuar como mensageiros secundários ou mediadores, apresentando um papel importante no metabolismo e estrutura celular e em vias de transdução de sinal. A fosfolipase D (PLD), uma das principais classes de fosfolipases, hidrolisa a ligação fosfodiéster na fosfatidilcolina, produzindo ácido fosfatídico e colina. A sua ação está descrita em diversos organismos, incluido leveduras, mamíferos, bactérias e plantas. Em mamíferos, duas isoformas de PLD foram identificadas: a PLD1 e a PLD2, e a sua atividade tem sido associada a um grande número de condições patofisiológicas, nomeadamente doenças cardíacas, cancro e doenças neurodegenerativas. Especificamente, a PLD1 e a PLD2 têm sido identificadas como tendo um papel extremamente importante na doença de Alzheimer (AD). *SPO14* é o ortólogo da PLD em levedura, codificando para a atividade PLD em *S. cerevisiae*, onde este gene é essencial para a meiose e a formação dos esporos. Apesar da sua semelhança no que toca à atividade catalítica e estrutura global, a PLD1 e PLD2 estão diferencialmente implicadas em diversas condições biológicas e vários aspetos da sua função distinta nas células estão ainda por desvendar. Com um conjunto robusto de vantagens manipulativas e sendo *SPO14*, provavelmente, a única fonte canónica de atividade PLD em *S. cerevisiae*, esta espécie apresenta-se como um modelo relevante e ideal para o estudo dos papéis diferenciais da PLD1 e PLD2 mamíferas.

O objetivo desta tese foi, então, estudar as enzimas mamíferas PLD1 e PLD2 usando o modelo de levedura, desenvolvendo mutantes para o SPO14, onde foram heterologamente expressas versões otimizadas do PLD1 e PLD2 de mamíferos.

Foi desenvolvido um conjunto de ferramentas moleculares valiosas, que permitirão a exploração de vários aspetos relevantes da relação genótipo-para-fenótipo da PLD1 e PLD2 no contexto da AD. Globalmente, estas ferramentas possibilitam investigação adicional sobre potenciais diferenças biológicas entre estas isoenzimas mamíferas, usando *S. cerevisiae* como modelo

ABSTRACT

Lipids are ubiquitous molecules with extremely diverse biological functions, from being stored energy sources, to acting as enzyme cofactors and intercellular messengers. Glycerophospholipids, also commonly called phospholipids, are a category of lipids mainly known for being major constituents of cell membranes and, when hydrolyzed by phospholipases, the resulting compounds can act as second messengers or mediators, playing important metabolic and structural roles as well as being involved in an array of signal transduction pathways. Phospholipase D (PLD), one of the major phospholipase classes, hydrolyzes the phosphodiester bond on phosphatidylcholine, producing phosphatidic acid and choline. Its action has been reported in several organisms including yeast, mammals, bacteria and plants. In mammals, two isoforms of PLD have been identified: PLD1 and PLD2, and their activity has been strongly associated with a number of pathophysiological conditions, namely heart disease, cancer and neurodegenerative diseases. Specifically, the PLD1 and PLD2 have been strongly implicated in Azlheimer's disease (AD). *SPO14* is the yeast ortholog of PLD, encoding the major phospholipase D activity in *S. cerevisiae*, where this gene is essential for meiosis and spore formation. Despite their similarity in catalytic function and overall structure, PLD1 and PLD2 are differentially implicated in various biological conditions and several aspects of PLD1's and PLD2's distinct function in cells are yet to be unveiled. With a robust set of manipulative advantages and with *SPO14* likely being the only source of canonical PLD activity in this species, *S. cerevisiae* presents itself as an ideal and relevant model to study the differential roles of mammalian PLD1 and PLD2 in the cell.

The aim of this thesis was to study mammalian PLD1 and PLD2 using the yeast model, by developing *SPO14* yeast mutants which were used to heterologously expressing codon optimized versions of mammalian *PLD1* and *PLD2* .

A set of valuable molecular tools was generated, which will allow for the exploration of several relevant aspects of the genotype-to-phenotype relationship of PLD1 and PLD2 in the context of AD. Overall, these tools permit further investigation of the potential biological differences between these mammalian isoenzymes using the *S. cerevisiae* model.

HETEROLOGOUS EXPRESSION OF PHOSPHOLIPASE D1 AND D2 IN THE YEAST MODEL

SCIENTIFIC OUTPUT

Poster Communications

1. Inês P. Ribeiro, Rosana Alves, Rafaela Ribeiro, Sandra Paiva and Tiago Gil Oliveira "*Heterologous expression of mammalian PLD1 and PLD2 in Saccharomyces cerevisiae*" (2021) 13th iMED Conference, 6 - 10 Outubro, Lisboa, Portugal.

TABLE OF CONTENTS

LIST OF ABBREVIATIONS AND ACRONYMS

AD	Alzheimer's Disease
ADP	Adenosine Diphosphate
APP	Amyloid Precursor Protein
ARF	ADP-Ribosylation Factor
ATP	Adenosine Triphosphate
CAI	Codon Adaptation Index
CL	Cardiolipin
CRISPR	Clustered Interspaced Short Palindromic Repeats
DAG	Diacylglycerol
DGK	Diacylglycerol Kinase
EDTA	Ethylenediamine Tetraacetic Acid
EGF	Epidermal Growth Factor
EGFR	Epidermal Growth Factor Receptor
ER	Endoplasmic Reticulum
GFP	Green Fluorescent Protein
His	Histidine
IMPACT	Imaging Phospholipase D Activity with Clickable Alcohols via Transphosphatidylation
IP_3	Inositol triphosphate
KO	Knock-out
LPA	Lyso-phosphatidic Acid
LPAAT	Lyso-phosphatidic Acid Acyl-Transferase
OD	Optical Density
PA	Phosphatidic Acid
PC	Phosphatidylcholine
PCA	Phenol:Chloroform:Isoamyl-Alcohol
PCR	Polymerase Chain Reaction
PE	Phosphatidylethanolamine
PEG	Polyethylene Glycol
PG	Phosphatidylglycerol
PH	Pleckstrin homology

PI	Phosphatidylinositol
PI(3,4,5)P_3	Phosphatidylinsitol 3,4,5-triphosphate
PI(3,4)P_2	Phosphatidylinsitol 3,4-biphosphate
PI(3,5)P_2	Phosphatidylinsitol 3,5-biphosphate
PI(3)P	Phosphatidylinsitol 3-phosphate
PI(4,5)P_2	Phosphatidylinsitol 4,5-biphosphate
PI(4)P	Phosphatidylinsitol 4-phosphate
PI(5)P	Phosphatidylinsitol 5-phosphate
PKC	Protein Kinase C
PLA	Phospholipase A
PLB	Phospholipase B
PLC	Phospholipase C
PLD	Phospholipase D
PLD1	Phospholipase D1
PLD2	Phospholipase D2
PLD3	Phospholipase D3
PLD4	Phospholipase D4
PLD5	Phospholipase D5
PLD6	Phospholipase D6
PS	Phosphatidylserine
PX	Phox
RTK	Receptor Tyrosine Kinase
SC	Synthetic Complete media
SRF1	Spo14 Regulatory Factor 1
TAE	Tris-Acetate-EDTA
Ura	Uracil
WT	Wild type
YPD	Yeast-extract Peptone Dextrose medium

LIST OF FIGURES

LIST OF TABLES

Chapter I - Introduction

I. Introduction

I.1. Lipids

Lipids are a heterogeneous and ubiquitous group of compounds that share the feature of being poorly soluble in water and are classically defined as being soluble in organic solvents [1]. These amphipathic molecules include fats and oils (triglycerides), phospholipids, waxes, and sterols, amongst others and their biological functions can be extremely diverse, however, four main functions can be highlighted [2]:

- Energy storage: for instance, glycerol esters (monoacylglycerol, diacylglycerol, and triacylglycerol) or sterols in lipid droplets can be used for membrane biogenesis and as reserves of caloric energy.
- Structural: amphiphilic lipids, such as phospholipids are responsible for the spontaneous formation of membranes due to their physical-chemical properties. These properties also allow for the compartmentalization of structures within cells, and therefore the formation of organelles. The main membrane lipids in eukaryotic cells are glycerophospholipids such as phosphatidylcholine (PC), phosphatidylinositol (PI), and phosphatidylserine (PS).
- First and second messengers: given their structural function in cell membranes, lipids are situated at the frontier between the intracellular and extracellular portions and can therefore participate in signal transduction pathways. The metabolization of membrane lipids can result in a signalling event that can be transmitted within the membrane to the cytoplasm through the hydrophobic and hydrophilic portions of these molecules, respectively. Lipid-derived signalling molecules include phosphatidic acid (PA) and diacylglycerol (DAG). Additionally, membrane lipids can be used as domain identifiers within membranes, and work as recruiters for proteins that organize subsequent effector complexes or secondary signalling cascades.
- Chemical tags: the compartmentalization achieved by lipid membranes allows for the segregation and isolation of specific biochemical reactions that result in higher efficiency and controlled spread of reaction products. For example, phosphoinositides can be interconverted by phosphatases and kinases to mark cellular membranes and recruit cytosolic proteins. Additionally, lipids can regulate the aggregation or dispersion of certain proteins.

In eukaryotic cells, variations in aliphatic chains and headgroups enable the existence of thousands of different lipid species [3]. As far as nomenclature, lipids can be classified into eight categories: fatty acyls, glycerolipids, glycerophospholipids, sphingolipids, sterol lipids, prenol lipids, saccharolipids and

polyketides [4]. Inside each category, lipids can be further subdivided in classes. Organisms can vary in the biological importance and presence of different lipid classes. In mammals, glycerolipids, sterols, sphingolipids, and glycerophospholipids are the lipid classes of most importance [5] – **Figure 1**.

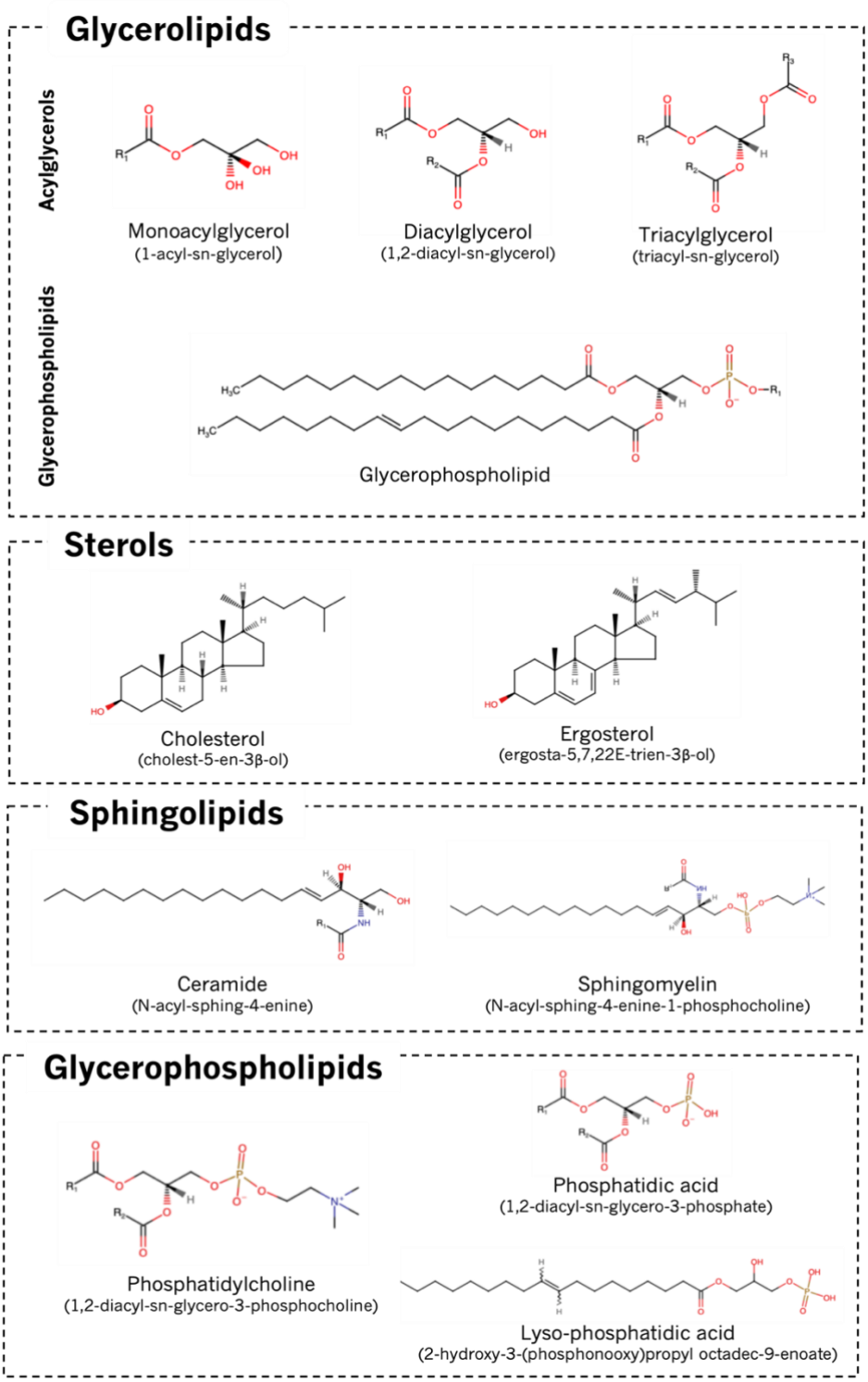

Figure 1. Four major lipid categories in mammals and examples of important members of each category.

In mammals, the four major lipid categories are glycerolipids, sterols, sphingolipids, and glycerophospholipids. Glycerolipids contain a glycerol molecule and can be divided into three main categories acylglycerols, glyceroglycolipids, and glycerophospholipids. Acylglycerols, or glycerides, are glycerol molecules that can be mono-, di-, or tri-esterified with fatty acids to form mono-, di-, and triglycerides, respectively**.** Sterols are non-polar lipids composed of an alkyl group on a hydroxylated sterane ring, a molecule composed of three rings with six atoms and one ring with five atoms, that can be esterified to a fatty acid. Sphingolipids are a class of membrane lipids composed of a sphingoid base linked to an N-acyl chain and a head group through a phosphate group. Phospholipids are composed of a glycerol backbone, linked to a polar head group by a phosphate residue and to one or two fatty acids, that can be saturated or unsaturated.

I.1.1. Glycerolipids

Glycerolipids comprise all lipids that contain a glycerol molecule. These can be divided into three classes: acylglycerols, glyceroglycolipids, and glycerophospholipids. Acylglycerols, or glycerides, are glycerol molecules that can be mono-, di-, or tri-esterified with fatty acids to form mono-, di-, and triglycerides, respectively [6]. Glyceroglycolipids are composed of an *sn*-1,2-diacylglycerol and a carbohydrate moiety linked by a glycosidic bond at the *sn*-3 position and are found in some bacteria and plants, in the membrane of thylakoids [7]. Glycerophospholipids have a glycerol backbone linked to a polar head group and one or two fatty acids [1].

I.1.2. Sterols

Sterols are one of the major components of cell membranes, with cholesterol being the predominant membrane sterol in mammals and ergosterol in yeast [2]. These are non-polar lipids composed of an alkyl group on a hydroxylated sterane ring – a molecule composed of three rings with six atoms and one ring with five atoms – that can be esterified to a fatty acid. In mammals, cholesterol is the major sterol playing a key role in membrane structure given its conic geometry, while in yeast and fungi ergosterol is the main sterol [8].

I.1.3. Sphingolipids

Sphingolipids are a class of membrane lipids composed of a sphingoid base – usually sphingosine, a long chain amino-alcohol – linked to an *N*-acyl chain and a head group through a phosphate group. This phosphate group places sphingolipids inside the phospholipid category of lipids [9]. Several sphingolipids can be produced by the substitution of the amino and alcohol moieties of sphingosine, with ceramide being the simpler one [10]. Sphingolipids have a distinctive characteristic when it comes to their location on cellular membranes, they can be found almost exclusively in the outer leaflet of most membrane bilayers [11]. Chemical diversity in sphingolipids is attributed to the length and type of sphingoid base present, the head group substituent, and the type and hydroxylation of the *N*-acyl chain [9]. The major representative of this class of lipids is sphingomyelin, a major component of cells membranes. Produced by transfer of the phosphorylcholine group from phosphatidylcholine to ceramide, sphingomyelin is found in large

amounts in the central nervous system, specifically in the myelin sheaths that surround the axons of some neurons [12,13].

I.1.4. Glycerophospholipids

Glycerophospholipids, commonly referred to as phospholipids, are often considered as a lipid class of their own, given their abundance and importance in membrane structure, metabolism, and molecular signalling. Phospholipids are amphiphilic species, composed of a glycerol backbone, linked to a polar head group by a phosphate residue and to one or two fatty acids, that can be saturated or unsaturated. The fatty acids are esterified to carbons *sn-1* and *sn-2* of the glycerol molecule whilst the phosphate group is esterified to carbon *sn-3*. Different combinations of fatty acids at *sn-1*, which tend to be saturated or monounsaturated, and at *sn-2*, which tend to be mono- or polyunsaturated, can confer chemical diversity to phospholipids [9]. Given their biophysical properties, these molecules can aggregate to spontaneously form lipid bilayers in water, with their hydrophobic carbon chains facing inwards and their hydrophilic head groups facing outwards. This phenomenon explains phospholipid's vital role in membrane structural integrity. Different head groups will result in different glycerophospholipids – Table 1.

Table 1. Most common head group substitutions and the resulting phospholipids.

Head group (X)	*Name of glycerophospholipid*
Choline	Phosphatidylcholine (PC)
Ethanolamine	Phosphatidylethanolamine (PE)
Glycerol	Phosphatidylglycerol (PG)
Hydroxyl	Phosphatidic Acid (PA)
Inositol	Phosphatidylinositol (PI)
Inositol-phosphate	Phosphatidylinositol phosphate - PI(3)P, PI(4)P or PI(5)P
Inositol-biphosphate	Phosphatidylinositol biphosphate - $PI(4,5)P_2$
Inositol-triphosphate	Phosphatidylinositol triphosphate - $PI(3,4,5)P_3$
Phosphatidylglycerol	Cardiolipin (CL)
Serine	Phosphatidylserine (PS)

These include phosphatidylcholine (PC), phosphatidylinositol (PI), and phosphatidylserine (PS) and are very abundant in cells, being present as membrane components and acting as signalling molecules [1,5]. The asymmetrical distribution of different species of phospholipids across the membrane leaflets, vertically and laterally, plays a pivotal role in cell dynamics, namely in cell division [14], oncogenesis [15], and apoptosis [16]. Phosphoinositides are generated by phosphorylation of the inositol hydroxyls of PI at positions 3, 4 or 5, resulting in monophosphorylated [PI(3)P, PI(4)P and PI(5)P], bisphosphorylated [$PI(3,4)P_2$, $PI(3,5)P_2$ and $PI(4,5)P_2$] and trisphosphorylated [$PI(3,4,5)P_3$] species, respectively. These seven derivatives are differentially enriched in the membrane of various organelles, and thus play a role in the specification of organelle and membrane identity [17]. Despite their relative low abundance, these membrane phospholipids have emerged as key regulators of several essential cellular processes in eukaryotic cells such as cytoskeletal function, membrane transport, and plasma membrane signaling [18,19]. PA is the simplest of phospholipids, having only a phosphomonoester as the head group.

I.1.4.1. Phosphatidic acid

Despite being the simplest phospholipid, PA is a key intermediate in various processes, from lipid storage to membrane lipid synthesis, and has been implicated as a regulator and mediator of multiple essential cellular pathways including signal transduction, cytoskeletal rearrangement, membrane trafficking, and secretion [20]. Structurally, this amphipathic lipid consists of a glycerol backbone esterified to two fatty acid chains and a phosphate, at positions *sn-1*, *sn-2,* and *sn-3*, respectively. Structural diversity is conferred by variations in fatty acid chain length and saturation. An alternative species, lysophosphatidic acid (LPA) can also be described, differing from PA by having only one fatty acid chain at the *sn-1* position. PA synthesis can be carried out by multiple enzymes and pathways, resulting in differences in the location and timing of the resulting species. Four important pathways for PA biosynthesis can be described, which are carried out in different organelles and under different stimuli [21]:

I. *De novo* synthesis, where PA is generated via sequential acylation of glycerol-3-phosphate by acyltransferases. In mammals, this process exists in most tissues, with different acyltransferase isoforms being located in the membranes of different organelles and expressed at various levels in different organs yielding distinct contributions to various cellular processes;

II. Phospholipase D (PLD) mediated hydrolysis of PC, where, in the presence of water, it results in the formation of PA and free choline;

III. DAG kinase (DGK) catalyzed phosphorylation of DAG, where PA is generated by the action of DAGKs on 1,2-diacyl-*sn*-glycerol. This reaction only happens under certain conditions, for example, those resulting from the action of phospholipase C (PLC) on other phospholipids;

IV. Acylation of lysophosphatidic acid, where LPA can be acylated by an LPA acyltransferase (LPAAT), resulting in the formation of PA. This pathway has important significance in membranes, where endophilin, an endocytic protein, has LPAAT activity and is thought to use the production of PA from LPA to alter the curvature of the plasma membrane bilayer [22];

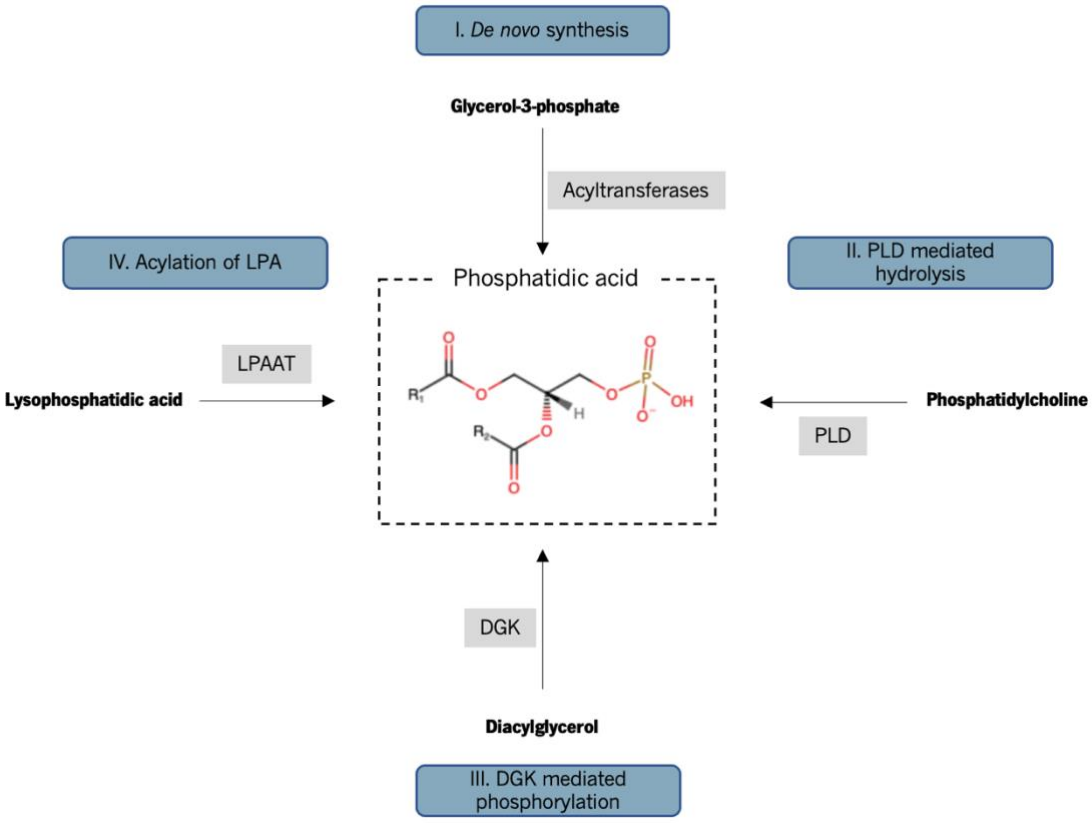

Figure 2. Phosphatidic acid biosynthesis by four different pathways.

PA formation can be achieved by four pathways in cells: from DAG by a reaction catalyzed by DGK; from LPA as a result of LPAAT activity; from PC by the action of PLD and synthesized de novo from glycerol-3-phosphate PA – phosphatidic acid, PC – phosphatidylcholine, DAG – diacylglycerol, LPA – lysophosphatidic acid, PLD – phospholipase D, DGK – DAG kinase, LPAAT - lysophosphatidic acid acyltransferase.

It is clear that lipids and lipid metabolism play very important roles in biological processes in all types of cells, with their functions being as diverse as their chemical structure. In the brain, particularly, lipids are key players in signalling and structure, with proven influence in a number of neuronal physiology and pathology processes [23]. This is of no surprise, given that both the nervous system and the brain are highly enriched in a wide variety of lipid species, with about half of the brain's dry weight being represented by lipids [24]. Alterations in the lipid homeostasis of the brain have been shown to be of great importance for central nervous system disorders [23]. These include neurodegenerative diseases such as Alzheimer's disease (AD) [25], Parkinson's disease [26], amyotrophic lateral sclerosis and multiple sclerosis [27,28].

I.2. Phospholipases

Phospholipases are a group of ubiquitously expressed enzymes that hydrolyze phospholipids [29]. These lipolytic enzymes can be divided into four main classes: phospholipases A (PLA), phospholipases B (PLB), PLC, and PLD [29] and although they all share a common substrate, they are very distinct when it comes to their function, mode of action, regulation and action site on the phospholipid molecule [30] (Figure 3). The PLA enzyme family comprises enzymes that have limited selectivity for the *sn-1* or *sn-2* acyl positions on the phospholipid molecule: PLA_1 and PLA_2, respectively. PLA_1 cleaves the phospholipid molecule at the *sn-1* position resulting in the formation of a fatty acid and a lysophospholipid, whilst phospholipase A_2 cleaves at the *sn-2* position resulting in the formation of arachidonic acid and LPA. Members of the PLA_1 family have been associated with blood clotting, digestion of dietary fat, and smooth muscle contraction [31,32]. Members of the PLA_2 family can be divided into six main groups in mammals, with most being expressed in different tissues and with no similarity when it comes to structure or regulatory and catalytic mechanisms [33]. PLB catalyzes the hydrolysis of ester bonds at the *sn-1* and *sn-2* positions of the phospholipid molecule. This enzyme has, therefore, a combination of the activity described for PLA_1 and PLA_2. These enzymes possess, additionally, acyltransferase activity which allows them to transfer a fatty acid to a lysophospholipid, resulting in a phospholipid [34]. The most well-characterized role of PLA_2 enzymes, and perhaps one of the most important, pertains to one of the products of the action of the enzyme on the phospholipid molecule – arachidonic acid. This long-chain fatty acid is a precursor for the synthesis of eicosanoids, which are an important mediator of inflammation [33]. PLCs catalyze the hydrolysis of the proximal phosphodiester bond between the glycerol backbone and the phosphate group on phospholipids. In mammals, thirteen members of the PLC family can be divided into six groups, depending on sequence

and structure. These enzymes are PI-specific, meaning they only hydrolyze phosphoinositides. More specifically, they hydrolyze the proximal phosphodiester bond on phosphatidylinositol biphosphate ($PI(4,5)P_2$) releasing DAG and inositol triphosphate (IP_3) [35]. Both these products are important second messengers that control various cellular processes. Whilst DAG remains anchored to the membrane after hydrolysis available as a substrate for the synthesis of other molecules such as PA, IP_3 diffuses into the cytosol becoming available for binding by its receptors such as the calcium channels of the endoplasmic reticulum. The resulting increase in cytosolic calcium induces a signalling cascade that can result in changes in intracellular activity. Additionally, both this increase in calcium and the newly synthesized DAG result in the activation of protein kinase C enzymes (PKCs). These will go on to phosphorylate their targets, activating several cell signalling pathways [36]. Given the previously described importance of phospholipids in cell mechanisms, the impact of dysregulation in phospholipase action has been extensively studied and implicates these enzymes in a number of human diseases and pathophysiological conditions including cancer, obesity, neurological diseases, cardiac ailments, metabolic diseases, platelet dysfunctions, amongst others [29]. Hence, it is of the utmost importance to fully investigate phospholipids' and phospholipases' mode of action and regulation in such mechanisms. These studies will advance the understanding of different pathophysiological conditions and will contribute to evaluating the use of phospholipids and phospholipases as potential therapeutic targets.

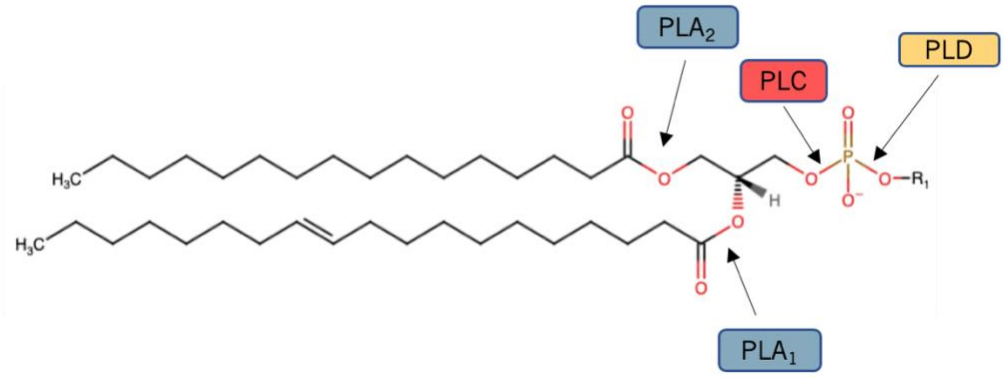

Figure 3. Action site of the four main phospholipases on the phospholipid molecule.

Phospholipases are a group of enzymes that hydrolyze phospholipids and can be divided into four main classes: phospholipases A (PLA), phospholipases B (PLB), phospholipases C (PLC), and phospholipases D (PLD). Dispite sharing the same susbtrate, their action site on the phospholipid molecule differs. PLA_1 cleaves at the *sn-1* position of the acyl chain; PLA_2 cleaves at the *sn-2* position of the acyl chain; PLC cleaves just before the phosphate group; PLD cleaves after the phosphate group. PLA_1 - Phospholipase A1; PLA_2 - Phospholipase A2; PLC – Phospholipase C; PLD – Phospholipase D.

I.2.1. Phospholipase D

PLD hydrolyzes the phosphodiester bond on the phospholipid molecule resulting in an exchange of the headgroup on PA at the terminal phosphodiester bond. PLDs' main substrate is PC, producing PA and choline [37] – Figure 4. This reaction is typically carried out using water as the nucleophile however, in the presence of primary alcohols, PLD prefers these compounds, by about 1000-fold, as substrate instead of water, resulting in the production of phosphatidylalcohols [38,39]. This alternative reaction is of particular importance given that one of its possible products, phosphatidylethanol, is used as a biomarker for chronic alcoholism. This characteristic has allowed for a lot of important studies on PLD activity and its quantification by measuring the produced phosphotidylalcohols. In fact, this promiscuity has allowed for the development of an innovative method for imaging PLD activity through the tagging of the alcohol derivatives with a fluorescent probe [40]. The enzyme was first identified in 1947 in the carrot by Hanahan *et al.,* who found that a raw fraction of the vegetable contained a lower concentration of PC when compared to a cooked fraction and postulated that the raw fraction contained an enzyme that was able to hydrolyze PC [41]. PLD enzymes have since been reported in an array of organisms, including bacteria [42,43], yeast [44,45], and viruses [46]. However, mammalian PLDs have been the target of the biggest interest since the 1970s, when the first mammalian phospholipase D activity was described in rats [47] and the first human PLD was cloned [48]. Hammond *et al.*, the first to clone a mammalian PLD, were also the first to position the HKD domains within the sequence of these enzymes. This same team later described the four highly conserved domains found in PLDs [49]. Around the same time, Ponting and Kerr defined, for the first time, the notion of a phospholipase D superfamily by showing that all the PLDs described so far shared the same primary structural characteristics [50]

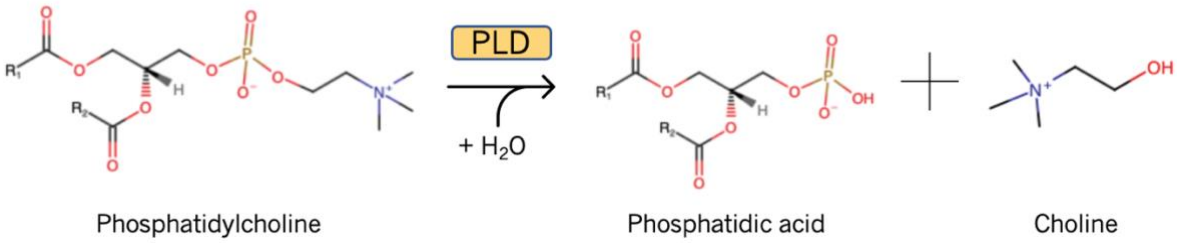

Figure 4. Reaction catalyzed by phospholipase D.

PLD uses water as the nucleophile to hydrolise the phosphodiester bond in phosphatidylcholine resulting in the formation of phosphatidic acid and free choline

I.2.2. Structure and cellular functions of mammalian PLD enzymes

I.2.2.1. PLD1 and PLD2

In the 1990s, two mammalian PLD isoforms with 50 % sequence homology - *PLD1* and *PLD2* - were cloned and characterized [48,51]. Structurally, mammalian PLD1 and PLD2 are comprised of four highly conserved domains (I-IV), two HKD motifs (HxKxxxxD sequence signature), a PX (Phox) and a PH (Pleckstrin Homology) domains in the N-terminal region [39], and a $PI(4,5)P_2$ binding site [52] (Figure 5). The C-terminal portion of PLD1 has been shown to be essential for catalytic activity since deletion of this region resulted in an inactivation of the enzyme. This is likely due to the fact that, unlike most enzymes, the C-terminus of PLD1 is directed towards the interior of the protein, with the terminal carboxylic acid forming a bond adjacent to the active site and the last four residues of the C-terminus forming a single-turn helix that leads to the active site [53]. This folding back into the structure works to stabilize the active site. A loop region can be found in PLD1 but not in PLD2 [54]. The HKD motif is crucial for PLD enzymatic activity [55]: the first His residue of the HKD motif attacks the phosphosubstrate followed by the activation of a water molecule by the second His residue; the water molecule then performs a nucleophilic attack on the phosphoinositide, releasing the product [53]. The PX and PH domains interact with lipids and proteins and are essential for PLD's subcellular localization [56,57]. The $PI(4,5)P_2$ binding motif mediates activation of PLD1 and PLD2 and is required for their catalytic activity [52]. Until recently, the loop domain on PLD1 was thought to be a regulatory region, mediating PLD1 inhibition resulting in PLD1's characteristic low basal activity [54]. In fact, insertion of this domain into PLD2 showed decreased enzymatic activity, which appeared to consolidate the loop as a regulatory domain [57]. However, recent work has shown that deletion of the loop region on recombinant human PLD1 does not result in a significant difference in the enzyme activity when compared to the full-length enzyme [53]. Since the loop is not essential for enzymatic activity and also appears to not have a regulatory role, as previously believed, a purpose for this PLD1 specific region is still to be found. Although a lot is known about the structure of PLD1 and PLD2, many aspects are still to be unveiled. Solving the crystal structure of human PLDs would greatly aid in this process. Whilst the catalytic domains of both PLD1 and PLD2 have recently been solved, solving of the entire crystal structure of these enzymes has proven difficult given the disordered regions that can be found in both enzymes (i.e., the loop in PLD1) [53,58]. 3D structure

predictions are available and can help enlighten some of these processes. AlphaFold, a recently developed artificial intelligence tool, predicts, with great speed and precision, protein 3D structures. Predictions for human PLD1 and PLD2 can be found in Figures 5c) and 5d), respectively.

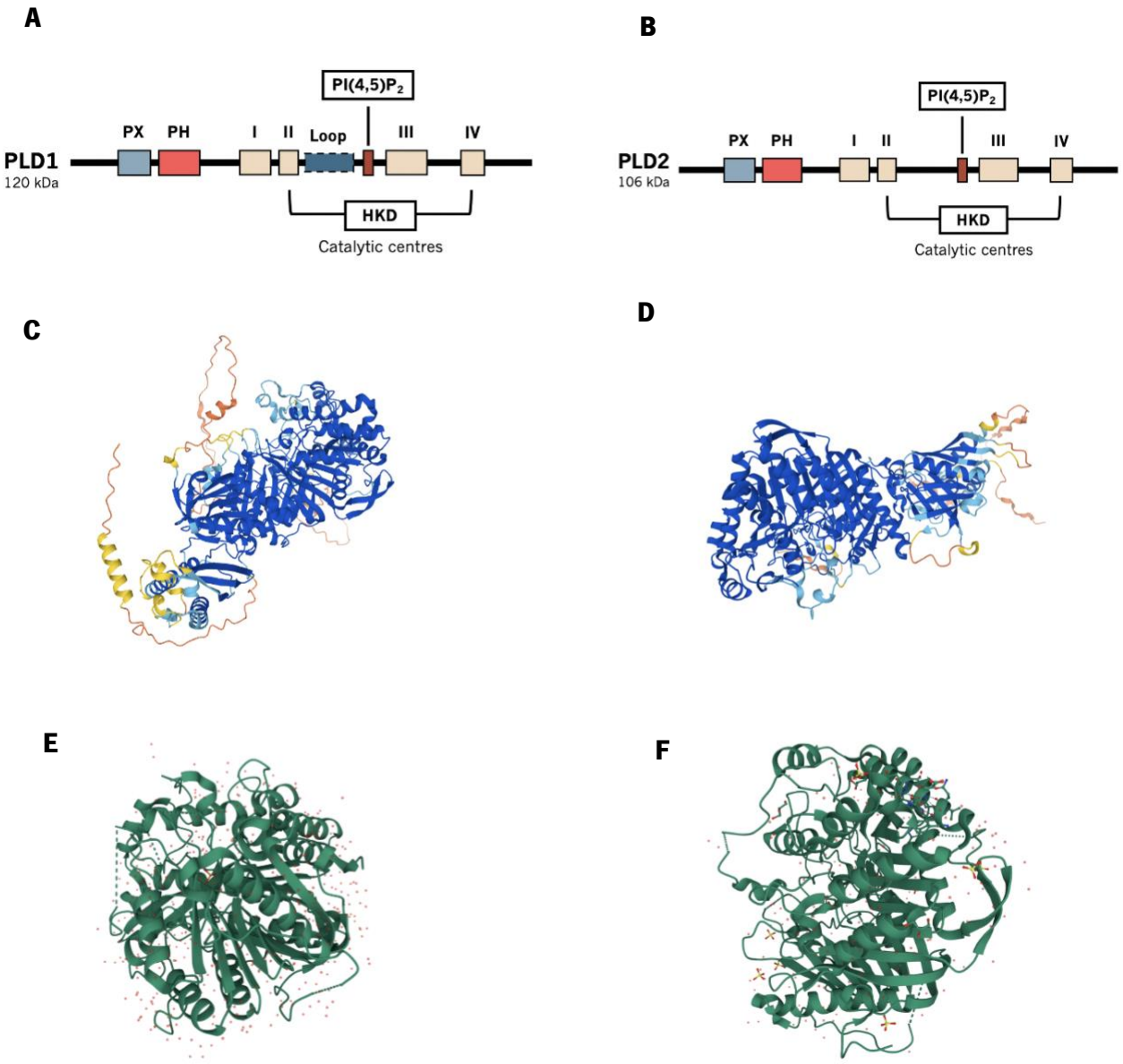

Figure 5. Structure of mammalian PLD1 and PLD2

A) and B) Characteristic domains of PLD1 and PLD2, respectively. Both isozymes contain PX and PH domains, essential for their subcellular localization. Similarly, both contain four (I-IV) highly conserved domains and two HKD motifs, critical for the enzyme's catalytic activity. A PI(4,5)P_2 binding region can also be found in both isozymes. A loop region can be found only in PLD1.

C) and D) **Predicted 3D protein structure of human PLD1 and PLD2, respectively** (AlphaFold Protein Structure Database). Alphafold produces a color coded, per residue confidence score between 0 and 100. Regions in dark blue and light blue present model confidence scores of "very high" and "confident", respectively, whilst regions in yellow and orange present confidence scores of "low" and "very low", respectively. For both PLD1 and PLD2, most of the residues in the predictions show a very high model confidence score

E) and F) Resolved crystal structures of the catalytic domains of human PLD1 [55] and PLD2 [89], respectively (Retrieved from RCSB PDB using Mol* [58]. PLD1 ID: 6U8Z PLD2 ID: 6OHO.) The resolved catalytic domain of human PLD1 shows 18 β-strands, 18 α-helices and a series of loops that combine, forming an asymmetric globular structure. For PLD2, a core containing 7 β-strands is found between 3 α-helices, running parallel to the strands on one side, and 1 long α-helices that runs perpendicular to the β-strands on the opposite side.

Despite both enzymes being ubiquitously expressed in almost all tissues and cell types [60], their subcellular localization differs, with PLD1 localizing, in steady-state normal conditions, predominantly at intracellular compartments such as the Golgi complex, the endosome, the lysosome, the endoplasmic reticulum, the plasma membrane, and in exocytotic vesicles, and PLD2 localizing mainly in the vicinity of the plasma membrane [61] with some reports of its presence at the Golgi complex [62,63], as well as associated with endosomal structures [64]. Interestingly, PLD1 and PLD2 cellular localization appear to be dynamic, changing throughout the cell cycle [65]. As an example, PLD1 can be recruited to the plasma membrane through the endosomal route upon stimulation [66,67]. Accordingly, PLD1 is involved in vesicle budding associated with the trans-Golgi network [68], Epidermal Growth Factor Receptor (EGFR) endocytosis [69], transport from the Golgi to the plasma membrane [63], exocytosis [70–74], regulation of the cytoskeleton [29,37] and phagocytosis [75], while PLD2 seems to function in phagocytotic traffic events associated with the Golgi [75,76] and G-protein coupled receptor endocytosis at the plasma membrane [64,77]. Even though PLD1 and PLD2 catalyze the same reaction, given the differences in intracellular localization, structure and activity in basal conditions, a difference in biological roles for PLD1 and PLD2 can be hypothesized.

I.2.2.2. PLD3, PLD4, PLD5, and PLD6

Additionally, PLD3, PLD4, PLD5, and mitochondrial PLD (MitoPLD/PLD6) have also been described and are known to share the same HxKxxxxD sequence signature [78–81]. Due to differences in structure and the presence or absence of certain domains, this enzyme superfamily can be divided into two groups that can be described as “classical” PLDs and “non-classical” PLDs. “Classical” PLDs comprise all PLD enzymes with a PX and PH domain, with two HKD motifs (or phosphodiesterase catalytic centres) and with canonical lipase activity, whilst “non-classical” PLDs comprise all PLD enzymes that lack one or both PX and PH domains, have one or two HKD motifs and do not have canonical lipase activity [82]. With no known phospholipase activity the “non-classical” PLD3 and PLD4 have recently been identified as 5’-ssDNA exonucleases that are needed to regulate endosomal nucleic-acid sensing [83]. PLD3 is a type II transmembrane protein and has been shown to localize to the ER, the golgi complex and lysosomes [84–86] This enzyme appears to be associated AD through the processing of amyloid precursor protein (APP) – *PLD3* gene expression was found to be lower in neurons of AD patients when compared to cognitively healthy individuals and this lower expression correlated with higher levels of APP and amyloid-beta. This same study also found a rare variant of the *PLD3* gene that increases the risk for AD [87]. Even though PLD4 contains two catalytic HKD domains

at the C-terminal end it does not have any known lipase activity. This PLD family member has, however, been associated with important processes such as the phagocytosis of microglia in the central nervous system [88] and shown to be involved in the activation of M1 macrophages promoting and inhibitory effect in colon cancer cells, *in vitro* [89]. Similarly to PLD3 and PLD4, PLD5 does not display any lipase activity. A recent study has associated PLD5 deregulation with thyroid cancer: survival analysis of mRNA expression profiles from thyroid cancer patients showed that up-regulation of PLD5 accelerated patients' death [90]. As the name suggests, MitoPLD or PLD6 is a mitochondrial protein responsible for hydrolyzing cardiolipin, a lipid molecule specific to the mitochondrion, forming PA in the mitochondrial surface and aiding in mitochondrial fusion [80]. This member exhibits only one HKD motif in its sequence, interestingly however it appears that PLD6 can dimerize to form an active enzyme by combining two HKD motifs in one catalytic pocket [91]. Recent studies have also highlighted the role of MitoPLD in the piRNA biogenesis pathway in the mouse germline [92].

I.2.3. Regulation of PLD1 and PLD2 activity

The first evidence of modulation of PLD activity was described in 1956 when the enzyme was partially purified for the first time. Authors reported that phospholipase D from cottonseed and cabbage were both susceptible to activity stimulation by NaCl [93]. The recent crystal structure solving of the catalytic domains of human PLD1 and PLD2 has highlighted some of the molecular mechanisms underlying substrate recognition and activation or inhibition of PLD1 and PLD2 [53,58]. In mammals, PLD activity can be regulated by a number of small GTPases such as ADP Ribosylation Factor (ARF) [94] and Rho GTPases [95], protein kinase C (PKC), and phosphoinositides. Furthermore, PLD has been shown to respond to receptor tyrosine kinases (RTK) such as EGF (Epidermal Growth Factor) signals in a number of cell types [96–98] with one particular study reporting that overexpression of *PLD1* and *PLD2* resulted in increased internalization and degradation of EGFRs. ARF, or ADP-Ribosylation Factors, were initially identified as positive regulators of PLD activity in human (HL60) [99] and porcine cells [100]. There are six known ARF proteins (ARF1 – ARF6) and all of them have been reported as activators of PLD1 activity *in vitro* [101], with ARF1 and ARF6 as the major activators [102]. However, PLD2 does not display a strong response to ARF activation [51,57]. PLD activation by PKC can be achieved through phosphorylation-dependent or phosphorylation-independent mechanisms. *In vitro*, PKCα regulates PLD1 activity but not PLD2 [51,103]. Furthermore, only PKCα and PKCβ have been reported as PLD1 activators *in vitro*, and this interaction is achieved through a non-

phosphorylation mechanism and in the absence of ATP [103,104]. Several studies have reported that PLD possesses PKC binding sites in both the N- and C- terminus [54,104,105]. Interestingly, there seems to be a synergistic interaction between PKCα and some of the other PLD activators, namely Rho and ARF [103]. When compared to activation by ARF and PKC, Rho GTPases appear as a less potent activator of PLD activity [103]. In PLD1, this regulation is achieved through the binding of the small GTPase RhoA to the C-terminal of the enzyme [106]. When RhoA binds to PLD1 the Michaelis constant, K_m, of PC is reduced [53]. With this result in mind, it has been hypothesized that PLD1 activation by RhoA is a result of conformational changes carried out when RhoA binds to one of the α-helices of PLD1's catalytic domain, increasing the enzyme's affinity for its substrate, PC. Other small GTPases of the Rho family, such as Cdc42 and Rac1, have been reported as regulators of PLD1 but not PLD2 [95,107,108]. As previously mentioned, the binding of the phosphoinositide $PI(4,5)P_2$ regulates activation of PLD1 and PLD2 and it is essential for their catalytic activity [52]. In fact, PLD1 requires $PI(4,5)P_2$ as a co-factor for basal activity and for activation by RhoA, Arf, and PKC [53]. $PI(3,4,5)P_3$ has also been reported as an activator of PLD, although less efficient than $PI(4,5)P_2$ [103,109]. A recent study has shown that binding of $PI(4,5)P_2$ strongly activates the PLD1 catalytic domain by 73-fold whilst $PI(3,4,5)P_3$ binding only resulted in an activation of 5-fold [53].

I.2.4. Phospholipase D1 and D2 in health and disease

Atypical expression and regulation of PLD activity have been strongly associated with a number of pathophysiological conditions, namely heart disease, cancer, and neurodegenerative diseases. PLD activity was shown to be increased in breast cancer and gastric carcinomas [110], while *PLD1/2* expression appears elevated in breast cancer [111,112], colorectal carcinomas [113], and renal cancers [114]. Additionally, *PLD1* expression was reported to play an important role in angiogenesis and metastasis, such as shown in studies using *PLD1* KO mice that were partially resistant to cancer growth [115]. Pertaining to heart disease, studies involving *PLD1* ablation in mice were associated with a protective effect in thrombosis and ischemic brain infarction [116] while *PLD2* appeared to be involved in high blood pressure associated pathologies [117] and has been identified as a risk factor for hypertensive disease [118].

I.2.5. PLD1 and PLD2 in the brain and neurodegeneration

The part that lipid-mediated signalling takes in neurodegenerative diseases, such as AD, has become more relevant in recent years [25]. Expression of *PLD1* and *PLD2* in the brain begins during the developmental phase and prolongs itself throughout postnatal life and in fact, appears to be regulated accordingly with the different developmental stages of the brain [119,120]. Several studies have associated PLDs with AD. A study from 2006 reported that PLD1 regulates APP trafficking, and it also corrects impaired neurite outgrowth/ branching capacity in familial Alzheimer's disease (FAD) mutant neurons, likely due to promotion of APP axonal transport [121]. APP is a precursor of amyloid-beta, the primary component of the amyloid plaques found in the brains of patients with AD. One of the clearest links between PLD activity and AD was established in a 2010 study, where ablation of *PLD2* resulted in a decrease in the synaptotoxic effect of Aβ42 oligomers (a highly cytotoxic amyloid-beta species). Moreover, PLD2 KO mice were protected from memory deficits when crossed with a transgenic mouse model of AD [122]. Similarly, in an AD *C. elegans* model that overexpresses Aβ, the ablation of the only nematode PLD gene was shown to also have a positive impact in several Aβ-deleterious phenotypes [123]. PLD has also been implicated as a potential neuroprotective target, with reports that PLD activity plays a role in buffering the cytotoxic effects of C16:PAF, a platelet-activating factor reported being elevated in the brain of patients with AD [124]. PLD1 was recently associated with longitudinal hippocampal axis functioning and organization and the ablation of *PLD1* in mice resulted in disruption of the dorsal hippocampus (DH) – ventral hippocampus (VH) structural differentiation with a predominant effect on DH [125]. Given the role that the hippocampus plays in memory and learning, these results seem to, once again, implicate the PLD pathway in neurological disorders.

I.3. A yeast ortholog: Spo14

In *Saccharomyces cerevisiae,* PLD activity was first described in the mitochondrial membrane where it was shown to play a role in the hydrolysis of mitochondrial enzymes during glucose repression under anaerobic conditions [126,127]. The *SPO14* gene codes for a 1638 amino acid and 195 kDa PC-specific PLD whose activity is critical for the regulation of prospore membrane formation during meiosis in starvation conditions [128] (Figure 4) highlighting the role of this gene in meiosis and spore formation [129]. Structurally, Spo14 is very similar to PLD1 and PLD2, containing PX [50] and PH [130] domains involved in protein and lipid interaction, four highly conserved domains (I-IV) two of

which contain HKD motifs as the catalytic centres' [55,131], and a PI(4,5)P_2 binding site [52]. In yeast, asexual reproduction or gemulation is the reproductive strategy carried out in favourable environmental conditions. However, oxygen deprivation or exposure to an unfermentable carbon source induces a switch in the reproduction system, resulting in the mating of yeast cells and sporulation. Sporulation allows for the formation of haploid nuclei after meiosis. These nuclei are surrounded by a prospore membrane whose formation and subsequent envelopment of the nuclei is dependent on Spo14. The defects in meiosis observed when *SPO14* is deleted can be rescued with the expression of a catalytically active Spo14 however, a catalytically inactive Spo14 mutant is not capable of rescuing the meiotic phenotype [55]. PLD activity of Spo14 is essential but not sufficient for meiosis, as a catalytically active Spo14 with a truncated N-terminal does not rescue the sporulation defect [128]. Therefore, this N-terminal region seems to play an important role in Spo14 subcellular localization. Localization wise, Spo14 is present throughout the cytoplasm in vegetative cells [73], re-localizing to the prospore membrane as the yeast enters meiosis II [128,132], the interaction of the PH domain with PI(4,5)P_2 induces this translocation of Spo14. Spo14 has also been reported to be required for vesicle fusion during sporulation in *S. cerevisiae* [133]. Together, these results reveal a possibility for a conserved role of PLD in membrane fusion. Spo14 is also involved in the metabolic pathways of crossbreeding between yeasts. The Ste20p kinase is responsible for the formation of the shmoo, a protuberance before the crossing between the yeasts. It triggers the formation of the protein complex called the polarisome which facilitates the polarization of cells and the rearrangement of the actin cytoskeleton. The production of PA by Spo14 results in the activation of Ste20p [134]. *SEC14* encodes a PI/PC transport protein essential for vesicle transport from the Golgi to the membrane. This requirement can be bypassed through a number of mutations in genes involved in the PC biosynthesis pathway. This is known as the *SEC14* bypass mechanism [135]. Spo14 activity is essential for the bypass phenotype as deletion of *SPO14* results in the elimination of the PI/PC excretion phenotypes [136]. These studies highlight a link between Sec14 and Spo14. Similar to what has been reported for mammalian PLD, Spo14 PLD activity *in vitro* is strongly activated by PI(4,5)P2 binding [52,109] however, it is unresponsive to ARF [128]. In yeast, PIP levels can be regulated by Vps13, a sorting protein involved in prospore membrane morphogenesis [137]. Another regulator of Spo14 activity is Spo14 Regulatory Factor 1, or SRF1, regulating Spo14 catalytic activity in mitotic cells [124].

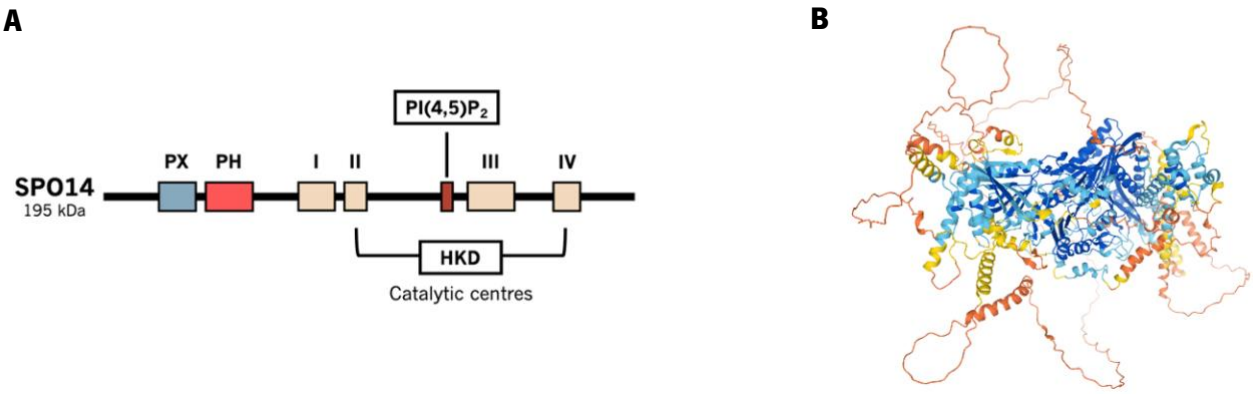

Figure 6. Structure of *S. cerevisiae* Spo14.

A) Domains of Spo14. Similarly to mammalian PLD1 and PLD2, Spo14 also contains PX and PH domains, the four highly conserved regions, I-IV, of which two share the conserved HKD motif involved in catalysis, and a PI(4,5)P2 binding site**.**

B) Predicted 3D protein structure of *S.cerevisiae* Spo14 (AlphaFold Protein Structure Database). Alphafold produces a color coded, per residue confidence score between 0 and 100. Regions in dark blue and light blue present model confidence scores of "very high" and "confident", respectively, whilst regions in yellow and orange present confidence scores of "low" and "very low", respectively. Given the high number of disordered regions in this enzyme, model confidence scores are mixed.

I.4. Yeast as a model organism: Using *S. cerevisiae* to study PLD1 and PLD2

Comprising a robust set of manipulative advantages, *S. cerevisiae* has been extensively used in scientific research and it is a well-established model organism. Importantly, it has been successfully used to study a variety of human diseases linked to the brain, specifically neurodegenerative diseases such as AD [138–141]. In fact, this species combines a set of characteristics that set it as one of the top models for eukaryotic cell biology research [142–145]:

I. Along with having a short generation time (around 90 minutes), its small size and straightforward growth conditions make it so that it can be easily cultured and very cost-effective. Additionally, it is a nonpathogenic species making manipulation in a laboratory more effortless.

II. As a unicellular eukaryote, *S. cerevisiae* shares a common cell architecture with higher multicellular eukaryotes.

III. A wide variety of yeast resources are readily available: a completely sequenced genome, specific and detailed databases, several sets of strains including deletion mutants and GFP-tagged strains.

IV. Availability of well-established transformation protocols, allowing for easy genetic manipulation using different genetic techniques (over and under expression, gene knockout or knockdown experiments, study gain- or loss-of-function phenotypes).

V. It can be grown as a haploid or a diploid organism, allowing for easier manipulation and identification of mutations and associated phenotypic traits.

VI. *SPO14* disruption does not compromise viability, nor does it exhibit growth defects under vegetative growth in *S. cerevisiae* [146].

As such, the yeast model provides a powerful heterologous expression system for the study and characterization of mammalian proteins. In fact, several studies have described the use of *S. cerevisiae* as a heterologous expression host for multiple important proteins of mammalian origin, including the GLUT glucose transporters [147], Na/H antiporters [148], Caspase-3 [149], and membrane proteins [150]. As for the use of *S. cerevisiae* in the study of PLD, some advantageous criteria can be highlighted: (1) approximately 17 % of yeast genes are orthologous for gene families associated with human diseases [151], and for the majority of these genes, the mammalian homolog functions in yeast and complements the deletion mutant [143]; (2) a single PLD ortholog has been identified and sequenced in *S. cerevisiae* - *SPO14* [73,129]. (3) yeast presents reduced complexity compared to the typically used mammalian models, which in certain biological conditions, can be useful for the study of essential mammals genes.

Since Spo14 is likely the only source of canonical PLD activity in yeast, the study of *SPO14* mutants presents itself as a relevant model to study the differential roles of mammalian PLD1 and PLD2.

I.5. Outline and aims of the thesis

Deregulation of the mechanisms underlying PLD1 and PLD2 activity plays a key role in a number of pathophysiological conditions, mainly neurodegenerative diseases such as AD. Despite their apparent similarity when it comes to catalytic function and overall structure, PLD1 and PLD2 are differentially implicated in various biological conditions. Therefore, understanding the basic cellular mechanisms by which both enzymes abide and are a part of, is of the utmost importance. Moreover, the eukaryotic model organism, *S. cerevisiae*, has proven to be a great model for studying mammalian proteins [147–149] and neurodegenerative diseases [124,138–141]. Despite being a simple unicellular organism, yeast shares a high level of complexity and similar cellular mechanisms with higher eukaryotes. Easy genetic manipulation and fast growth in accessible and easily achievable conditions in combination with the currently available genetic design and manipulation techniques make this organism a great model

for studying the differential roles of mammalian enzymes such as PLD1 and PLD2. Taking all of this into account, the present work aimed at heterologously expressing codon-optimized versions of mammalian *PLD1* and *PLD2* genes in the yeast *S. cerevisiae SPO14* deletion mutant as a way to explore potential biological differences between these mammalian isoenzymes. Importantly, a set of valuable molecular tools was generated in order to further investigate the localization and expression of *PLD1* and *PLD2* which is relevant for this thesis, but also contributes for other future projects that intend to study PLD biology using multimodal and multispecies approaches.

Chapter II - Materials and methods

II. Materials and methods

II.1. Yeast strains and growth conditions

The *S. cerevisiae* yeast strains used in this work are listed in Table 2. Yeast strains were maintained in YPD plates (1 % yeast extract (w/v), 1 % peptone (w/v), 2 % glucose (w/v) and 2 % agar (w/v)). When yeast pre-inoculums or inoculums were needed, strains were grown in YPD liquid media (1 % yeast extract (w/v), 1 % peptone (w/v), 2 % glucose (w/v)). For growth in selective media, plates were prepared according to each strain's selective requirements.

Table 2. List of *S. cerevisiae* strains used in this work

Strain	Genotype	Source
IR01	23344c; MATα *ura3 spo14::kanMX*	This work
IR04	BY4741; MATa *ura3Δ0; leu2Δ0; his3Δ1; met15Δ0; YKR031c::kanMX*	Euroscarf
IR07	23344c; MATα *ura3*	Laboratory collection
IR10	23344c; MATα *ura3 spo14::HygMX4*	This work
IR17	W303; MATα *his3, leu2, trp1, ura3*	Peter Griac's Lab
IR23	W303; MATa *ura3, his3, leu2, trp1, spo14::URA3*	Peter Griac's Lab
IR71	23344C; MATα ura3 *spo14::kanMX* p416-GPD_coPLD1-GFP	This work
IR74	23344C; MATα *ura3 spo14::kanMX* p416-GPD_coPLD2-GFP	This work
IR77	23344c; MATα *ura3* p416-GPD	Laboratory collection
IR78	CEN.PK113-7 D; MATa	Nijkamp J., *et al* [152]
IR79	23344c; MATα *ura3 spo14::PLD1*	This work

II.2. Primer design

The primers used in this work were designed using the "ApE – A Plasmid Editor" software, a sequence editing tool, and are listed in Table 3**.**

Table 3. List of oligonucleotides used in this work

Primer	Sequence (5' → 3')	Source
196_pMEC_MX4_fwd	ACTTTTCGGGGAAATGTGC	Laboratory collection (MEC group)
253_kanC3	CCTCGACATCATCTGCCCAGAT	Laboratory collection (MEC group)
473_MSW_rev	GTATAGCGACCAGCATTC	Laboratory collection (MEC group)
576_pBR322_2	GAAAAATAAACAAATAGGGGTTCCG	Laboratory collection (MEC group)
gRNA_HygMX4-FW	TCTCTACAGGGGCGCGGCGTGTTTTAGAGCTAGAAATAGCAAGTTAAAAT	This work
gRNA_HygMX4-RV	ACGCCGCGCCCCTGTAGAGAGATCATTTATCTTTCACTGCGGAG	This work
Long-down-SPO14-hPLD1-RV	GAATGCATAATGAAAACTGTTTATGTATCAGCGTCGAATGCTTATAACAGATAA AAGGAAAATACAGGTAATGGTGTGTTCCTGGTCGTTTTTATATTCCCTTATGTC CAAACTTCCATT	This work
Long-down-SPO14-mPLD2-RV	GAATGCATAATGAAAACTGTTTATGTATCAGCGTCGAATGCTTATAACAGATAA AAGGAAAATACAGGTAATGGTGTGTTCCTGGTCGTTTTTATATTCCCTTATGTC CAAACTTCCAAT	This work
Long-up-SPO14-hPLD1-FW	GCAGGACATTATAGGCACGACCGGTCACTGATAATTCACACGACGCATTGAG AGGCACGTACGCAAGAAGAAAAGGTAGGATAGATAAACAAGGGTGATGTCATT GAAGAACGAACCAAG	This work
Long-up-SPO14-mPLD2-FW	GCAGGACATTATAGGCACGACCGGTCACTGATAATTCACACGACGCATTGAG AGGCACGTACGCAAGAAGAAAAGGTAGGATAGATAAACAAGGGTGATGACTGT TACACAAAAGAATTT	This work
pGPD-co-hPLD1-GFP-fw	CTAGTGGATCCATGTCATTGAAGAACGAACCAAGA	This work
pGPD-co-hPLD1-GFP-rv	CATGTCGACAAGCTTGATATCGAATTCTGTCCAAACTTCCATTGGAA	This work
pGPD-co-mPLD2-GFP-fw	GAACTAGTGGATCCATGACTGTTACACAAAAGAA	This work
pGPD-co-mPLD2-GFP-rv	CATGTCGACAAGCTTGATATCGAATTCTGTCCAAACTTCCAATGGAA	This work
Screening-down-SPO14-rv	CTGTTTATGTATCAGCGTCGAATG	This work
Screening-hPLD1-fw	GCATGGTACAAATTTCTTGAAGGAT	This work

Screening-hPLD1-rv	CCACTTTGCTAAAGCGTTTTCT	This work
Screening-mPLD2-fw	GGTAGAGATTTCTTGCAATTGCATC	This work
Screening-mPLD2-rv	GCTCTCAAGATAGCATCTGCAA	This work
Screening-up-SPO14-fw	GGTGAAGATTGCTACAGCCCTT	This work
1114_GFP-R	CCATCTAATTCAACAAGAATTGGGACAAC	Laboratory collection (MEC group)
1356_sgDNA_seq_pRCC-K_v2	CACACCCTACAATGTTCTG	Laboratory collection (MEC group)
primerA_spo14_del	TAAGCAACACTTGCTGATTACAGTC	This work
primerD-spo14-del	ATTATTAAGCAATTGAACACGGAAA	This work
K3	CCATCCTATGGAACTGCCT	Laboratory collection
150_MX4fwd	AAAATCTTGCTAGGATACAGTTCTC	Laboratory collection (MEC group)
149_MX4rev	ACAAATGACAAGTTCTTGAAAACAA	Laboratory collection (MEC group)
256_KanB	CTGCAGCGAGGAGCCGTAAT	Laboratory collection (MEC group)

II.3. Plasmids

The plasmids used in this work are listed in Table 4. The respective nucleotide sequences and any further relevant features are available in Chapter VI – Appendices.

Table 4. List of plasmids used in this work

Plasmid	**Source**
hPLD1_pUC57	GenScript ®
mPLD2_pCCI-4K	GenScript ®
pRCC-K	Generoso, W.C. *et al.* [153]
pRCC-K_gRNA-HygMX4	This work
p416_GPD-JEN1-GFP	Soares-Silva *et al.* [154]

p416_GDP-coPLD1-GFP	This work
p416_GPD-coPLD2-GFP	This work
pAG32	Goldstein *et al.* [155]

II.4. Polymerase Chain Reaction (PCR)

Polymerase chain reaction, or PCR, is a fast and cheap technique used to obtain several copies of a DNA fragment. PCR uses a series of repetitive and temperature-dependent conditions to amplify DNA. One PCR cycle consists of three steps – denaturation of the DNA template, binding of the primers to a specific region of the template, and extension of the primed ends by a polymerase, resulting in the synthesis of new copies of the template DNA. In this work, three different DNA polymerases were used, depending on the protocol and the final use of the amplified product: Taq DNA polymerase was used in colony PCR verifications, Phusion™ High–Fidelity DNA Polymerase (Thermo Scientific) was used to amplify the deletion cassettes, the genes *PLD1*, and *PLD2* for cloning into p416-GPD-GFP and to amplify the pRCC-K plasmid. Platinum™ II Hot-Start DNA Polymerase (Thermo Scientific) was used to amplify *PLD1* and *PLD2* for genomic integration. The annealing temperature of each primer pair in a PCR reaction was obtained using the WebPCR online software. Distinct annealing temperature gradients were selected to optimize and identify the ideal annealing temperature for each reaction (annealing temperatures for each primer pair can be found in Chapter VI – Appendices. The manufacturer's recommendations were followed when using the Phusion™ High–Fidelity DNA Polymerase and Platinum™ II Hot-Start DNA Polymerase.

II.5. Colony PCR

Colony PCR refers to the technique where single colonies are screened through PCR for the presence of a specific DNA sequence. A 2x PCR master mix was prepared containing 200 µL of 10x *Taq* buffer, 80 µL of 50 mM $MgCl_2$, 40 µL of 10 mM dNTPs, 50 µL of *Taq* polymerase (0.05 U/µL) and 630 µL of ultrapure water. The mix was vortexed and 10 µL were added into as many tubes as needed. Any remaining mix was stored at -20 °C. Afterwards, 1 µL of each primer was added into the correct tubes and 8 µL of ultrapure water was added to reach the final volume of 20 µL per tube. For each plate resulting from a yeast transformation protocol, an average of 10 colonies were chosen, numbered, and streaked onto a new plate using a sterile pipette tip. After streaking, the pipette tip was submerged in the PCR mix and swirled around to release any remaining cells into the PCR tube. With the exception

of the annealing temperature, which was adapted to each primer pair in a reaction and can be found in Chapter VI – Appendices, every colony PCR performed throughout this study followed the same cycling conditions: 10 minutes at 94 °C followed by 30 cycles of 10 seconds at 94 °C, 30 seconds at annealing temperature and 1 minute at 72 °C, and a final extension run of 10 minutes at 72 °C at the end of the 30 cycles.

II.6. Yeast genomic DNA extraction

Genomic DNA extraction was performed using phenol-chloroform-isoamyl alcohol (PCA). This method is based on the different solubility of biomolecules in the three components present in the PCA mixture. Phenol will digest protein structures and not DNA given its insolubility in phenol. Chloroform increases the efficiency of phenol denaturation of proteins, protects DNA by allowing for the separation between the organic phase and the aqueous phase, and will denature lipids. Isoamyl alcohol will precipitate and increase the purity of DNA. Briefly, yeast cell biomass was collected from a plate and added into an Eppendorf tube along with glass beads, 150 µL of 10x Tris-EDTA, and 150 µL of PCA. Cells were disrupted in the cell disrupter for 5 minutes at top speed followed by 10-minute centrifugation at 14000 rpm. After centrifugation, the top aqueous layer containing the DNA was removed and stored at -20 °C.

II.7. Construction of *SPO14* deletion strains

S.cerevisiae SPO14 deletion strains (*Δspo14*) were constructed for the subsequent heterologous expression of mammalian *PLD1* and *PLD2* genes. The *SPO14* gene was deleted via replacement with a drug resistance cassette through homologous recombination. For this genomic DNA was obtained from strain IR04 (Table 2) and the KanMX cassette was amplified via PCR using primers primerA-spo14-del and primerD-spo14-del (Table 3). The amplified cassette was transformed into strain IR07 (Table 2) using the LiAc/SS-DNA/PEG protocol described below. Transformants were grown in selective media plates containing geneticin (1 % yeast extract (w/v), 1 % peptone (w/v), 2 % glucose (w/v), 2 % agar (w/v), and 200 µg/ml of geneticin) and allowed to grow at 30 °C for 2-4 days. Transformants were further tested for correct insertion of the KanMX cassette through colony PCR. The new *SPO14* deletion strain (IR01 – Table 2) was then subject to resistance cassette switching. The HygMX cassette was amplified via PCR from plasmid pAG32 with primers 150_MX4fwd and 149_MX4rev (Table 3) and transformed into the newly constructed deletion strain IR01 (Table 2) in the same manner.

Transformants were grown in selective media plates containing geneticin (1 % yeast extract (w/v), 1 % peptone (w/v), 2 % glucose (w/v), 2 % agar (w/v), and 300 μg/ml of hygromycin) and allowed to grow at 30 °C for 2-4 days. Transformants were further tested for correct insertion of the HygMX cassette through colony PCR.

II.8. Codon usage optimization

The degenerate nature of the genetic code allows for single amino acids to be coded by more than one codon, which can result in the same protein being encoded by different nucleic acid sequences. Different organisms can have different codon usage frequencies, leading to difficulties in expressing proteins in heterologous hosts. Therefore, the codon usage of human *PLD1* and mouse *PLD2* was optimized to better fit the codon usage of the *S. cerevisiae* host strain. The optimized mammalian *PLD1* and *PLD2* genes were synthesized by Genscript and cloned into the pUC57 and pCCI-4K vectors, respectively. The mammalian *PLD1* and *PLD2* chosen for optimization in this work, from human and mouse origin respectively, were chosen based on the availability in our lab of the corresponding non-optimized versions. This ensures transversality throughout any experiments done in different host organisms. The *PLD1* and *PLD2* genes used for experiments throughout this work and mentioned henceforth are always the codon-optimized versions.

II.9. DNA precipitation

In order to achieve higher efficiency when integrating *PLD1* and *PLD2* in the yeast genome, the amplified genes were precipitated, resulting in a more concentrated product. Firstly, one volume of 5 M ammonium acetate was added into the samples and vortexed. Samples were centrifuged at 12000 rpm for 15 minutes at 4 °C. After centrifugation, one volume of 100 % isopropanol was added and samples were incubated at – 20 °C for 30 minutes. Followed another centrifugation at 12000 rpm for 15 minutes at 4 °C. The supernatant was gently aspirated and 200 μl of ice-cold 70 % ethanol was added to the pellet. Samples were vortexed and centrifuged at 12000 rpm for 3 minutes at 4 °C. The supernatant was aspirated gently and the pellet was allowed to air dry for 5 minutes. After drying, the pellet was resuspended in nuclease-free water.

II.10. Agarose gel electrophoresis

Agarose gel electrophoresis was performed for visualization of different DNA fragments throughout this work. All agarose gel electrophoresis experiences were performed using a 1 % agarose gel (1 % (w/v) agarose and 1X TAE (Tris-Acetate-EDTA) buffer). Agarose gels were pre-stained with Midori Green Advance nucleic acid stain (Nippon Genetics Europe) and all DNA samples were prepared with loading buffer (5 % (w/v) glycerol, 0.1 mM EDTA, 0.4 % (w/v) bromophenol blue) before being loaded into the gel. Gels were run at 200 V for 20 minutes and visualized in a UV transilluminator (VMR, Genosmart)

II.11. Cloning strategy

Two cloning strategies were performed in this work, to achieve different results. For subcellular localization studies, the codon-optimized mammalian *PLD1* and *PLD2* genes were cloned into a plasmid carrying the *GFP* reporter gene using traditional cloning. For studies involving sporulation and evaluation of PLD activity, the optimized genes were integrated into the genome of *S. cerevisiae* using the CRISPR-Cas9 editing tool.

II.11.1. Construction of GFP tagged *PLD1* and *PLD2* by restriction enzyme-based cloning

In traditional cloning, restriction endonucleases are used to cleave both the DNA insert and the vector, generating complementary end sequences that can be joined together by a DNA ligase before the transformation into the desired species. By using two restriction enzymes whose resulting cut sites are not compatible, the insert will be cloned directionally and the occurrence of re-ligation of the vector after digestion will decrease significantly. In order to clone the codon-optimized versions of human *PLD1* and mouse *PLD2* into the p416-GPD-GFP plasmid, both genes were amplified by polymerase chain reaction with primers containing recognition sites for the BamHI (Thermo Scientific) and SalI (Thermo Scientific) restriction enzymes. *PLD1* was amplified using primers pGPD-co-hPLD1-GFP-fw and pGPD-co-hPLD1-GFP-rv (Table 3), while *PLD2* was amplified using primers pGPD-co-mPLD2-GFP-fw and pGPD-co-mPLD2-GFP-rv (Table 3). PCR amplification was followed by digestion at of both genes with BamHI and SalI using the conditions recommended by Thermo Scientific's DoubleDigest Calculator: 0,5 µl of BamHI; 1 µl of SalI; 1 µl BamHI buffer; 2 µl of DNA insert and 3,5 µl of ultra-pure water. The digestion was carried out at 37 °C for 4 hours. Simultaneously, the

p416_GPD-JEN1-GFP vector [154] was digested using the same enzymes and reaction conditions (0,5 µl of BamHI; 1 µl of SalI; 1 µl BamHI buffer; 2 µl of plasmid vector and 3,5 µl of ultra-pure water). After digestion, the vector was loaded in an agarose gel and the empty vector (p416_GPD-GFP) was extracted from the gel and purified using the NZYGelpure kit (NZYTech). Briefly, the desired DNA fragment was excised from the gel with a scalpel and solubilized at 55 °C with 300 µL of Binding Buffer for each 100 mg of gel weight for 10 minutes, or until the gel slice was completely dissolved. The mixture was then loaded into an NZYTech spin column inside a collection tube and centrifuged for 1 minute at top speed (12000 rpm). The flow-through was discarded and the column was washed with 600 µL of Wash Buffer and centrifuged for 1 minute at top speed. After discarding the flow-through, the column was dried by centrifugation for 1 minute at top speed. Finally, 50 µL of DNA Elution Buffer was added and the column was incubated for 1 minute at room temperature. DNA was eluted by centrifugation for 1 minute at top speed and DNA was quantified using the NanoDrop® ND-1000 system. vector and DNA insert were ligated *in vitro* in a 1:1 molar ratio using T4 DNA ligase (Thermo Scientific™) (10 µl of digested insert; 5 µl of digested vector; 1 µl of T4 DNA ligase; 2 µl of 10X T4 DNA ligase buffer; 2 µl of ultra-pure water) and incubated at 22 °C for 1 hour. After ligation, 10 µl of each reaction were transformed, individually, into XL1-blue chemically competent *E. coli* cells. After transformation, single colonies were chosen from selection plates and plasmid DNA was extracted, digested with XbaI (Thermo Scientific) or EcoRV (Thermo Scientific), single and double-cut enzymes, respectively, to verify the size of the constructs (0,5 µl of XbaI or EcoRV; 1 µl of buffer Tango or buffer R; 1 µl of plasmid and 7,5 µl of ultra-pure water, incubated at 37 °C for 1 hour). Several of the constructs showing the correct size were sent for sequencing (sequencing results and alignments are available in Chapter VI – Appendices). The constructs whose sequence was correct were transformed into the IR01 *S. cerevisiae* strain (Table 2).

II.11.2. Genomic integration of mammalian *PLD1* and *PLD2* in the yeast genome using the CRISPR-Cas9 system

The budding yeast *S. cerevisiae* can reproduce sexually or asexually, depending on environmental conditions. In favourable conditions, where nutrient sources are readily available, yeast reproduces asexually by budding, a daughter cell simply buds out from the parent cell. This generates daughter cells that are genetic clones of the parental cells since these cells are

only undergoing mitosis. When nutrient sources are scarce or unavailable, yeast switches to sexual reproduction, mating with other yeast cells of a different mating type and sporulating. In order to test phenotypes that are associated with sporulation and meiosis and to yield a strain that expresses *PLD1* and *PLD2* in levels that are similar to physiological conditions, the optimized phospholipase D genes were integrated into the yeast genome.

The CRISPR-Cas9 genome editing technique was performed following the protocol developed by Generoso *et al.*, [153] where a single plasmid is used to carry the Cas9 nuclease and the gRNA recognition sequences. Firstly, the Cas9 bearing plasmid was amplified by PCR in three fragments, with primers containing the protospacer sequences (gRNA_HygMX4-FW and gRNA_HygMX4-RV – Table 3), and with primers for amplification of the remaining two fragments (196_pMEC_MX4_fwd, 253_kanC3, 473_MSW_rev, 576_pBR322_2 – Table 3) The protospacer containing primers were chosen according to the CRISPR gRNA Design tool provided by DNA 2.0. Afterwards, the plasmid was assembled using the Gibson Assembly® Master Mix (New England Biolabs) following the conditions provided by the manufacturer. Meanwhile, the *PLD1* and *PLD2* genes were amplified by PCR, in a total of four reactions per gene. The resulting DNA was then concentrated in order to allow for a higher concentration of donor DNA to be transformed into the yeast, increasing the efficiency of the transformation. The assembled plasmid and each donor gene were transformed into the IR10 yeast strain (Table 2) following the LiAc/ SS carrier DNA/PEG protocol and plated in selection plates containing geneticin (1 % yeast extract (w/v), 1 % peptone (w/v), 2 % glucose (w/v), 2 % agar (w/v) and 200 μg/ml of geneticin), to allow for the selection of transformants carrying the pRCC-K_gRNA-HygMX4 plasmid. Cells were grown at 30 °C for 2-4 days. Afterwards, cells were replica plated into media containing hygromycin (1 % yeast extract (w/v), 1 % peptone (w/v), 2 % glucose (w/v), 2 % agar (w/v), and 300 μg/ml of hygromycin), which allowed for the growth of colonies that did not have the *PLD1* or *PLD2* genome integration. Colonies that grew in media containing geneticin but did not grow in media containing hygromycin were selected for colony PCR.

II.12. *E. coli* transformation

E. coli transformation with the desired plasmids was performed following the heat shock transformation protocol adapted from Inoue *et al.,* [156]. *E. coli* XL1-blue competent cells were defrosted on ice. Once completely defrosted, 50 μl of competent cells were aliquoted for each transformation, into as many tubes as needed and 1 μl of plasmid DNA was added (approximately 100

ng), and cells were incubated on ice for 20 minutes. After the incubation on ice, cells were heat-shocked at 42 °C for 45 seconds and immediately returned to the ice for an additional 10 minutes. Afterwards, 200 µl of SOC medium was added to the tubes, and cells were allowed to recover in a shaking incubator at 37 °C for 1 hour. Cells were plated in LB-Amp selection plates (0,5 % yeast extract (w/v), 1 % peptone (w/v), 1 % sodium chloride (w/v), 2 % agar (w/v) and 100 µg/ml ampicillin) and allowed to grow overnight at 37 °C.

II.13. Plasmid DNA extraction

Plasmid DNA extraction was performed using the *NZYMiniprep Kit* (NZYTech) by following the provided protocol. For plasmid extraction from *E. coli*, cells were grown in 5 ml of LB media with appropriate antibiotics (Geneticin or ampicillin) overnight at 37 °C with agitation (200 rpm). The following morning, cells were collected by centrifugation at 13000 rpm for 1 minute. The supernatant was discarded, and cell lysis was performed by resuspending the pellet in 250 µl of A1 buffer and vigorously vortexed. Once the pellet was completely dissolved, 250 µl of buffer A2 were added and mixed by gently inverting the tube 6-8 times. Cells were incubated at room temperature for 4 minutes followed by the addition of 300 µl of A3 buffer. The tube was inverted 6-8 times and the lysate was clarified by centrifuging the tube for 10 minutes at 13000 rpm. The supernatant was loaded onto the spin columns provided by the kit and centrifuged for 1 minute at 13000 rpm to allow for the binding of DNA onto the silica column. The flow-through was discarded and the DNA was washed by adding 500 µl of AY buffer was loaded onto the column followed by another 1-minute centrifugation at 13000 rpm to dry. The flow-through was discarded and 600 µl of A4 buffer were added followed by 1-minute centrifugation at 13000 rpm. The silica membrane was dried by re-inserting the column into the tube and centrifuging for 2 minutes at 13000 rpm. The silica column was placed into a new 1,5 ml tube and 50 µl of AE buffer were carefully added to the center of the column and incubated for 1 minute at room temperature in order to elute DNA. The tube was centrifuged for 1 minute at 13000 rpm and the resulting flow-through was quantified using the NanoDrop® ND-1000 system and stored at -20 °C for later use.

II.14. Yeast transformation

The transformation of yeast strains with the desired DNA sequences was performed following two transformation protocols.

II.14.1. Electroporation protocol

For the expression of *PLD1-GFP* and *PLD2-GFP* in yeast, the corresponding plasmid constructs were transformed into the IR01 yeast strain (Table 2) using an electroporation transformation protocol. Transformation using electroporation uses an electrical pulse at an optimized voltage discharged through the cell. The voltage allows for the formation of temporary pores across the plasma membrane. Additionally, it helps increase the membrane potential across the cell. These two conditions allow the charged molecules in DNA to travel across the pores formed throughout the membrane which results in a large number of transfected cells. Firstly, a pre-culture was prepared by growing the IR01 strain (Table 2) in 5 ml of YPD medium overnight at 30 °C with the agitation of 200 rpm. The following morning, cell culture was prepared by diluting the pre-culture in 50 ml of YPD medium to an optical density at 640 nm (OD_{640}) of approximately 0.2 and grown until OD_{640} reached 1.5. Once the cell culture reached the desired optical density, cells were collected by centrifugation at 3500 rpm for 5 minutes at room temperature and washed two times, first with 50 ml of sterile distilled H_2O followed by a wash with 25 ml of sterile distilled H_2O. The cell pellet was resuspended in 8 ml of sterile distilled H_2O, 1 ml of TE 10X (0.1 M Tris-CL and 0.01 M EDTA), and 1 ml of LiAc 1 M and incubated at 30 °C for 30 min with the agitation of 200 rpm. After incubation, 250 µl of DTT 1 M was added to the cells and further incubated at 30 °C for 1 hour with the agitation of 200 rpm. Following the incubation, 40 ml of ice-cold sterile distilled H_2O was added, and cells were collected by centrifugation at 3500 rpm for 5 minutes at 4 °C. From this step onwards, cells were always kept on ice. Cells were then washed twice, first with 25 ml of cold sterile distilled H_2O and then with 5 ml of cold 1 M sorbitol. The pellet was resuspended in 500 µl of cold 1 M sorbitol. For each transformation, 45 µl of the now competent cells were transferred into as many tubes as needed and 1 µg of plasmid DNA was added into the corresponding tubes. The contents of each tube were transferred into the sterile electroporation cuvettes and electroporated at 1,5 kV, 200 Ω, 25 µF. Immediately after electroporation, 1 ml of sterile distilled water was added to the cuvettes and the contents were transferred back into the tubes. Afterwards, cells were collected by centrifugation at 3500 rpm for 5 minutes and resuspended in 400 µl of sterile distilled water, plated into synthetic complete medium without uracil (SC-ura) plates (2 % glucose (w/v), 2 % agar (w/v), 1850 mg/L of Kaiser SC double dropout -His -

Ura (FORMEDIUM), 6,7 g/L of yeast nitrogen base w/o amino acids (BD Difco™) and 76 mg/L of histidine) and allowed to grow at 30 °C for 2-4 days.

II.14.2. Lithium acetate/single-stranded carrier DNA/PEG protocol

For the integration of *PLD1* and *PLD2* in the yeast genome transformation was performed following the LiAc/ SS-DNA/PEG protocol, adapted from Gietz *et al.,* [157]. This is a high-efficiency version of the yeast transformation method using the Lithium acetate /single-stranded carrier DNA/PEG method. Firstly, a pre-culture was prepared by growing the *S. cerevisiae* IR53 strain (Table 2) in 5 ml of YPD medium overnight at 30 °C with the agitation of 200 rpm. The following morning, a cell culture was prepared by diluting the pre-culture in 50 ml of YPD medium to an optical density at 640 nm (OD_{640}) of approximately 0.4 and grown until OD_{640} reached 1.5. Once the cell culture reached the desired optical density, cells were harvested by centrifugation at 3500 rpm for 3 minutes and washed two times in 25 ml of sterile distilled H_2O. After washing, cells were resuspended in 1 ml of 100 mM LiAc, and the suspension was transferred into a 1,5 ml microcentrifuge tube. Cells were centrifuged at 13000 rpm for 15 seconds and LiAc was removed. The cell pellet was resuspended by adding 400 µl of 100 mM LiAc to a final volume of 500 µl and vortexed until the pellet was fully mixed. Afterwards, 50 µl of cell suspension was added into as many tubes as needed and centrifuged and the LiAc was removed. Following the thorough removal of remaining LiAc, the reagents for the transformation mix were added to each tube, in order: 240 µl of PEG 50 % (w/v); 36 µl of LiAc 1 M; 25 µl of previously boiled salmon sperm DNA 2 mg/ml; 40 µl of sterile distilled H_2O and 10 µl of PCR product or 50 µl of sterile distilled H_2O for the negative control. Tubes were vortexed until the cell pellet was completely dissolved and incubated at 30 °C for 30 minutes followed by incubation at 42 °C for 25 minutes. After incubation at 42 °C, tubes were centrifuged at 8000 rpm for 30 seconds and the transformation mix was completely removed. Afterwards, 1 ml of sterile distilled H_2O was added to the cell pellet and vortexed to uniformly resuspend the pellet. Cells were plated into YPD medium and allowed to grow at 30 °C for 2-4 days. For transformations that required antibiotic gene selection, cells were transferred into glass tubes with 1 ml of YPD and incubated for 3 hours at 30 °C to allow for the good expression of the antibiotic resistance gene.

II.15. Growth assays

Cells from strains IR23, IR71, IR74, IR78, IR77 (Table 2) were grown overnight in YPD or SC-ura medium at 30 °C with the agitation of 200 rpm. The following morning, cells were harvested by centrifugation at 3000 rpm for 5 minutes and washed three times with sterile distilled water. After the final wash, cells were resuspended in 10 ml of sterile water and diluted to an OD_{640} = 1 in 1 ml of water, and serial dilutions to 10^{-4} were prepared for each strain. In a laminar flow chamber 3 µl drops of each dilution, for every strain, were plated in SC-URA, SC-ura supplemented with 0.4 % (v/v) of ethanol and SC-URA + 2.5 µg/ml C16:PAF, SC-ura + 5 µg/ml C16:PAF, and SC-ura + 7.5 µg/ml C16:PAF. Cells were grown at 30 °C for 2 days.

II.16. Imaging of phospholipase D activity

For evaluating PLD activity a newly developed method by the Baskin Lab at Cornell was followed. This method, named IMPACT (**Im**aging **P**hospholipase D **A**ctivity with **C**lickable Alcohols via **T**ransphosphatidylation) allows us to image phospholipase D activity through a click chemistry reaction. The method is based on the promiscuity of PLD enzymes, which, in addition to using water for phospholipid hydrolysis, can also accept a variety of primary alcohols in a transphosphatidylation reaction. By tagging the resultant lipids with fluorescent reporters via click chemistry we end up with fluorescent lipids that act as reporters of PLD activity. Firstly, two pre-cultures were prepared by growing IR01, IR04, IR71 and IR74 *S. cerevisiae* strains (Table 2) in 5 ml of YPD medium overnight at 30 °C with the agitation of 200 rpm. The following morning, cell cultures were prepared by diluting the pre-cultures in 50 ml of YPD medium to an optical density at 640 nm (OD_{640}) of approximately 0.2 and grown until OD_{640} reached 3. Once the cell culture reached the desired optical density, cells were harvested by centrifugation at 3500 rpm for 3 minutes and resuspended in 1 ml of YPD medium supplemented with 10 mM of 5-hexyn-1-ol (hexynol for short) and incubated for 1 hour at 30 °C with the agitation of 200 rpm. After incubation with the primary alcohol, cells were collected by centrifugation at 10,000 x g for 1 minute and washed three times in 0.1 M potassium phosphate buffer pH 6.5 (0.1 M K_2HPO_4, 0.1 M KH_2PO_4). Afterwards, cells were fixed by resuspension of the pellet in 680 µl of potassium phosphate buffer containing 3.7 % paraformaldehyde (v/v) followed by an incubation of 45 minutes at room temperature with gentle shaking. Meanwhile, click master mix was prepared by combining, in the following order, 100 mM Tris pH 8.0, 1 mM $CuSO_4$ (from a freshly prepared 20 mM stock), 40 µM AZDye 594 Azide (Click Chemistry Tools), and 50 mM of sodium ascorbate (from a

freshly prepared 500 mM stock). At the end of the incubation period, fixed cells were washed three times with 0.1 M potassium phosphate buffer and 1 ml of click master mix was added to each tube. Cells were incubated for 30 minutes at 30 °C for fluorescent tagging. The labelled cells were then washed three times with 0.1 M potassium phosphate buffer and stored in 100 µl of 0.1 M potassium phosphate buffer at 4 °C until imaging.

II.17. Fluorescent and confocal microscopy of yeast cells

For imaging of yeast cells expressing *PLD1-GFP* and *PLD2-GFP*, cells were grown in SC-ura plates at 30 °C overnight. The following day, biomass was collected from the plates, cells were resuspended in 1 ml of sterile ultra-pure water and pelleted by centrifugation at 13,000 rpm for 30 seconds. Afterwards, 5 µl of cells were aspirated from the pellet, mounted onto a coverslip, and imaged immediately after using the Leica DM5000B epifluorescent microscope. Images were acquired with a Leica DFC 350FX R2 digital camera using the LAS AF V2.6.0 software.

For imaging yeast cells after IMPACT, the labelled cells were pelleted by centrifugation and potassium phosphate buffer was removed. Cells were then stained with DAPI nuclear stain by incubating the cells for 60 seconds at room temperature with 0.5µg/ml of DAPI in PBS (137 mM NaCl, 2.7 mM KCl, 10 mM Na_2HPO_4, 1.8 mM KH_2PO_4). Cells were washed with PBS and pelleted by centrifugation. Afterwards, 5 µl of cells were aspirated from the pellet, mounted onto a coverslip, and imaged immediately after using the Olympus LPS Confocal FV1000 microscope.

Chapter III – Results and discussion

III. Results and discussion

III.1. Construction of *SPO14* deletion strains

One of the aims of this work was to use the yeast model as a heterologous system to study the heterologous expression of the mammalian *PLD1* and *PLD2* genes. For this purpose, *S. cerevisiae* strains deleted in *SPO14,* the yeast ortholog of mammalian *PLD1* and *PLD2,* were developed. In order to study phenotypes associated with the deletion of *SPO14* and see if the expression of the mammalian genes could complement any of the phenotypes, construction of *SPO14* deletion strains was carried out. Briefly, an antibiotic resistance cassette is amplified by PCR with primers that contain several base pairs of homology to the upstream and downstream regions of the ORF of the gene of interest. When transformed into the desired strain, the amplified cassette will be integrated by homologous recombination into the desired locus, replacing the desired gene. To delete the *SPO14* gene from the IR07 yeast strain (Table 2), genomic DNA was extracted from strain IR04 (Table 2) and the KanMX antibiotic resistance cassette was amplified via PCR using primers primerA-spo14-del and primerD-spo14-del (Table 3). The size of the amplified cassette was confirmed by DNA gel electrophoresis using a 1 % TAE agarose gel, and images were acquired using a UV transilluminator (Genosmart, VWR) - Figure 7.

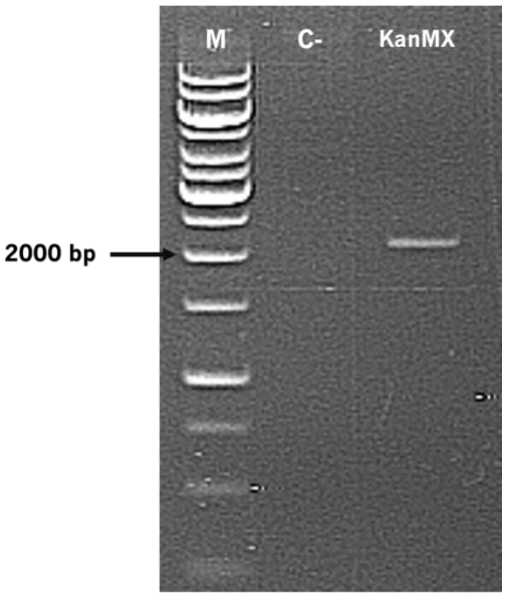

Figure 7. DNA agarose gel of the PCR amplification of KanMX cassette from strain IR04.

M represents the molecular weight marker (Thermo ScientificTM GeneRulerTM 1 kb DNA Ladder), C- represents the negative control for this PCR reaction and KanMX shows the amplified KanMX cassette (2165 bp) with primers primerA-spo14-del and primerD-spo14-del.

After confirmation of the correct size of the PCR product, the cassette was transformed into the IR07 strain (Table 2) using the LiAc/SS-DNA/PEG protocol and resulting transformants were plated into selective medium containing geneticin (200 μg/ml) to allow for selective growth of cells containing the KanMX cassette, which confers antibiotic resistance to geneticin in yeast. As a way to further select transformants with the correct integration of the KanMX cassette in the *SPO14* locus, colony PCR was performed. For this, seven isolated colonies growing in the selective medium were picked and tested using primers K3 and primerD-spo14-del (Table 3). This specific set of primers allows for confirmation of the presence of the KanMX cassette in the genome of the transformed strain, for the confirmation of the integration in the correct locus and that the cassette has been inserted in the correct orientation. The resulting samples were loaded onto a 1 % TAE agarose gel and images were acquired using a UV transilluminator (Genosmart, VWR) – Figure 8. Colonies 1 through 5 tested positive for the correct integration of the KanMX cassette in the *SPO14* locus.

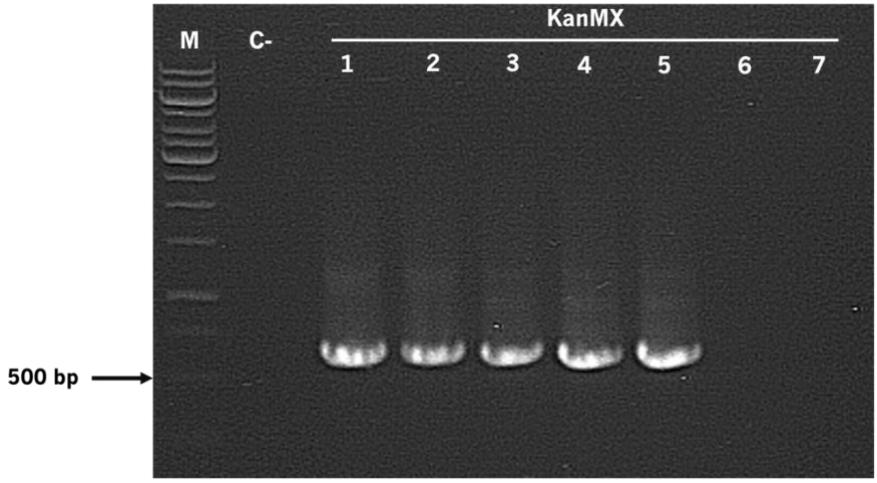

Figure 8. DNA agarose gel of the colony PCR for KanMX cassette integration in the *SPO14* locus.

M represents the molecular weight marker (Thermo Scientific™ GeneRuler™ 1 kb DNA Ladder), C- represents the negative control for this PCR reaction. Lanes 1-7 show the amplification of a fragment of the KanMX cassette (579 bp) with primers K3 and primerD-spo14-del. Colonies 1-5 show the correct integration of the KanMX cassette in the *SPO14* locus.

To allow for later studies when deletion of additional genes could be necessary and for experiments that required expression of plasmids that contained the KanMX resistance marker as well, the *SPO14* deletion strain constructed above (IR01 – Table 2) was subject to resistance marker switching. To do so, a new resistance cassette was selected -HygMX- and amplified from the pAG32 plasmid with primers 150_MX4fwd and 149_MX4rev (Table 3). The size of the amplified cassette was confirmed by

DNA gel electrophoresis using a 1 % TAE agarose gel, and images were acquired using a UV transilluminator (Genosmart, VWR) – Figure 9.

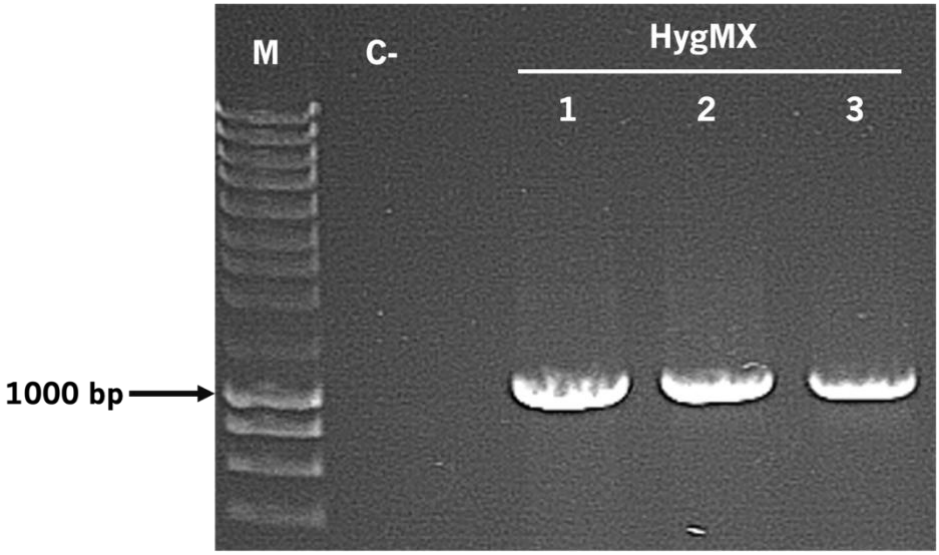

Figure 9. DNA agarose gel of the PCR amplification of HygMX cassette from pAG32.

M represents the molecular weight marker (NZYDNA Ladder III, NZYTech), C- represents the negative control for this PCR reaction. HygMX (lanes 1-3) show the amplified HygMX cassette (1128 bp) with primers 150_MX4fwd and 149_MX4rev.

After confirmation of the correct size of the PCR product, the cassette was transformed into the IR01 strain (Table 2) using the LiAc/SS-DNA/PEG protocol and resulting transformants were plated into selective medium containing hygromycin (300 μg/ml) to allow for selective growth of cells containing the HygMX cassette, which confers antibiotic resistance to hygromycin in yeast. As a way to further select transformants with the correct integration of the HygMX cassette in the *SPO14* locus, colony PCR was performed. For this, seven isolated colonies growing in the selective medium were picked and tested using primers 256_KanB and primerA-spo14-del (Table 3). This specific set of primers allows for confirmation of the presence of the HygMX cassette in the genome of the transformed strain, for the confirmation of the integration in the correct locus and that the cassette has been inserted in the correct orientation. The resulting samples were loaded onto a 1 % TAE agarose gel and images were acquired using a UV transilluminator (Genosmart, VWR) – Figure 10. All tested colonies were positive for the integration of the HygMX cassette in the *SPO14* locus.

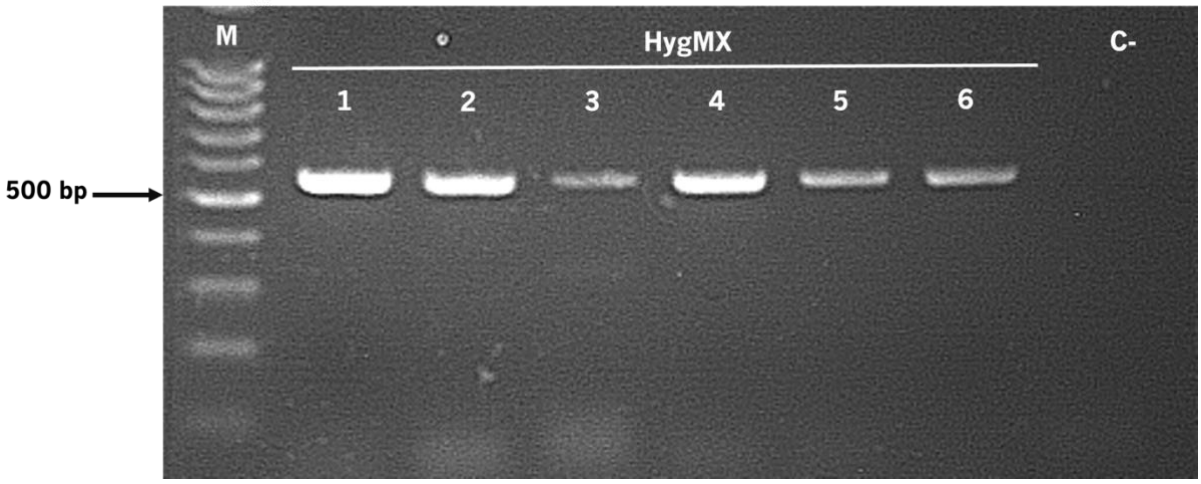

Figure 10. DNA agarose gel of the colony PCR for HygMX cassette integration in the *SPO14* locus.

M represents the molecular weight marker (Bioron 100 bp plus DNA Ladder), C- represents the negative control for this PCR reaction. Lanes 1-6 show the amplification of a fragment of the HygMX cassette (526 bp) with primers 256_KanB and primerA-spo14-del. Colonies 1-6 show the correct integration of the HygMX cassette in the *SPO14* locus.

III.2. Construction of p416_GPD-coPLD1-GFP and p416_GPD-coPLD2-GFP

The *GFP* reporter gene is a powerful genetic tool that allows for studying intracellular molecular mechanisms and events. Mainly, the GFP fluorescent protein is used to image the expression of a gene of interest inside the cell. In order to study the physical location of *PLD1* and *PLD2* when heterologously expressed in yeast, the codon-optimized mammalian genes were cloned, through the classical cloning technique, into a *GFP* carrying vector. The resulting plasmid yields a fusion of GFP at the C-terminal end of PLD1 or PLD2. Firstly, codon-optimized *PLD1* and *PLD2* were amplified from plasmids hPLD1_pUC57 and mPLD2_pCCI-4K with primers pGPD-co-hPLD1-GFP-fw plus pGPD-co-hPLD1-GFP-rv and pGPD-co-mPLD2-GFP-fw plus pGPD-co-mPLD2-GFP-rv (Table 3), respectively. The size of the amplified genes was confirmed by DNA gel electrophoresis using a 1 % TAE agarose gel, and images were acquired using a UV transilluminator (Genosmart, VWR) - Figure 11.

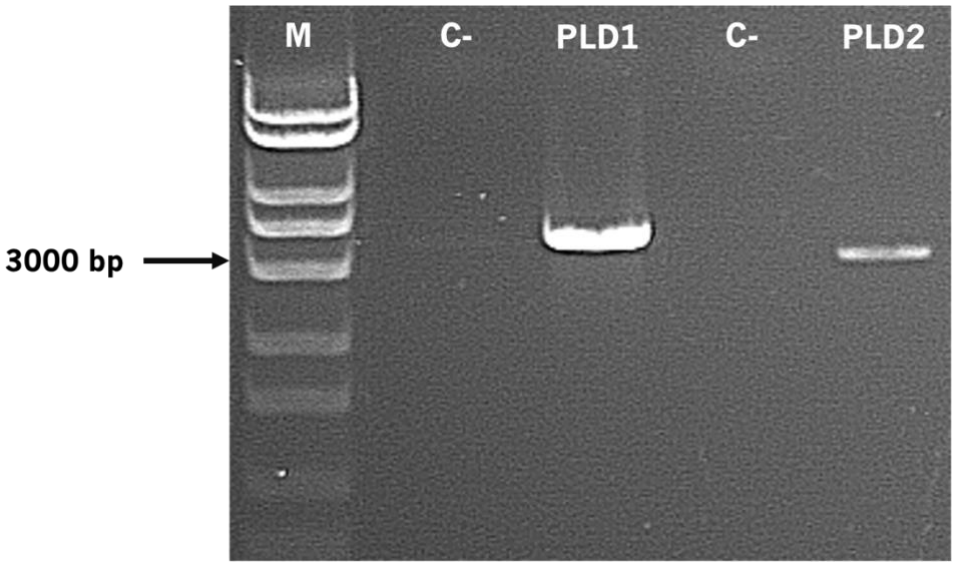

Figure 11. DNA agarose gel of the PCR amplification of codon-optimized PLD1 and PLD2 from hPLD1_pUC57 and mPLD2_PCCI-4K, respectively.

M represents the molecular weight marker (1 kb Penn State DNA Ladder), C- represents the negative control for PCR amplification of PLD1 and PLD2 respectively. PLD1 and PLD2 show the amplified PLD1 (3260 bp) and PLD2 (2873 bp) genes with primers pGPD-co-hPLD1-GFP-fw plus pGPD-co-hPLD1-GFP-rv and pGPD-co-mPLD2-GFP-fw plus pGPD-co-mPLD2-GFP-rv, respectively.

Subsequently, both amplified genes were digested with restriction endonucleases BamHI and SalI. Additionally, the plasmid vector harbouring *GFP*, p416_GPD-Jen1-GFP was also digested with restriction endonucleases BamHI and SalI and extracted from the gel, followed by purification of the vector- Figure 12.

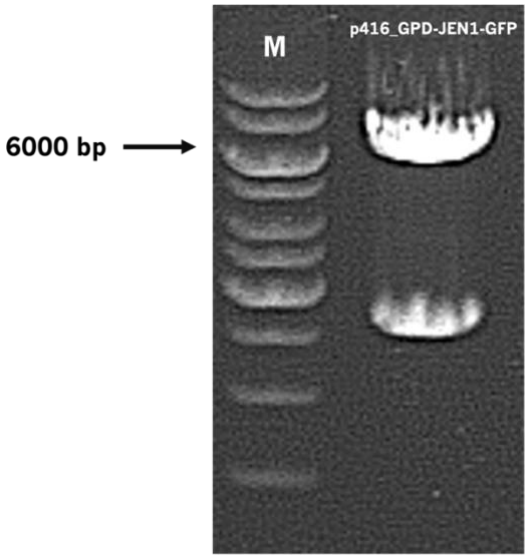

Figure 12. DNA agarose gel of the digestion of p461_GPD-JEN1-GFP with BamHI and SalI.

M represents the molecular weight marker (Thermo Scientific™ GeneRuler™ 1 kb DNA Ladder). The lane identified as p416_GPD-JEN1-GFP shows the corresponding plasmid digested with BamHI and SalI (6468 bp + 1872 bp).

The purified vector and the amplified genes were individually ligated using T4 DNA ligase and the resulting constructs (p416_GPD-coPLD1-GFP and p416_GPD-coPLD2-GFP) were transformed into chemically competent *E.coli* cells. Following transformation, cells were plated on selective media containing ampicillin (100 µg/ml). To further select transformants with the desired genetic constructs, colony PCR was performed. For this, three isolated colonies growing in the selective medium were picked and tested for each construct. PCR reaction was carried out using primers pGPD-co-hPLD1-GFP-fw and screening-hPLD1-rv for p416-coPLD1-GFP and pGPD-co-mPLD2-GFP-fw screening-mPLD2-rv for p416-coPLD2-GFP (Table 3). The resulting samples were loaded onto a 1 % TAE agarose gel and images were acquired using a UV transilluminator (Genosmart, VWR) – Figure 13. All tested colonies were confirmed to correctly harbour the respective construct by colony PCR.

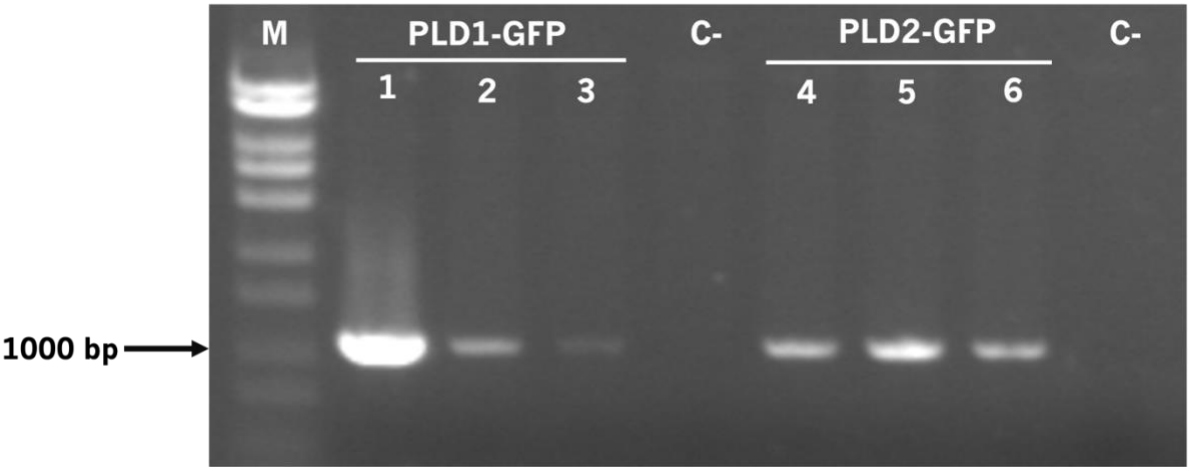

Figure 13. DNA agarose gel of the colony PCR for p416-coPLD1-GFP and p416-coPLD2-GFP.

M represents the molecular weight marker (1 kb Penn State DNA Ladder). *PLD1-GFP* (lanes 1-3) shows the amplification of a *PLD1-GFP* fragment of the p416-coPLD1-GFP vector (1073 bp) from 3 different colonies. *PLD2-GFP* (lanes 4-6) shows the amplification of a *PLD2-GFP* fragment of the p416-coPLD2-GFP vector (1078 bp) from 3 different colonies. C- represents the negative control for PCR reactions.

Two plasmid constructs were retrieved for each gene from positive colonies by miniprep plasmid DNA extraction and digested with single or double cut enzymes to check for the correct size of the plasmids after cloning. Both p416_GPD-coPLD1-GFP and p416_GPD-coPLD2-GFP were digested with XbaI or EcoRV, single and double-cut enzymes, respectively, and the resulting samples were loaded onto a 1 % TAE agarose gel and images were acquired using a UV transilluminator (Genosmart, VWR) – Figure 14.

To further confirm the correct assembly of the plasmid constructs and the correct sequence of the insert genes, *PLD1* and *PLD2*, one construct for each gene was sent to be sequenced using primers pGPD-co-hPLD1-GFP-fw and 1114_GFP-R for p416_GPD-coPLD1-GFP and pGPD-co-mPLD2-GFP-fw and 1114_GFP-R for p416_GPD-coPLD2-GFP (Table 3). Alignment results for both constructs can be found in Chapter VI – Appendices.

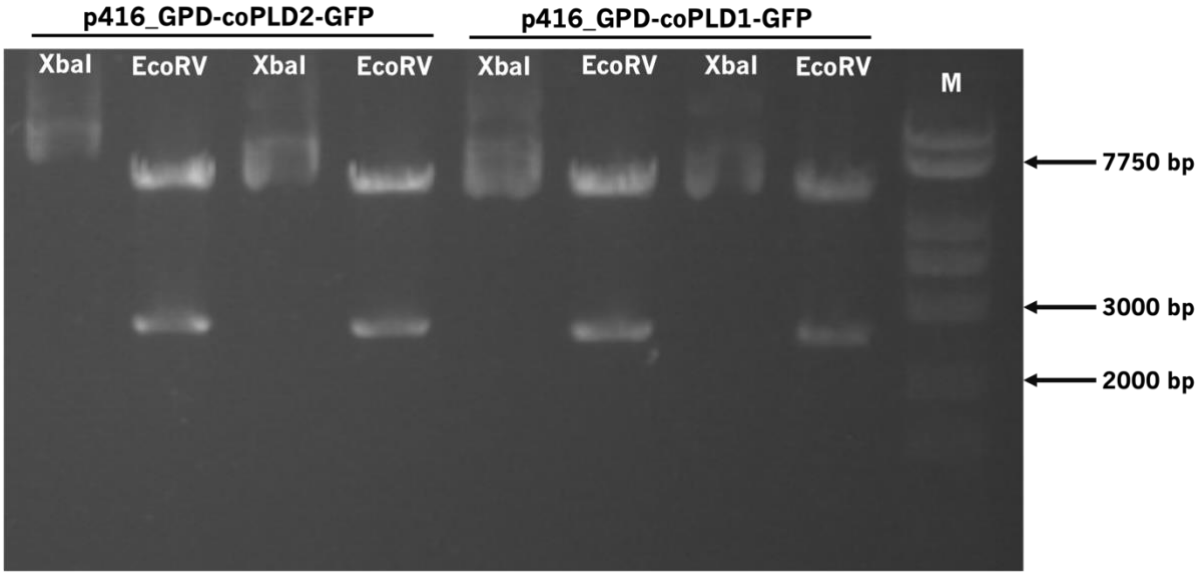

Figure 14. DNA agarose gel of the DNA fragments obtained by digestion of plasmids p461_GPD-coPLD1-GFP and p416_GPD-coPLD2-GFP with XbaI and EcoRV restriction enzymes.

M represents the molecular weight marker (1 kb Penn State DNA ladder). Lanes identified with p416_GPD-coPLD1-GFP show the corresponding extracted plasmid digested with XbaI (9714 bp), single cut enzyme and EcoRV, double cut enzyme (7302 bp + 2412 bp). Lanes identified with p416_GPD-coPLD2-GFP show the corresponding extracted plasmid digested with XbaI (9324 bp), single cut enzyme and EcoRV, double cut enzyme (6912 bp + 2412 bp).

The resulting constructs are an essential and powerful tool for any further experiments regarding the study of mammalian *PLD1* and *PLD2* using the yeast model, as they can now be expressed in any desired strain, yielding a *PLD1* and/or *PLD2* heterologous expression model in *S.cerevisiae*.

III.3. Analysis of *PLD1-GFP* and *PLD2-GFP* expression and localization by fluorescence microscopy

After the plasmid constructs for both genes were confirmed to be correctly assembled by sequencing, the previously developed *SPO14* deletion strain, IR01 (Table 2), was transformed with p416_GPD-coPLD1-GFP or p416_GPD-coPLD2-GFP. The resulting yeast strains heterologously expressing the codon-optimized mammalian *PLD1* and *PLD2* genes were evaluated for localization of *PLD1-GFP* and *PLD2-GFP* through fluorescence microscopy – Figure 15.

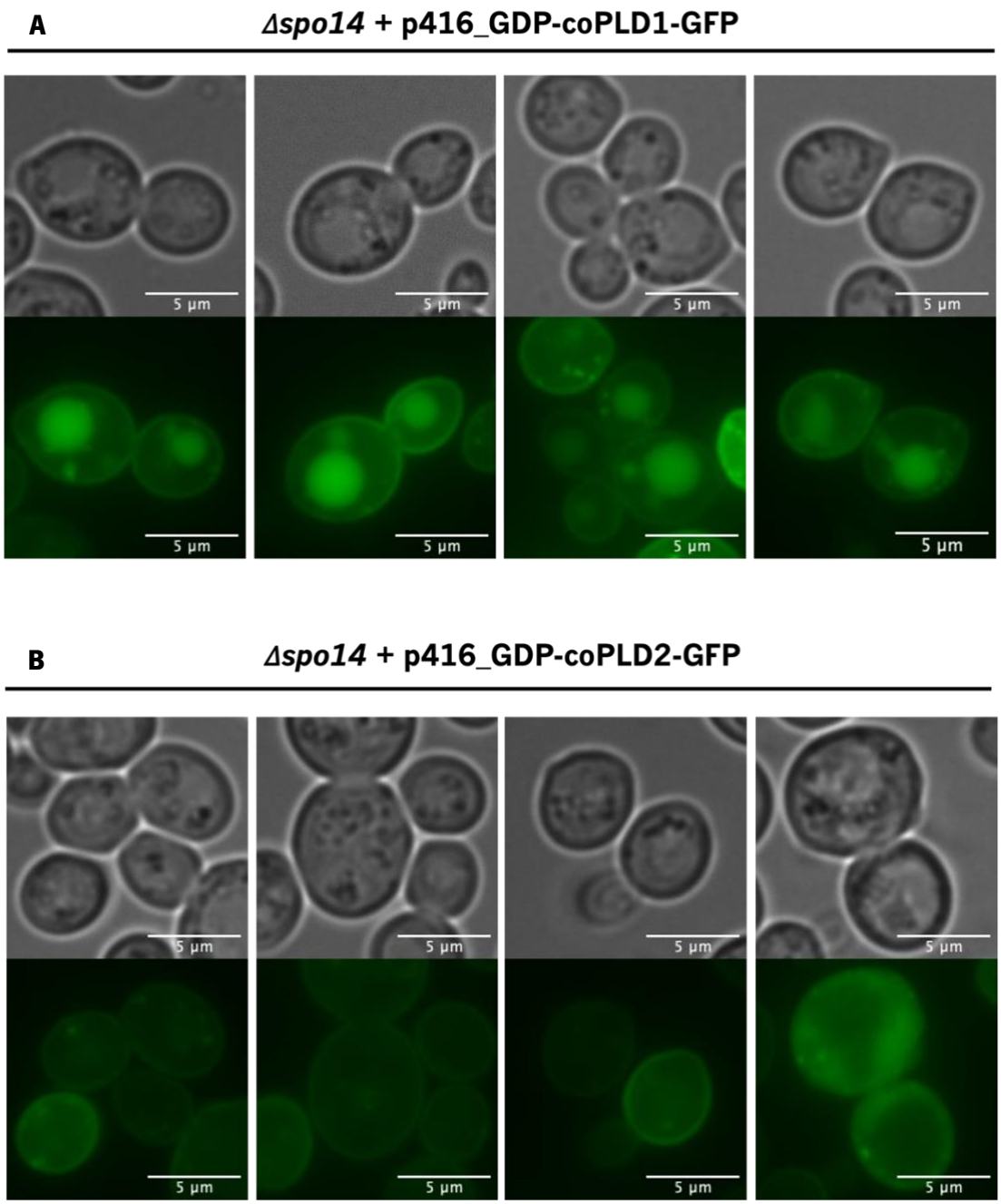

Figure 15. Analysis of PLD1-GFP (A) and PLD2-GFP (B) expression and localization by fluorescence microscopy.

Yeast Δ*spo14* cells carrying p416_GPD-coPLD1-GFP or p416_GPD-coPLD2-GFP plasmids were grown on selective SC-ura plates. Biomass was collected and diluted in water. A volume of 5 µL of cells was instantly visualized using Leica DM5000B epifluorescent microscope with appropriate filters.

In mammals, *PLD1* and *PLD2* expression can be found in different locations of the intracellular environment. PLD1 is usually found at intracellular compartments such as the Golgi complex, the endosome, the lysosome and the endoplasmic reticulum and at the plasma membrane, and exocytotic vesicles, whilst PLD2 localizes mainly in the vicinity of the plasma membrane [60] and in the Golgi complex [61,62]. In yeast, Spo14 is usually found throughout the cytoplasm and relocates to the prospore membrane when yeast cells undergo meiosis [128,132]. In this work, fluorescent microscopy of the yeast strains overexpressing the mammalian codon-optimized *PLD1* or *PLD2* seems to also reveal a difference in the intracellular localization of *PLD1-GFP* (Figure 15-A) and *PLD2-GFP* (Figure 15-B). Both *PLD1-GFP* and *PLD2-GFP* show expression at the plasma membrane, replicating what has been reported to be their location in mammalian organisms [64,158]. *PLD1-GFP* shows strong fluorescence in the vacuole. Vacuoles, like lysosomes, are the cell primary organ for digestion and degradation of cell components such as proteins and lipids. Both organelles are similarly involved in autophagy, an important mechanism that maintains cell homeostasis by inducing clearing of damaged cell organelles and toxic products, as well as being an energy retrieval mechanism used when cells experience glucose starvation [159]. Importantly, PLD1 appears to have a regulatory role in autophagy, specifically in the clearance of protein aggregates [160] and in the promotion of cancer cell death [161]. Additionally, both *PLD-GFP* fusions seem to be strongly expressed in what appear to be vesicles throughout the cell, which could potentially be endosomes. This again appears to be mimicking the endosomal localization reported for PLD1 and PLD2 in mammals [61–64]. This is of course speculative and further co-localization studies with organelle-specific stains will be necessary for a clear description of the intracellular localization of overexpressed *PLD1-GFP* and *PLD2-GFP*.

III.4. Genomic integration of codon-optimized *PLD1* and *PLD2* in the *SPO14* locus of a mutant strain

Heterologous expression of a gene of interest via a plasmid construct is a powerful tool for genetic engineering in yeast. However, despite its easy applicability and quick protocol, plasmid gene expression lacks stability as a plasmid can easily be lost if the antibiotic or auxotrophic selection is removed. A chromosomally integrated gene is not subject to this instability. Additionally, genomic integration allows for stable expression and long-term maintenance of the gene of interest in the transformed cells and their progeny. In order to integrate codon-optimized mammalian *PLD1* and *PLD2* in the yeast genome, the CRISPR Cas9 editing tool was used. For this, a technique developed by

Generoso *et al.*, [153] was used, whereby a single plasmid (pRCC-K) carries the Cas9 DNA endonuclease and the guide RNA (gRNA) sequence that guides the enzyme to its intended cutting site in the genome. The pRCC-K plasmid was amplified in three parts in order to insert the gRNA sequence needed to direct the Cas9 endonuclease to the HygMX cassette used to delete *SPO14*: the first fragment was amplified with primers gRNA_HygMX4-FW and 253_KanC3 (Table 3), the second fragment was amplified with primers 473_MSW_rev and 576_pBR322_2 (Table 3), and the third fragment was amplified with primers 196_pMEC_MX4_fwd and gRNA_HygMX4-RV (Table 3) - Figure 16.

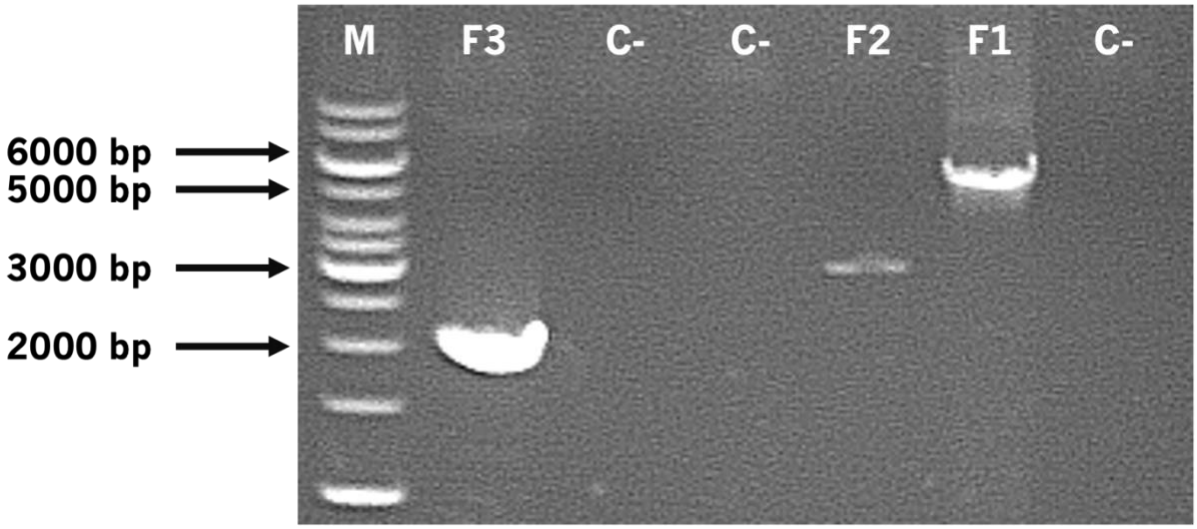

Figure 16. DNA agarose gel of the PCR amplification of the pRCC-K plasmid in three fragments.

M represents the molecular weight marker (Thermo Scientific™ GeneRuler™ 1 kb DNA Ladder), C- represents the negative control for PCR amplification of each fragment. F3 shows the amplification of fragment 3 of the plasmid with primers 196_pMEC_MX4_fwd and gRNA_HygMX4-RV (2068 bp). F2 shows the amplification of fragment 2 of the plasmid with primers 473_MSW_rev and 576_pBR322_2 (3020 bp). F1 shows the amplification of fragment one of the plasmid with primers gRNA_HygMX4-FW and 253_KanC3 (5315 bp).

Following amplification, all three fragments of the pRCC-K plasmid were subjected to enzymatic digestion with DpnI to get rid of any remaining template plasmid in the resulting PCR products. After digestion, the Gibson assembly technique was used to ligate all three fragments, generating pRCC-K_gRNA-HygMX. Chemically competent *E.coli* cells were transformed with the newly developed plasmid. Cells were grown overnight at 37 °C on selective media containing ampicillin (100 µg/ml). Subsequently, plasmid DNA was extracted via Miniprep. Additionally, *PLD1* and *PLD2* were amplified by PCR from hPLD1_pUC57 and mPLD2_pCCI-4K respectively, with primers Long-up-SPO14-hPLD1-FW and Long-down-SPO14-hPLD1-RV for *PLD1* and Long-up-SPO14-mPLD2-FW and Long-down-SPO14-

mPLD2-RV (Table 3) for *PLD2* - Figure 17. This amplification results in a DNA product containing *PLD1* or *PLD2* flanked on each side by a 50 base pair sequence homologous to the genomic regions before and after the *SPO14* locus, allowing for the integration of the genes through homologous recombination after cleavage by the Cas9 enzyme. These products will henceforth be mentioned as donors.

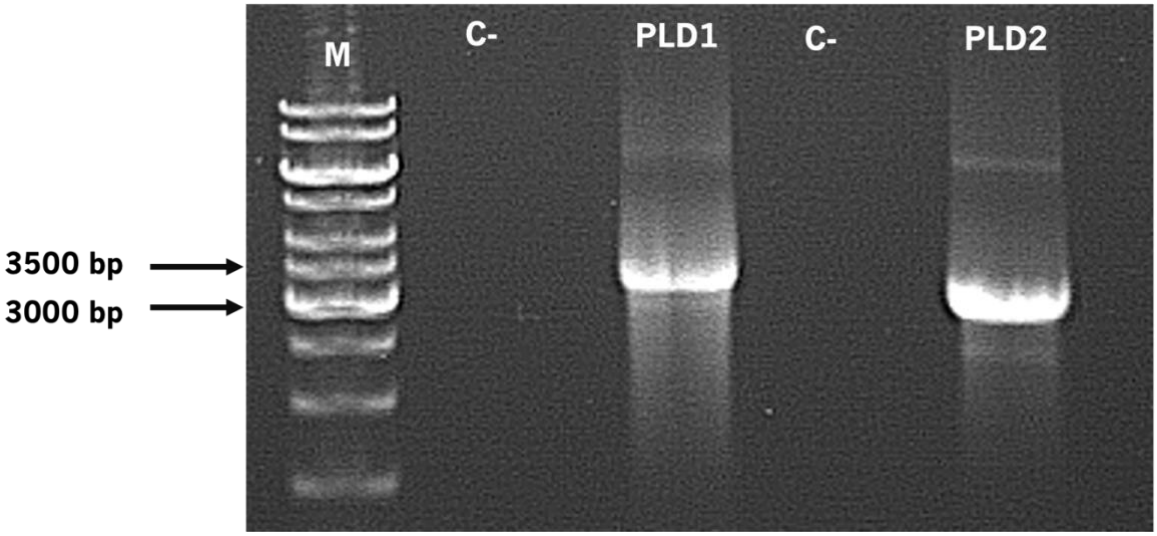

Figure 17. DNA agarose gel of the PCR amplification of codon optimized *PLD1* and *PLD2* from hPLD1_pUC57 and mPLD2_PCCI-4K, respectively.

M represents the molecular weight marker (Thermo Scientific™ GeneRuler™ 1 kb DNA Ladder), C- represents the negative control for PCR amplification of *PLD1* and *PLD2* respectively. PLD1 and PLD2 show the amplified *PLD1* (3423 bp) and *PLD2* (3033 bp) genes with primers Long-up-SPO14-hPLD1-FW plus Long-down-SPO14-hPLD1-RV and Long-up-SPO14-mPLD2-FW plus Long-down-SPO14-mPLD2-RV for PLD2, respectively.

After amplification of *PLD1* and *PLD2*, both pRCC-K_gRNA-HygMX and donor *PLD1* or *PLD2* were transformed into the *SPO14* deletion strain IR10 (Table 2). The resulting transformants were plated on selective media containing geneticin (200 μg/ml) and allowed to grow at 30 °C until isolated colonies were visible. Once isolated colonies were visible, cells were replica plated into selective plates containing hygromycin (300 μg/ml) and geneticin (200 μg/ml). Colonies that did not grow after replica plating were selected from the original plates containing only geneticin (200 μg/ml) for colony PCR. The colony PCR reaction was carried out using primers screening-down-SPO14-rv and screening-hPLD1-fw for *PLD1* and screening-down-SPO14-rv and screening-mPLD2-fw for *PLD2*. The resulting samples were loaded onto a 1 % TAE agarose gel and images were acquired using a UV transilluminator (Genosmart, VWR) – Figure 13. All tested colonies were confirmed to correctly harbour the respective construct by colony PCR.

Two positive colonies were found for the correct integration of *PLD1* in the *SPO14* locus (Figure 18- colonies 1 and 2), however, no positive transformants were found for the integration of *PLD2*. Integration of *PLD2* in the yeast genome will be attempted again and the sporulation and meiosis efficiency of these strains stably expression the mammalian genes will be evaluated.

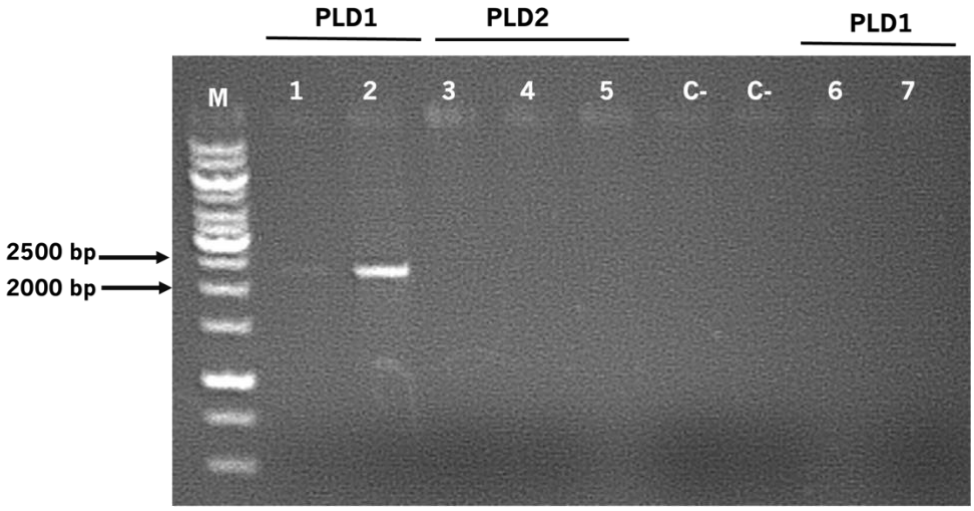

Figure 18. DNA agarose gel of the colony PCR for genomic integration of PLD1 and PLD2 in the yeast genome.

M represents the molecular weight marker (Thermo Scientific™ GeneRuler™ 1 kb DNA Ladder). PLD1 (lanes 1-2 and 6-7) shows the amplification of a part of the *PLD1* gene from the yeast genome (2324 bp) from four different colonies. PLD2 (lanes 3-5) shows the amplification of a part of the *PLD2* gene from the yeast genome from three different colonies. C- represents the negative controls of the PCR reactions for the amplification of *PLD1* or *PLD2*, respectively.

III.5. Imaging of mammalian PLD1 and PLD2 activity in *S. cerevisiae*

The IMPACT (**Im**aging **P**hospholipase D **A**ctivity with **C**lickable Alcohols via **T**ransphosphatidylation) protocol allows for imaging of phospholipase D activity with clickable alcohols via transphosphatydilation. This method is based on the promiscuity of PLD enzymes, which, in addition to using water for phospholipid hydrolysis, can also accept a variety of primary alcohols in a transphosphatidylation reaction. Tagging the resultant lipids with fluorescent reporters via click chemistry reactions results in fluorescent lipids that act as reporters of PLD activity. In order to image and compare phospholipase D activity in the different constructed strains, the IMPACT protocol was applied. Briefly, a wild type strain (IR17), a *SPO14* deletion strain (IR01) and both strains expressing *PLD1-GFP* or *PLD2-GFP* (IR71 and IR74, respectively) (Table 2) were subject to IMPACT labelling and

stored. Immediately before imaging, labelled cells were treated with DAPI DNA stain and imaged by confocal microscopy - Figure 18.

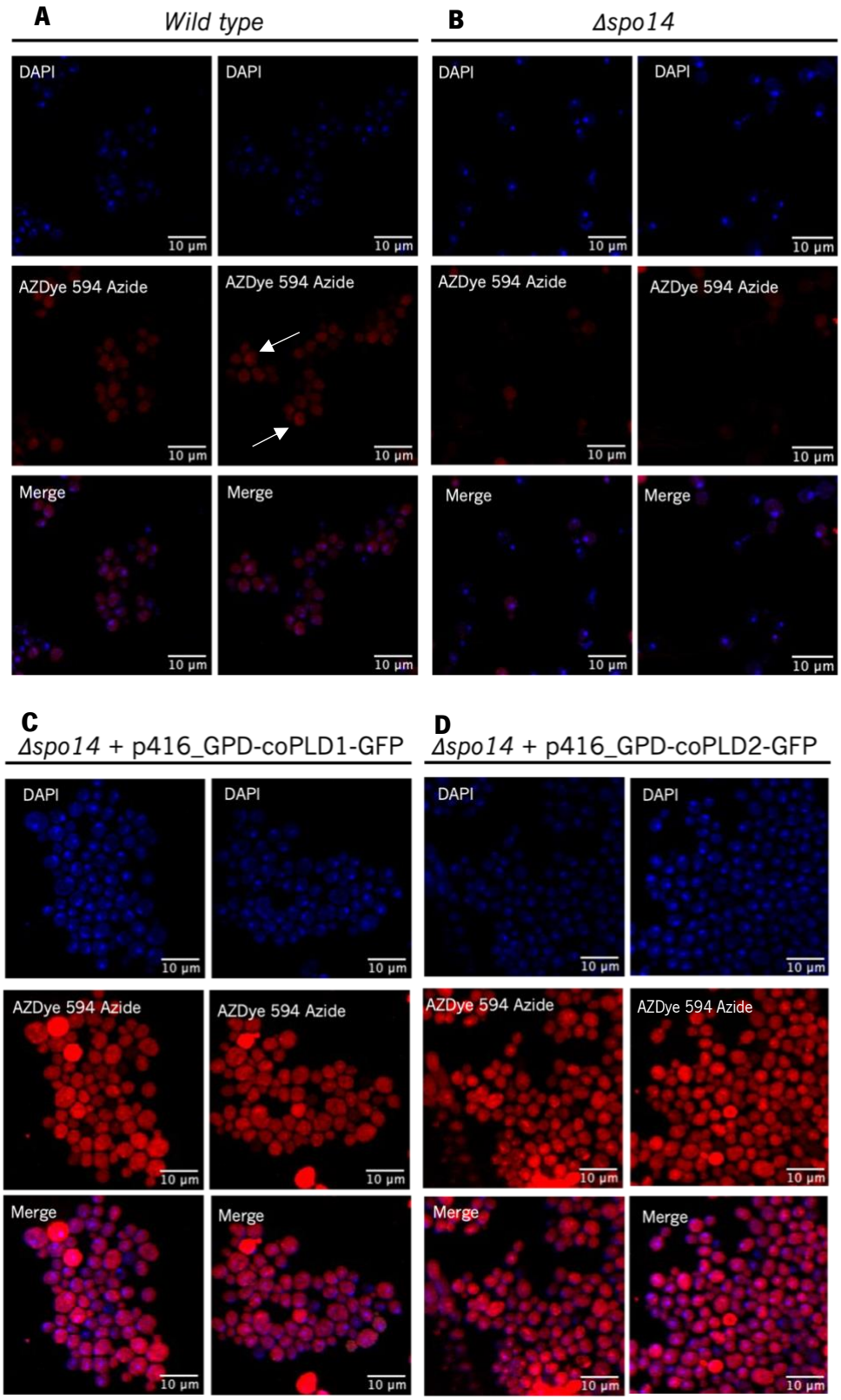

Figure 19. Analysis of PLD activity by confocal microscopy.

Yeast wild type (A), Δspo14 (B) and Δspo14 cells carrying p416_GPD-coPLD1-GFP (C) or p416_GPD-coPLD2-GFP (D) plasmids were labelled by IMPACT protocol. Immediately prior to confocal microscopy, cells were stained with DAPI. A volume of 5 µL of cells for each strain was instantly visualized using Olympus LPS Confocal FV1000 microscope with appropriate filters.

The Alexa Fluor derived AZDYE 594 azide, a red fluorescent marker, was used to report on PLD activity whilst the blue stain DAPI was used to fluorescently tag the nucleus. In the wild type strain (Figure 19-A), basal levels of PLD activity in red can be observed. PLD activity related fluorescence can be seen throughout the cell, with some cells showing high IMPACT-derived fluorescence in certain regions of the intracellular space (Figure 19-A, marked by white arrows). This signal is likely to be ER-associated given its proximity to the nucleus and the previous results using IMPACT to study active PLD location inside the cell [162,163]. Overall, for this strain, the level of PLD-activity derived fluorescence is according to what would be expected for wild type cells. It would be interesting, however, to examine whether this activity could be altered by exposure to known PLD1 and PLD2 stimulants and inhibitors in mammal cells. In the *SPO14* deletion strain (Figure19-B), little to no PLD-activity derived fluorescence can be observed. Given that *SPO14* is the only reported source of canonical phospholipase D activity in yeast, this would be expected. Additionally, this result is a positive indicator of the correct construction of the *SPO14* deletion strain used in this assay (IR01 - Table 2). As for the *PLD1* (Figure 19-C) and *PLD2* (Figure 19-D) expressing strains, functional expression of the mammalian PLDs through a plasmid vector results in higher PLD activity in yeast in both strains. This is expected, as increasing the copy number of a gene, in this case, compared to the wild type strain, yields higher expression and consequently activity of the said gene. This assay report directly on PLD-derived PA production. The fact that the IMPACT protocol resulted in such a clear difference in strains harbouring heterologous *PLD1* and *PLD2* reveals the correct performance of these enzymes when expressed in yeast. This is a good indicator of the validity of these tools for future projects.

This experiment was performed with the constructed strains harbouring the *PLD1* or *PLD2* carrying plasmids, which result in overexpression of both genes due to the nature of the expression method used. Despite resulting in expression levels and consequently activity levels that are not necessarily similar to what is to be expected for the expression of these genes in basal conditions, the plasmid constructs harbouring the mammalian *PLD1* and *PLD2* worked well in this assay. Using these constructs, resulted in a clear difference in PLD activity related fluorescence between the wild type, the SPO14 deletion strain and the strains harbouring the constructs. This difference between strains, allows for clear separation of the phenotypes which not only proves the strength of the developed yeast-based tools, but also confirms the correct optimization and application of this assay. Ideally, this experiment should also be performed using the strains expressing *PLD1* or *PLD2* via genomic integration, to elucidate possible differences in expression levels at naturally occurring, basal conditions.

III.6. Growth assays: Evaluation of C16:PAF sensitivity

A previous study by Kennedy *et al.*, [124] reported that the absence of the *SPO14* gene renders yeast cells more sensitive to C16:PAF, a glycerolipid with a function in platelet aggregation during inflammation response. This lipid has previously been associated with AD in different molecular contexts, and its metabolism was found to be disrupted in the posterior/entorhinal cortex of the brains of patients with AD. In mice, a similar disruption was found following a pathogenic increase of the cortical ratio between $A\beta_{42}$ and $A\beta_{40}$. Acute elevation of C16:PAF was also reported to be a signal for tau hyperphosphorylation [164,165].

Given the previously mentioned importance of C16:PAF for AD and the study that reported a link between PLD1 and C16:PAF [124], we set to perform a growth assay to determine if the expression of the mammalian *PLD1* or *PLD2* could complement the growth phenotype of a *SPO14* deletion mutant. Evaluation of growth phenotypes by growth assays is a quick, simple and easily scalable tool to study the sensitivity of desired strains to relevant molecules and compounds or to unravel possible gene interactions.

A wild type yeast strain (IR78), a wild type yeast strain carrying the empty p416-GDP vector (IR77), a *SPO14* deletion strain (IR23) and the *SPO14* deletion strains carrying p416_GPD-coPLD1-GFP (IR71) or p416_GPD-coPLD2-GFP (IR74) (Table 2) were grown, in serial dilutions, on SC-ura media containing different concentrations of C16:PAF – Figure 19.

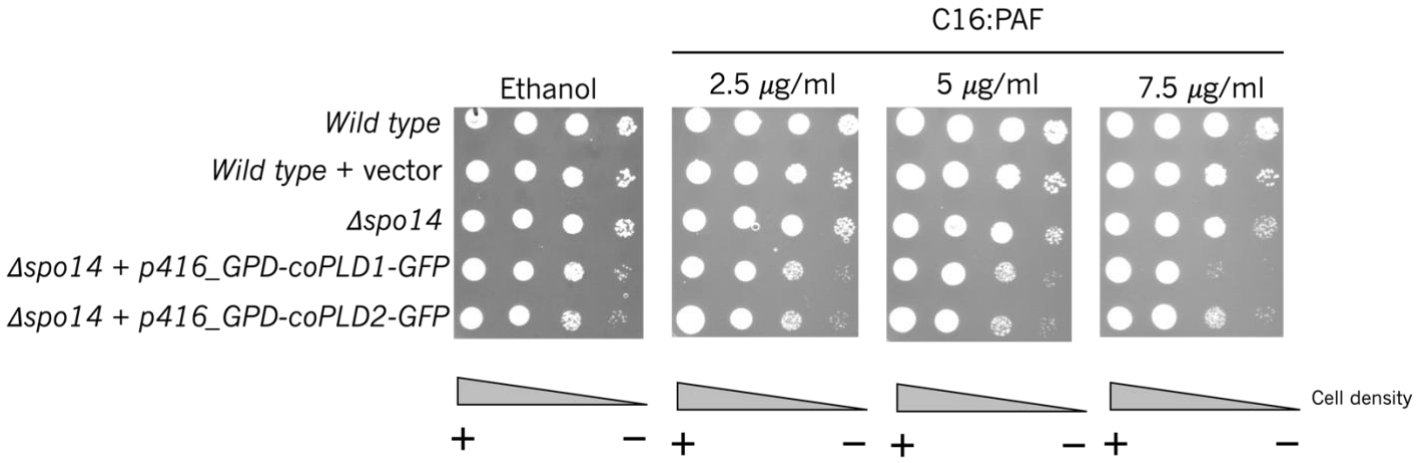

Figure 20. Growth phenotypes of serial dilutions to 10^{-4} of wild type, wild type + vector, Δspo14 and Δspo14 cells carrying p416_GPD-coPLD1-GFP or p416_GPD-coPLD2-GFP.

Cells are plated in SC-ura media containing different dilutions of C16:PAF (2.5 μg/ml, 5 μg/ml or 7.5 μg/ml) and 0.4 % ethanol as a control for the C16:PAF vehicle**.** The different concentrations of the lipid were chosen as per the previously mentioned paper were the C16:PAF sensitivity phenotype was reported [124]. Experiments were performed in triplicate.

The growth phenotype of a wild type strain, the *SPO14* deletion mutant and the *SPO14* deletion strains expressing the plasmid constructs harbouring the codon-optimized PLD1 or PLD2 was evaluated when exposed to increasing concentrations (2.5 μg/ml, 5 μg/ml or 7.5 μg/ml) of C16:PAF -Figure 19. Kennedy and co-workers [124] described that *Δspo14* cells were sensitive to C16:PAF in concentrations as low as 2.5 μg/ml (in YPD media) and 5 μg/ml (in SD-Leu media). We observed that cells lacking *SPO14* do not display a significant difference in sensitivity to C16:PAF when compared with the wild type cells and the wild type cells harbouring the empty vector (Figure 19, first three rows of panels 2 through 4). This is in contrast with what has been described by Kennedy, *et al.*, [124]. However, it is important to note that the backgrounds of the *SPO14* deletion strain used in the Kennedy *et al.*, and in this assay are different (SC288c and W303, respectively). This factor may influence the behaviour of the strains in the growth assay. All other relevant growth conditions were maintained, including the carbon source (2 % glucose) as well as the incubation time and temperature (2 days at 30 °C). Although we could not replicate this phenotype, a difference between the growth of the deletions strains harbouring p416_GPD-coPLD1-GFP or p416_GPD-coPLD2-GFP could be observed, with the first appearing more sensitive to the toxic lipid compound. The apparent higher resistance of cells overexpressing mammalian PLD2 is an interesting finding, given the relationship between C16:PAF and amyloid-beta toxicity [155,156], since PLD2 has also been strongly linked to amyloid-beta toxicity in the context of AD [122]. Ideally, this growth assay should be repeated with any other available *SPO14* deletion strains given the discrepancy between these results and what has been published regarding the sensitivity of *SPO14* deletion mutants to C16:PAF. Additionally, further controls should be included, such as the *SPO14* deletion strain carrying the empty plasmid vector. Given the preferential affinity of PLD to primary alcohols, the dilution of the lipid molecule in different solvents should also be tested to exclude the possibility that any of the visible phenotypes could be due to a decrease in PLD-derived PA availability instead of the C16:PAF itself. Another aspect to consider is the mode of expression of the mammalian genes. In this case, despite the low copy number nature of the chosen vector (p416-GPD), overexpression of *PLD1-GFP* and *PLD2-GFP* will always occur. In yeast, plasmid burden has been characterized and shown to result in defects for the growth phenotype in most cases [166]. Therefore, and ideally, the C16:PAF sensitivity growth assay should be repeated using strains with genomic integration of *PLD1* and *PLD2*.

Chapter IV – Final remarks and future perspectives

IV. Final remarks and future perspectives

The implication of PLD1 and PLD2 in cell homeostasis is clear. Dysregulation of the mechanisms surrounding the normal function of these enzymes has been implicated in a series of pathologies, including, but not limited to, neurodegenerative diseases such as AD. Importantly, AD is a progressive neurodegenerative disorder and is currently the sixth-leading cause of death and accounts as the cause for 60 to 80% of all cases of dementia [167]. With the World Health Organization (WHO) estimating a 40 % increase in AD and dementia-related deaths until 2030, the full understanding of the mechanisms behind this pathology is more needed than ever. Although higher mammalian models such as rodents and primates are most commonly used to study AD, the study of the underlying mechanisms and pathways at the molecular level requires extensive genetic manipulation and screening. This is more easily achieved in simpler research model organisms such as the yeast *S. cerevisiae.* Additionally, yeast research is not subject to the same ethical barriers encountered when higher mammalian model organisms are used. In fact *S. cerevisiae* has been successfully used a model to study the role of another mammalian protein that is extremely relevant for AD - Apolipoprotein E4 (ApoE4). Studies in yeast uncovered the impact of ApoE4 expression, the biggest genetic risk factor for AD, in the dysregulation of specific pathways associated with lipid metabolism [141]. This work establishes the use of yeast as model organism to study genotype-to-phenotype relationships in the context of AD.

In this work, a set of yeast-based tools was developed to further research the role of PLD1 and PLD2 in pathologies such as AD. A good indicator of the possible validity of these tools is the fluorescent microscopy of the yeast strains expressing the GFP-tagged PLDs, revealing that mammalian PLD1 and PLD2 appear to maintain their subcellular localization from what has been described in mammals. Despite the limitations of plasmid based gene overexpression, the plasmid constructs developed in this work are an excellent and versatile tool that can be used in several ways in multiple different strains, to provide valuable information PLD1 and PLD2. Additionally, the optimization and application of an IMPACT protocol to the strains heterologously expressing the codon-optimized mammalian *PLD1* and *PLD2* sets a precedent for future application of the method in various strains of interest and different relevant research models such as cell lines and mammals such as rodents.

Although very similar in structure and basic enzymatic function, PLD1 and PLD2 have been differently implicated in AD pathology. The codon-optimized mammalian *PLD1* and *PLD2* genes, the

PLD1-GFP and *PLD2-GFP* carrying plasmids and the strains expressing mammalian *PLD1* and *PLD2* in the genome will help unravel the molecular pathways surrounding PLD activity by investigating new genetic interactions and potential regulators of mammalian PLD activity at the cellular level, using yeast, a powerful eukaryotic system for heterologous expression which is easy to grow and genetically manipulate. Ideally, in the future, these strains will be used to perform drug screening as they are a powerful model for screening of drugs that interact with these two mammalian enzymes or modulate their activity. Any candidate targets that might be found by drug screening in yeast would then be tested in higher models relevant for the pathology, such as human induced pluripotent stem cells from AD patients and, additionally, rodent models. Ultimately, the hope is to find new therapeutic strategies for AD using the yeast model as a starting point.

Chapter V - References

V. References

[1] **Nelson, D.L. and Cox, M.M.** (2009) Lehninger Principles of Biochemistry. W.H Freeman, New York.

[2] **Van Meer, G., Voelker, D.R., and Feigenson, G.W.** (2008) Membrane lipids: Where they are and how they behave. *Nature Reviews Molecular Cell Biology*. 9 (2), 112–124.

[3] **Sud, M., Fahy, E., Cotter, D., Brown, A., Dennis, E.A., Glass, C.K., et al.** (2007) LMSD: LIPID MAPS structure database. *Nucleic Acids Research*. 35 (SUPPL. 1), S527–S532.

[4] **Fahy, E., Subramaniam, S., Murphy, R.C., Nishijima, M., Raetz, C.R.H., Shimizu, T., et al.** (2009) Update of the LIPID MAPS comprehensive classification system for lipids. *Journal of Lipid Research*. 50 (SUPPL.), S9–S14.

[5] **Miranda, A.M. and Oliveira, T.G.** (2015) Lipids under stress - A lipidomic approach for the study of mood disorders. *BioEssays*. 37 (11), 1226–1235.

[6] **Diehl, K.L., Ivy, M.A., Rabidoux, S., Petry, S.M., Müller, G., and Anslyn, E. V.** (2015) Differential sensing for the regio- and stereoselective identification and quantitation of glycerides. *Proceedings of the National Academy of Sciences of the United States of America*. 112 (30), E3977–E3986.

[7] **Vill, V. and Hashim, R.** (2002) Carbohydrate liquid crystals: Structure - Property relationship of thermotropic and lyotropic glycolipids. *Current Opinion in Colloid and Interface Science*. 7 (5–6), 395–409.

[8] **Dufourc, E.J.** (2008) Sterols and membrane dynamics. *Journal of Chemical Biology*. 1 (1–4), 63–77.

[9] **Harayama, T. and Riezman, H.** (2018) Understanding the diversity of membrane lipid composition. *Nature Reviews Molecular Cell Biology*. 19 (5), 281–296.

[10] **Futerman, A.H. and Hannun, Y.A.** (2004) The complex life of simple sphingolipids. *EMBO Reports*. 5 (8), 777–782.

[11] **Courtney, K.C., Pezeshkian, W., Raghupathy, R., Zhang, C., Darbyson, A., Ipsen, J.H., et al.** (2018) C24 Sphingolipids Govern the Transbilayer Asymmetry of Cholesterol and Lateral Organization of Model and Live-Cell Plasma Membranes. *Cell Reports*. 24 (4), 1037–1049.

[12] **Slotte, J.P. and Ramstedt, B.** (2007) The functional role of sphingomyelin in cell membranes. in: Eur. J. Lipid Sci. Technol., pp. 977–981.

[13] **Schneider, N., Hauser, J., Oliveira, M., Cazaubon, E., Mottaz, S.C., O'Neill, B. V., et al.** (2019) Sphingomyelin in brain and cognitive development: Preliminary data. *ENeuro*. 6 (4), 1–13.

[14] **Emoto, K., Kobayashi, T., Yamaji, A., Aizawa, H., Yahara, I., Inoue, K., et al.** (1996) Redistribution of phosphatidylethanolamine at the cleavage furrow of dividing cells during cytokinesis. *Proceedings of the National Academy of Sciences of the United States of America*. 93 (23), 12867–12872.

[15] **Stafford, J.H. and Thorpe, P.E.** (2011) Increased exposure of phosphatidylethanolamine on the surface of tumor vascular endothelium. *Neoplasia*. 13 (4), 299–308.

[16] **Fadok, V.A., Voelker, D.R., Campbell, P.A., Cohen, J.J., Bratton, D.L., and Henson, P.M.** (1992) Exposure of phosphatidylserine on the surface of apoptotic lymphocytes triggers specific recognition and removal by macrophages. *Journal of Immunology (Baltimore, Md. : 1950)*. 148 (7), 2207–16.

[17] **Shewan, A., Eastburn, D.J., and Mostov, K.** (2011) Phosphoinositides in cell architecture. *Cold Spring*

Harbor Perspectives in Biology. 3 (8), 1–17.

[18] **Raghu, P., Joseph, A., Krishnan, H., Singh, P., and Saha, S.** (2019) Phosphoinositides: Regulators of Nervous System Function in Health and Disease. *Frontiers in Molecular Neuroscience*. 12.

[19] **Phan, T.K., Williams, S.A., Bindra, G.K., Lay, F.T., Poon, I.K.H., and Hulett, M.D.** (2019) Phosphoinositides: multipurpose cellular lipids with emerging roles in cell death. *Cell Death and Differentiation*. 26 (5), 781–793.

[20] **Kim, S.C. and Wang, X.** (2020) Phosphatidic acid: An emerging versatile class of cellular mediators. *Essays in Biochemistry*. 64 (3), 533–546.

[21] **Raben, D.M. and Barber, C.N.** (2017) Phosphatidic acid and neurotransmission. *Advances in Biological Regulation*. 63 15–21.

[22] **Bai, J., Hu, Z., Dittman, J.S., Pym, E.C.G., and Kaplan, J.M.** (2010) Endophilin functions as a membrane-bending molecule and is delivered to endocytic zones by exocytosis. *Cell*. 143 (3), 430–441.

[23] **Cermenati, G., Mitro, N., Audano, M., Melcangi, R.C., Crestani, M., De Fabiani, E., et al.** (2015) Lipids in the nervous system: From biochemistry and molecular biology to patho-physiology. *Biochimica et Biophysica Acta - Molecular and Cell Biology of Lipids*. 1851 (1), 51–60.

[24] **Piomelli, D., Astarita, G., and Rapaka, R.** (2007) A neuroscientist's guide to lipidomics. *Nature Reviews Neuroscience*. 8 (10), 743–754.

[25] **Di Paolo, G. and Kim, T.W.** (2011) Linking lipids to Alzheimer's disease: Cholesterol and beyond. *Nature Reviews Neuroscience*. 12 (5), 284–296.

[26] **Ruipérez, V., Darios, F., and Davletov, B.** (2010) Alpha-synuclein, lipids and Parkinson's disease. *Progress in Lipid Research*. 49 (4), 420–428.

[27] **Ingre, C., Chen, L., Zhan, Y., Termorshuizen, J., Yin, L., and Fang, F.** (2020) Lipids, apolipoproteins, and prognosis of amyotrophic lateral sclerosis. *Neurology*. 94 (17), E1835–E1844.

[28] **Pineda-Torra, I., Siddique, S., Waddington, K.E., Farrell, R., and Jury, E.C.** (2021) Disrupted Lipid Metabolism in Multiple Sclerosis: A Role for Liver X Receptors? *Frontiers in Endocrinology*. 12.

[29] **Tappia, P.S. and Dhalla, N.S.** (2014) Phospholipases in health and disease. Springer, New York.

[30] **Vance, D.E. and Vance, J.E., Eds.** (1991) New Comprehensive Biochemistry. Elsevier, New York.

[31] **Inoue, K., Arai, H., and Aoki, J.** (2005) Phospholipase A1 Structures, Physiological and Patho-physiological Roles in Mammals. in: Lipases Phospholipases Drug Dev., pp. 23–39.

[32] **Stahelin, R. V.** (2016) Phospholipid Catabolism. in: Biochem. Lipids, Lipoproteins Membr. Sixth Ed., pp. 237–257.

[33] **Dennis, E.A., Cao, J., Hsu, Y.H., Magrioti, V., and Kokotos, G.** (2011) Phospholipase A2 enzymes: Physical structure, biological function, disease implication, chemical inhibition, and therapeutic intervention. *Chemical Reviews*. 111 (10), 6130–6185.

[34] **Chen, S.C.A., Wright, L.C., Santangelo, R.T., Muller, M., Moran, V.R., Kuchel, P.W., et al.** (1997) Identification of extracellular phospholipase B, lysophospholipase, and acyltransferase produced by Cryptococcus neoformans. *Infection and Immunity*. 65 (2), 405–411.

[35] **Nakamura, Y. and Fukami, K.** (2017) Regulation and physiological functions of mammalian phospholipase C. *Journal of Biochemistry*. 161 (4), 315–321.

[36] **Kadamur, G. and Ross, E.M.** (2013) Mammalian phospholipase C. *Annual Review of Physiology*. 75.

[37] **McDermott, M., Wakelam, M.J.O., and Morris, A.J.** (2004) Phospholipase D. *Biochemistry and Cell Biology*. 82 (1), 225–253.

[38] **Gustavsson, L.** (1995) ESBRA 1994 Award Lecture. Phosphatidylethanol formation: Specific effects of ethanol mediated via phospholipase D. *Alcohol and Alcoholism*. (30), 391–406.

[39] **Frohman, M.A., Sung, T.C., and Morris, A.J.** (1999) Mammalian phospholipase D structure and regulation. *Biochimica et Biophysica Acta - Molecular and Cell Biology of Lipids*. 1439 (2), 175–186.

[40] **Bumpus, T.W., Liang, D., and Baskin, J.M.** (2020) IMPACT: Imaging phospholipase D activity with clickable alcohols via transphosphatidylation. *Methods in Enzymology*. 641 75–94.

[41] **Hanahan, D.J. and Chaikoff, I.L.** (1947) The phosphorus-containing lipides of the carrot. *The Journal of Biological Chemistry*. 168 (1), 233–240.

[42] **Stuckey, J.A. and Dixon, J.E.** (1999) Crystal structure of a phospholipase D family member. *Nature Structural Biology*. 6 (3), 278–284.

[43] **Lagunavicius, A., Sasnauskas, G., Halford, S.E., and Siksnys, V.** (2003) The metal-independent type IIs restriction enzyme BfiI is a dimer that binds two DNA sites but has only one catalytic centre. *Journal of Molecular Biology*. 326 (4), 1051–1064.

[44] **Esposito, M.S., Esposito, R.E., Arnaud, M., and Halvorson, H.O.** (1970) Conditional mutants of meiosis in yeast. *Journal of Bacteriology*. 104 (1), 202–210.

[45] **Harkins, A.L., Yuan, G., London, S.D., and Dolan, J.W.** (2010) An oleate-stimulated, phosphatidylinositol 4,5-bisphosphate-independent phospholipase D in Schizosaccharomyces pombe. *FEMS Yeast Research*. 10 (6), 717–726.

[46] **Koonin, E. V.** (1996) A duplicated catalytic motif in a new superfamily of phosphohydrolases and phospholipid synthases that includes poxvirus envelope proteins. *Trends in Biochemical Sciences*. 21 (7), 242–243.

[47] **Saito, M. and Kanfer, J.** (1973) Solubilization and properties of a membrane-bound enzyme from rat brain catalyzing a base-exchange reaction. *Biochemical and Biophysical Research Communications*. 53 (2), 391–398.

[48] **Hammond, S.M., Altshuller, Y.M., Sung, T.C., Rudge, S.A., Rose, K., Engebrecht, J.A., et al.** (1995) Human ADP-ribosylation factor-activated phosphatidylcholine-specific phospholipase D defines a new and highly conserved gene family. *Journal of Biological Chemistry*. 270 (50), 29640–29643.

[49] **Sung, T.C., Roper, R.L., Zhang, Y., Rudge, S.A., Temel, R., Hammond, S.M., et al.** (1997) Mutagenesis of phospholipase D defines a superfamily including a trans-Golgi viral protein required for poxvirus pathogenicity. *EMBO Journal*. 16 (15), 4519–4530.

[50] **Ponting, C.P. and Kerr, I.D.** (1996) A novel family of phospholipase D homologues that includes phospholipid synthases and putative endonucleases: Identification of duplicated repeats and potential active site residues. *Protein Science*. 5 (5), 914–922.

[51] **Colley, W.C., Sung, T.C., Roll, R., Jenco, J., Hammondt, S.M., Altshuller, Y., et al.** (1997) Phospholipase D2, a distinct phospholipase D isoform with novel regulatory properties that provokes cytoskeletal reorganization. *Current Biology*. 7 (3), 191–201.

[52] **Sciorra, V.A., Rudge, S.A., Prestwich, G.D., Frohman, M.A., Engebrecht, J.A., and Morris, A.J.** (1999) Identification of a phosphoinositide binding motif that mediates activation of mammalian and yeast phospholipase D

isoenzymes. *EMBO Journal*. 18 (21), 5911–5921.

[53] **Bowling, F.Z., Salazar, C.M., Bell, J.A., Huq, T.S., Frohman, M.A., and Airola, M. V.** (2020) Crystal structure of human PLD1 provides insight into activation by PI(4,5)P2 and RhoA. *Nature Chemical Biology*. 16 (4), 400–407.

[54] **Sung, T.C., Zhang, Y., Morris, A.J., and Frohman, M.A.** (1999) Structural analysis of human phospholipase D1. *Journal of Biological Chemistry*. 274 (6), 3659–3666.

[55] **Sung, T.C., Roper, R.L., Zhang, Y., Rudge, S.A., Temel, R., Hammond, S.M., et al.** (1997) Mutagenesis of phospholipase D defines a superfamily including a trans-Golgi viral protein required for poxvirus pathogenicity. *EMBO Journal*. 16 (15), 4519–4530.

[56] **Sugars, J.M., Cellek, S., Manifava, M., Coadwell, J., and Ktistakis, N.T.** (2002) Hierarchy of membrane-targeting signals of phospholipase D1 involving lipid modification of a pleckstrin homology domain. *The Journal of Biological Chemistry*. 277 (32), 29152–29161.

[57] **Sung, T.C., Altshuller, Y.M., Morris, A.J., and Frohman, M.A.** (1999) Molecular analysis of mammalian phospholipase D2. *Journal of Biological Chemistry*. 274 (1), 494–502.

[58] **Metrick, C.M., Peterson, E.A., Santoro, J.C., Enyedy, I.J., Murugan, P., Chen, T.Y., et al.** (2020) Human PLD structures enable drug design and characterization of isoenzyme selectivity. *Nature Chemical Biology*. 16 (4), 391–399.

[59] **Sehnal, D., Bittrich, S., Deshpande, M., Svobodová, R., Berka, K., Bazgier, V., et al.** (2021) Mol∗Viewer: Modern web app for 3D visualization and analysis of large biomolecular structures. *Nucleic Acids Research*. 49 (W1), W431–W437.

[60] **Liscovitch, M., Czarny, M., Fiucci, G., and Tang, X.** (2000) Phospholipase D: Molecular and cell biology of a novel gene family. *Biochemical Journal*. 345 (3), 401–415.

[61] **Jenkins, G.M. and Frohman, M.A.** (2005) Phospholipase D: a lipid centric review. *CMLS Cellular and Molecular Life Sciences*. (62), 2305–2316.

[62] **Freyberg, Z., Bourgoin, S., and Shields, D.** (2002) Phospholipase D2 is localized to the rims of the Golgi apparatus in mammalian cells. *Molecular Biology of the Cell*. 13 (11), 3930–3942.

[63] **Denmat-Ouisse, L.A., Phebidias, C., Honkavaara, P., Robin, P., Geny, B., Min, D.S., et al.** (2001) Regulation of Constitutive Protein Transit by Phospholipase D in HT29-cl19A Cells. *Journal of Biological Chemistry*. 276 (52), 48840–48846.

[64] **Du, G., Huang, P., Liang, B.T., and Frohman, M.A.** (2004) Phospholipase D2 Localizes to the Plasma Membrane and Regulates Angiotensin II Receptor Endocytosis. *Molecular Biology of the Cell*. 15 (3), 1024–1030.

[65] **Peng, X. and Frohman, M.A.** (2012) Mammalian phospholipase D physiological and pathological roles. *Acta Physiologica*. 204 (2), 219–226.

[66] **Brown, F.D., Thompson, N., Saqib, K.M., Clark, J.M., Powner, D., Thompson, N.T., et al.** (1998) Phospholipase D1 localises to secretory granules and lysosomes and is plasma-membrane translocated on cellular stimulation. *Current Biology*. 8 (14), 835–838.

[67] **Donaldson, J.G.** (2009) Phospholipase D in endocytosis and endosomal recycling pathways. *Biochimica et Biophysica Acta - Molecular and Cell Biology of Lipids*. 1791 (9), 845–849.

[68] **Chen, Y.G., Siddhanta, A., Austin, C.D., Hammond, S.M., Sung, T.C., Frohman, M.A., et al.** (1997)

Phospholipase D stimulates release of nascent secretory vesicles from the trans-Golgi network. *Journal of Cell Biology*. 138 (3), 495–504.

[69] **Lee, C.S., Kim, I.S., Park, J.B., Lee, M.N., Lee, H.Y., Suh, P.G., et al.** (2006) The phox homology domain of phospholipase D activates dynamin GTPase activity and accelerates EGFR endocytosis. *Nature Cell Biology*. 8 (5), 477–484.

[70] **Vitale, N., Caumont, A.S., Chasserot-Golaz, S., Du, G., Wu, S., Sciorra, V.A., et al.** (2001) Phospholipase D1: A key factor for the exocytotic machinery in neuroendocrine cells. *EMBO Journal*. 20 (10), 2424–2434.

[71] **Vitale, N., Mawet, J., Camonis, J., Regazzi, R., Bader, M.F., and Chasserot-Golaz, S.** (2005) The small GTPase RalA controls exocytosis of large dense core secretory granules by interacting with ARF6-dependent phospholipase D1. *Journal of Biological Chemistry*. 280 (33), 29921–29928.

[72] **Liu, L., Liao, H., Castle, A., Zhang, J., Casanova, J., Szabo, G., et al.** (2005) SCAMP2 interacts with Arf6 and phospholipase D1 and links their function to exocytotic fusion pore formation in PC12 cells. *Molecular Biology of the Cell*. 16 (10), 4463–4472.

[73] **Rose, K., Rudge, S.A., Frohman, M.A., Morris, A.J., and Engebrecht, J.** (1995) Phospholipase D signaling is essential for meiosis. *Proceedings of the National Academy of Sciences of the United States of America*. 92 (26), 12151–12155.

[74] **Choi, W.S., Kim, Y.M., Combs, C., Frohman, M.A., and Beaven, M.A.** (2002) Phospholipases D1 and D2 Regulate Different Phases of Exocytosis in Mast Cells. *The Journal of Immunology*. 168 (11), 5682–5689.

[75] **Corrotte, M., Chasserot-Golaz, S., Huang, P., Du, G., Ktistakis, N.T., Frohman, M.A., et al.** (2006) Dynamics and function of phospholipase D and phosphatidic acid during phagocytosis. *Traffic*. 7 (3), 365–377.

[76] **Iyer, S.S., Barton, J.A., Bourgoin, S., and Kusner, D.J.** (2004) Phospholipases D1 and D2 Coordinately Regulate Macrophage Phagocytosis. *The Journal of Immunology*. 173 (4), 2615–2623.

[77] **Shen, Y., Xu, L., and Foster, D.A.** (2001) Role for Phospholipase D in Receptor-Mediated Endocytosis. *Molecular and Cellular Biology*. 21 (2), 595–602.

[78] **Pedersen, K.M., Finsen, B., Celis, J.E., and Jensen, N.A.** (1998) Expression of a novel murine phospholipase D homolog coincides with late neuronal development in the forebrain. *Journal of Biological Chemistry*. 273 (47), 31494–31504.

[79] **Yoshikawa, F., Banno, Y., Otani, Y., Yamaguchi, Y., Nagakura-Takagi, Y., Morita, N., et al.** (2010) Phospholipase D family member 4, a transmembrane glycoprotein with no phospholipase D activity, expression in spleen and early postnatal microglia. *PLoS ONE*. 5 (11), e13932.

[80] **Choi, S.Y., Huang, P., Jenkins, G.M., Chan, D.C., Schiller, J., and Frohman, M.A.** (2006) A common lipid links Mfn-mediated mitochondrial fusion and SNARE-regulated exocytosis. *Nature Cell Biology*. 8 (11), 1255–1262.

[81] **Ota, T., Suzuki, Y., Nishikawa, T., Otsuki, T., Sugiyama, T., Irie, R., et al.** (2004) Complete sequencing and characterization of 21,243 full-length human cDNAs. *Nature Genetics*. 36 (1), 40–45.

[82] **Gomez-Cambronero, J. and Ganesan, R.** (2018) Targeting phospholipase D genetically and pharmacologically for studying leukocyte function. in: Methods Mol. Biol., pp. 297–314.

[83] **Gavin, A.L., Huang, D., Huber, C., Mårtensson, A., Tardif, V., Skog, P.D., et al.** (2018) PLD3 and PLD4

are single-stranded acid exonucleases that regulate endosomal nucleic-acid sensing. *Nature Immunology*. 19 (9), 942–953.

[84] **Munck, A., Böhm, C., Seibel, N.M., Hosseini, Z.H., and Hampe, W.** (2005) Hu-K4 is a ubiquitously expressed type 2 transmembrane protein associated with the endoplasmic reticulum. *FEBS Journal*. 272 (7), 1718–1726.

[85] **Mukadam, A.S., Breusegem, S.Y., and Seaman, M.N.J.** (2018) Analysis of novel endosome-to-Golgi retrieval genes reveals a role for PLD3 in regulating endosomal protein sorting and amyloid precursor protein processing. *Cellular and Molecular Life Sciences*. 75 (14), 2613–2625.

[86] **Gonzalez, A.C., Schweizer, M., Jagdmann, S., Bernreuther, C., Reinheckel, T., Saftig, P., et al.** (2018) Unconventional Trafficking of Mammalian Phospholipase D3 to Lysosomes. *Cell Reports*. 22 (4), 1040–1053.

[87] **Cruchaga, C., Karch, C.M., Jin, S.C., Benitez, B.A., Cai, Y., Guerreiro, R., et al.** (2014) Rare coding variants in the phospholipase D3 gene confer risk for Alzheimer's disease. *Nature*. 505 (7484), 550–554.

[88] **Otani, Y., Yamaguchi, Y., Sato, Y., Furuichi, T., Ikenaka, K., Kitani, H., et al.** (2011) PLD4 is involved in phagocytosis of microglia: Expression and localization changes of PLD4 are correlated with activation state of microglia. *PLoS ONE*. 6 (11), e27544.

[89] **Gao, L., Zhou, Y., Zhou, S.X., Yu, X.J., Xu, J.M., Zuo, L., et al.** (2017) PLD4 promotes M1 macrophages to perform antitumor effects in colon cancer cells. *Oncology Reports*. 37 (1), 408–416.

[90] **Han, Y. and Zhou, L.** (2020) MiRNA-4665-3p Regulates Expression of PLD5 in Thyroid Cancer Patients and Predicts Death. *Journal of Biomaterials and Tissue Engineering*. 9 (7), 871–880.

[91] **Huang, H., Gao, Q., Peng, X., Choi, S.Y., Sarma, K., Ren, H., et al.** (2011) PiRNA-Associated Germline Nuage Formation and Spermatogenesis Require MitoPLD Profusogenic Mitochondrial-Surface Lipid Signaling. *Developmental Cell*. 20 (3), 376–387.

[92] **Watanabe, T., Chuma, S., Yamamoto, Y., Kuramochi-Miyagawa, S., Totoki, Y., Toyoda, A., et al.** (2011) MITOPLD Is a Mitochondrial Protein Essential for Nuage Formation and piRNA Biogenesis in the Mouse Germline. *Developmental Cell*. 20 (3), 364–375.

[93] **TOOKEY, H.L. and BALLS, A.K.** (1956) Plant phospholipase D. I. Studies on cottonseed and cabbage phospholipase D. *The Journal of Biological Chemistry*. 218 (1), 213–224.

[94] **Cockcroft, S., Thomas, G.M.H., Fensome, A., Geny, B., Cunningham, E., Gout, I., et al.** (1994) Phospholipase D: A downstream effector of ARF in granulocytes. *Science*. 263 (5146), 523–526.

[95] **Malcolm, K.C., Ross, A.H., Qiut, R.G., Symonst, M., and Exton, J.H.** (1994) Activation of rat liver phospholipase D by the small GTP-binding protein RhoA. *Journal of Biological Chemistry*. 269 (42), 25951–25954.

[96] **Kaszkin, M., Seidler, L., Kast, R., and Kinzel, V.** (1992) Epidermal-growth-factor-induced production of phosphatidylalcohols by HeLa cells and A431 cells through activation of phospholipase D. *Biochemical Journal*. 287 (1), 51–57.

[97] **Rydzewska, G. and Morisset, J.** (1995) Activation of pancreatic acinar cell phospholipase d by epidermal, insulin-like, and basic fibroblast growth factors involves tyrosine kinase. *Pancreas*. 10 (1), 59–65.

[98] **Dean, N.M. and Boynton, A.L.** (1995) EGF-Induced increase in diacylglycerol, choline release, and DNA synthesis is extracellular calcium dependent. *Journal of Cellular Physiology*. 164 (3), 449–458.

[99] **Brown, H.A., Gutowski, S., Moomaw, C.R., Slaughter, C., and Sternwels, P.C.** (1993) ADP-ribosylation factor, a small GTP-dependent regulatory protein, stimulates phospholipase D activity. *Cell*. 75 (6), 1137–1144.

[100] **Brown, H.A., Gutowski, S., Kahn, R.A., and Sternweis, P.C.** (1995) Partial purification and characterization of Arf-sensitive phospholipase D from porcine brain. *Journal of Biological Chemistry*. 270 (25), 14935–14943.

[101] **Cockcroft, S., Way, G., O'Luanaigh, N., Pardo, R., Sarri, E., and Fensome, A.** (2002) Signalling role for ARF and phospholipase D in mast cell exocytosis stimulated by crosslinking of the high affinity FcεR1 receptor. *Molecular Immunology*. 38 (16–18), 1277–1282.

[102] **Rudge, S.A. and Wakelam, M.J.O.** (2009) Inter-regulatory dynamics of phospholipase D and the actin cytoskeleton. *Biochimica et Biophysica Acta - Molecular and Cell Biology of Lipids*. 1791 (9), 856–861.

[103] **Hammond, S.M., Jenco, J.M., Nakashima, S., Cadwallader, K., Gu, Q.M., Cook, S., et al.** (1997) Characterization of two alternately spliced forms of phospholipase D1: Activation of the purified enzymes by phosphatidylinositol 4,5-bisphosphate, ADP-ribosylation factor, and RHO family monomeric GTP-binding proteins and protein kinase C-α. *Journal of Biological Chemistry*. 272 (6), 3860–3868.

[104] **Min, D.S., Park, S.K., and Exton, J.H.** (1998) Characterization of a rat brain phospholipase D isozyme. *Journal of Biological Chemistry*. 273 (12), 7044–7051.

[105] **Park, S.K., Min, D.S., and Exton, J.H.** (1998) Definition of the protein kinase C interaction site of phospholipase D. *Biochemical and Biophysical Research Communications*. 244 (2), 364–367.

[106] **Yamazaki, M., Zhang, Y., Watanabe, H., Yokozeki, T., Ohno, S., Kaibuchi, K., et al.** (1999) Interaction of the small G protein RhoA with the C terminus of human phospholipase D1. *Journal of Biological Chemistry*. 274 (10), 6035–6038.

[107] **Exton, J.H.** (2002) Regulation of phospholipase D. *FEBS Letters*. 531 (1), 58–61.

[108] **Bowman, E.P., Uhlinger, D.J., and Lambeth, J.D.** (1993) Neutrophil phospholipase D is activated by a membrane-associated Rho family small molecular weight GTP-binding protein. *Journal of Biological Chemistry*. 268 (29), 21509–21512.

[109] **Sciorra, V.A., Rudge, S.A., Wang, J., McLaughlin, S., Engebrecht, J.A., and Morris, A.J.** (2002) Dual role for phosphoinositides in regulation of yeast and mammalian phospholipase D enzymes. *Journal of Cell Biology*. 159 (6), 1039–1049.

[110] **Uchida, N., Okamura, S.I., and Kuwano, H.** (1999) Phospholipase D activity in human gastric carcinoma. *Anticancer Research*. 19 (1 B), 671–675.

[111] **Uchida, N., Okamura, S.I., Nagamachi, Y., and Yamashita, S.** (1997) Increased phospholipase D activity in human breast cancer. *Journal of Cancer Research and Clinical Oncology*. 123 (5), 280–285.

[112] **Noh, D.Y., Ahn, S.J., Lee, R.A., Park, I.A., Kim, J.H., Suh, P.G., et al.** (2000) Overexpression of phospholipase D1 in human breast cancer tissues. *Cancer Letters*. 161 (2), 207–214.

[113] **Yamada, Y., Hamajima, N., Kato, T., Iwata, H., Yamamura, Y., Shinoda, M., et al.** (2003) Association of a polymorphism of the phospholipase D2 gene with the prevalence of colorectal cancer. *Journal of Molecular Medicine*. 81 (2), 126–131.

[114] **Zhao, Y., Ehara, H., Akao, Y., Shamoto, M., Nakagawa, Y., Banno, Y., et al.** (2000) Increased activity and intranuclear expression of phospholipase D2 in human renal cancer. *Biochemical and Biophysical Research Communications*. 278 (1), 140–143.

[115] **Chen, Q., Hongu, T., Sato, T., Zhang, Y., Ali, W., Cavallo, J.A., et al.** (2012) Key roles for the lipid signaling enzyme phospholipase D1 in the tumor microenvironment during tumor angiogenesis and metastasis. *Science Signaling*. 5 (249), ra79.

[116] **Huang, P. and Frohman, M.A.** (2007) The potential for phospholipase D as a new therapeutic target. *Expert Opinion on Therapeutic Targets*. 11 (5), 707–716.

[117] **Tsukahara, T., Tsukahara, R., Fujiwara, Y., Yue, J., Cheng, Y., Guo, H., et al.** (2010) Phospholipase D2-dependent inhibition of the nuclear hormone receptor PPARγ by cyclic phosphatidic acid. *Molecular Cell*. 39 (3), 421–432.

[118] **Hong, K.W., Jin, H.S., Lim, J.E., Cho, Y.S., Go, M.J., Jung, J., et al.** (2010) Non-synonymous single-nucleotide polymorphisms associated with blood pressure and hypertension. *Journal of Human Hypertension*. 24 (11), 763–774.

[119] **Peng, J.H.F. and Rhodes, P.G.** (2000) Developmental expression of phospholipase D2 mRNA in rat brain. *International Journal of Developmental Neuroscience*. 18 (6), 585–589.

[120] **Zhao, D., Berse, B., Holler, T., Cermak, J.M., and Blusztajn, J.K.** (1998) Developmental changes in phospholipase D activity and mRNA levels in rat brain. *Developmental Brain Research*. 109 (2), 121–127.

[121] **Cai, D., Zhong, M., Wang, R., Netzer, W.J., Shields, D., Zheng, H., et al.** (2006) Phospholipase D1 corrects impaired βAPP trafficking and neurite outgrowth in familial Alzheimer's disease-linked presenilin-1 mutant neurons. *Proceedings of the National Academy of Sciences of the United States of America*. 103 (6), 1936–1940.

[122] **Oliveira, T.G., Chan, R.B., Tian, H., Laredo, M., Shui, G., Staniszewski, A., et al.** (2010) Phospholipase D2 ablation ameliorates Alzheimer's disease-linked synaptic dysfunction and cognitive deficits. *Journal of Neuroscience*. 30 (49), 16419–16428.

[123] **Bravo, F.V., Da Silva, J., Chan, R.B., Di Paolo, G., Teixeira-Castro, A., and Oliveira, T.G.** (2018) Phospholipase D functional ablation has a protective effect in an Alzheimer's disease Caenorhabditis elegans model. *Scientific Reports*. 8 (1), 3540.

[124] **Kennedy, M.A., Kabbani, N., Lambert, J.P., Swayne, L.A., Ahmed, F., Figeys, D., et al.** (2011) Srf1 is a novel regulator of phospholipase D activity and is essential to buffer the toxic effects of C16:0 platelet activating factor. *PLoS Genetics*. 7 (2), e1001299.

[125] **Santa-Marinha, L., Castanho, I., Silva, R.R., Bravo, F.V., Miranda, A.M., Meira, T., et al.** (2020) Phospholipase D1 Ablation Disrupts Mouse Longitudinal Hippocampal Axis Organization and Functioning. *Cell Reports*. 30 (12), 4197-4208.e6.

[126] **Dharmalingam, K. and Jayaraman, J.** (1971) Mechanism of glucose repression of mitochondriogenesis: Induction of phospholipases. *Biochemical and Biophysical Research Communications*. 45 (5), 1115–1118.

[127] **Grossman, S., Cobley, J., Hogue, P.K., Kearney, E.B., and Singer, T.P.** (1973) Relation of phospholipase D activity to the decay of succinate dehydrogenase and of covalently bound flavin in yeast cells undergoing glucose repression. *Archives of Biochemistry and Biophysics*. 158 (2), 744–753.

[128] **Rudge, S.A., Morris, A.J., and Engebrecht, J.A.** (1998) Relocalization of phospholipase D activity mediates membrane formation during meiosis. *Journal of Cell Biology*. 140 (1), 81–90.

[129] **Honigberg, S.M., Conicella, C., and Espositio, R.E.** (1992) Commitment to meiosis in Saccharomyces cerevisiae: Involvement of the SP014 gene. *Genetics*. 130 (4), 703–716.

[130] **Steed, P.M., Clark, K.L., Boyar, W.C., and Lasala, D.J.** (1998) Characterization of human PLD2 and the analysis of PLD isoform splice variants. *The FASEB Journal*. 12 (13), 1309–1317.

[131] **Morris, A.J., Engebrecht, J.A., and Frohman, M.A.** (1996) Structure and regulation of phospholipase D. *Trends in Pharmacological Sciences*. 17 (5), 182–185.

[132] **Rudge, S.A., Sciorra, V.A., Iwamoto, M., Zhou, C., Strahl, T., Morris, A.J., et al.** (2004) Roles of Phosphoinositides and of Spo14p (phospholipase D)-generated Phosphatidic Acid during Yeast Sporulation. *Molecular Biology of the Cell*. 15 (1), 207–218.

[133] **Nakanishi, H., Morishita, M., Schwartz, C.L., Coluccio, A., Engebrecht, J.A., and Neiman, A.M.** (2006) Phospholipase D and the SNARE Sso1p are necessary for vesicle fusion during sporulation in yeast. *Journal of Cell Science*. 119 (7), 1406–1415.

[134] **Harkins, A.L., London, S.D., and Dolan, J.W.** (2008) An upstream regulator and downstream target of phospholipase D1 activity during pheromone response in Saccharomyces cerevisiae. *FEMS Yeast Research*. 8 (2), 237–244.

[135] **Cleves, A.E., McGee, T.P., Whitters, E.A., Champlon, K.M., Altken, J.R., Dowhan, W., et al.** (1991) Mutations in the CDP-choline pathway for phospholipid biosynthesis bypass the requirement for an essential phospholipid transfer protein. *Cell*. 64 (4), 789–800.

[136] **Sreenivas, A., Patton-Vogt, J.L., Bruno, V., Griac, P., and Henry, S.A.** (1998) A role for phospholipase D (Pld1p) in growth, secretion, and regulation of membrane lipid synthesis in yeast. *Journal of Biological Chemistry*. 273 (27), 16635–16638.

[137] **Park, J.S. and Neiman, A.M.** (2012) VPS13 regulates membrane morphogenesis during sporulation in Saccharomyces cerevisiae. *Journal of Cell Science*. 125 (12), 3004–3011.

[138] **Zhang, W., Espinoza, D., Hines, V., Innis, M., Mehta, P., and Miller, D.L.** (1997) Characterization of β-amyloid peptide precursor processing by the yeast Yap3 and Mkc7 proteases. *Biochimica et Biophysica Acta - Molecular Cell Research*. 1359 (2), 110–122.

[139] **Feng, B.Y., Toyama, B.H., Wille, H., Colby, D.W., Collins, S.R., May, B.C.H., et al.** (2008) Small-molecule aggregates inhibit amyloid polymerization. *Nature Chemical Biology*. 4 (3), 197–199.

[140] **Outeiro, T.F. and Lindquist, S.** (2003) Yeast Cells Provide Insight into Alpha-Synuclein Biology and Pathobiology. *Science*. 302 (5651), 1772–1775.

[141] **Narayan, P., Sienski, G., Bonner, J.M., Lin, Y.T., Seo, J., Baru, V., et al.** (2020) PICALM Rescues Endocytic Defects Caused by the Alzheimer's Disease Risk Factor APOE4. *Cell Reports*. 33 (1), 108224.

[142] **Mell, J.C. and Burgess, S.M.** (2003) Yeast as a Model Genetic Organism. in: Encycl. Life Sci., pp. 1–8.

[143] **Botstein, D. and Fink, G.R.** (2011) Yeast: An experimental organism for 21st century biology. *Genetics*. 189 (3), 695–704.

[144] **Mohammadi, S., Saberidokht, B., Subramaniam, S., and Grama, A.** (2015) Scope and limitations of yeast as a model organism for studying human tissue-specific pathways. *BMC Systems Biology*. 9 (1), 1–21.

[145] **Hanson, P.K.** (2018) Saccharomyces cerevisiae: A Unicellular Model Genetic Organism of Enduring Importance. *Current Protocols in Essential Laboratory Techniques*. 16 (1), e21.

[146] **Rudge, S.A., Pettitt, T.R., Zhou, C., Wakelam, M.J.O., and Engebrecht, J.A.** (2001) SPO14 separation-of-function mutations define unique roles for phospholipase D in secretion and cellular differentiation in

Saccharomyces cerevisiae. *Genetics*. 158 (4), 1431–1444.

[147] **Wieczorke, R., Dlugai, S., Krampe, S., and Boles, E.** (2003) Characterisation of mammalian GLUT glucose transporters in a heterologous yeast expression system. *Cellular Physiology and Biochemistry*. 13 (3), 123–134.

[148] **Flegelova, H., Haguenauer-Tsapis, R., and Sychrova, H.** (2006) Heterologous expression of mammalian Na/H antiporters in Saccharomyces cerevisiae. *Biochimica et Biophysica Acta - General Subjects*. 1760 (3), 504–516.

[149] **Wright, M.E., Han, D.K., and Hockenbery, D.M.** (2000) Caspase-3 and inhibitor of apoptosis protein(s) interactions in Saccharomyces cerevisiae and mammalian cells. in: FEBS Lett., pp. 13–18.

[150] **Jidenko, M., Nielsen, R.C., Sørensen, T.L.M., Møller, J. V., Le Maire, M., Nissen, P., et al.** (2005) Crystallization of a mammalian membrane protein overexpressed in Saccharomyces cerevisiae. *Proceedings of the National Academy of Sciences of the United States of America*. 102 (33), 11687–11691.

[151] **Heinicke, S., Livstone, M.S., Lu, C., Oughtred, R., Kang, F., Angiuoli, S. V., et al.** (2007) The Princeton Protein Orthology Database (P-POD): A comparative genomics analysis tool for biologists. *PLoS ONE*. 2 (8), e766.

[152] **Nijkamp, J.F., van den Broek, M., Datema, E., de Kok, S., Bosman, L., Luttik, M.A., et al.** (2012) De novo sequencing, assembly and analysis of the genome of the laboratory strain Saccharomyces cerevisiae CEN.PK113-7D, a model for modern industrial biotechnology. *Microbial Cell Factories*. 11.

[153] **Generoso, W.C., Gottardi, M., Oreb, M., and Boles, E.** (2016) Simplified CRISPR-Cas genome editing for Saccharomyces cerevisiae. *Journal of Microbiological Methods*. 127 203–205.

[154] **Soares-Silva, I., Paiva, S., Diallinas, G., and Casal, M.** (2007) The conserved sequence NXX[S/T]HX[S/T]QDXXXT of the lactate/pyruvate:H+ symporter subfamily defines the function of the substrate translocation pathway. *Molecular Membrane Biology*. 24 (5–6), 464–474.

[155] **Goldstein, A.L. and McCusker, J.H.** (1999) Three new dominant drug resistance cassettes for gene disruption in Saccharomyces cerevisiae. *Yeast*. 15 (14), 1541–1553.

[156] **Inoue, H., Nojima, H., and Okayama, H.** (1990) High efficiency transformation of Escherichia coli with plasmids. *Gene*. 96 (1), 23–28.

[157] **Gietz, R.D. and Schiestl, R.H.** (2007) High-efficiency yeast transformation using the LiAc/SS carrier DNA/PEG method. *Nature Protocols*. 2 (1), 31–34.

[158] **Freyberg, Z., Sweeney, D., Siddhanta, A., Bourgoin, S., Frohman, M., and Shields, D.** (2001) Intracellular localization of phospholipase D1 in mammalian cells. *Molecular Biology of the Cell*. 12 (4), 943–955.

[159] **Lousa, C.D.M. and Denecke, J.** (2016) Lysosomal and vacuolar sorting: Not so different after all! *Biochemical Society Transactions*. 44 (3), 891–897.

[160] **Dall'Armi, C., Hurtado-Lorenzo, A., Tian, H., Morel, E., Nezu, A., Chan, R.B., et al.** (2010) The phospholipase D1 pathway modulates macroautophagy. *Nature Communications*. 1 (9), 1–11.

[161] **Cai, M., He, J., Xiong, J., Tay, L.W.R., Wang, Z., Rog, C., et al.** (2016) Phospholipase D1-regulated autophagy supplies free fatty acids to counter nutrient stress in cancer cells. *Cell Death and Disease*. 7 (11), e2448-e2448.

[162] **Bumpus, T.W. and Baskin, J.M.** (2017) Clickable Substrate Mimics Enable Imaging of Phospholipase D Activity. *ACS Central Science*. 3 (10), 1070–1077.

[163] **Liang, D., Wu, K., Tei, R., Bumpus, T.W., Ye, J., and Baskin, J.M.** (2019) A real-time click chemistry

imaging approach reveals stimulus-specific subcellular locations of phospholipase D activity. *Proceedings of the National Academy of Sciences of the United States of America*. 116 (31), 15453–15462.

[164] **Chishti, M.A., Yang, D.S., Janus, C., Phinney, A.L., Horne, P., Pearson, J., et al.** (2001) Early-onset Amyloid Deposition and Cognitive Deficits in Transgenic Mice Expressing a Double Mutant Form of Amyloid Precursor Protein 695. *Journal of Biological Chemistry*. 276 (24), 21562–21570.

[165] **Ryan, S.D., Whitehead, S.N., Swayne, L.A., Moffat, T.C., Hou, W., Ethier, M., et al.** (2009) Amyloid-β42 signals tau hyperphosphorylation and compromises neuronal viability by disrupting alkylacylglycerophosphocholine metabolism. *Proceedings of the National Academy of Sciences of the United States of America*. 106 (49), 20936–20941.

[166] **Karim, A.S., Curran, K.A., and Alper, H.S.** (2013) Characterization of plasmid burden and copy number in Saccharomyces cerevisiae for optimization of metabolic engineering applications. *FEMS Yeast Research*. 13 (1), 107–116.

[167] **Haque, R.U. and Levey, A.I.** (2019) Alzheimer's disease: A clinical perspective and future nonhuman primate research opportunities. *Proceedings of the National Academy of Sciences of the United States of America*. 116 (52), 26224–26229.

Chapter VI – Appendices

VI. Appendices

VI.1. Codon optimization of mammalian *PLD1* and *PLD2*

VI.1.1. Codon Adaptation Index prediction and optimization

To predict the levels of expression of a heterologous protein the Codon Adaptation Index (CAI) can be calculated. The ideal CAI is 1.0, although CAI values above 0.8 are considered sufficient for good expression levels in the host. The CAI for *hPLD1* and *mPLD2* for expression in *S. cerevisiae* were calculated using Genscript's Rare Codon Analysis Tool. *PLD1* showed a CAI of 0.66 and *PLD2* a CAI of 0.57, both too low to ensure good heterologous expression in yeast. Therefore, to improve the heterologous expression of mammalian *PLD1* and *PLD2* in *S. cerevisiae* the codon usage frequency of both genes was optimized. The optimized genes were synthesized by Genscript and cloned into vectors pUC57 and pCCI-4K. After optimization, the CAI of both genes showed a significant improvement, with *PLD1* showing a CAI of 0.91 and *PLD2* showing a CAI of 0.93 – Figure 21.

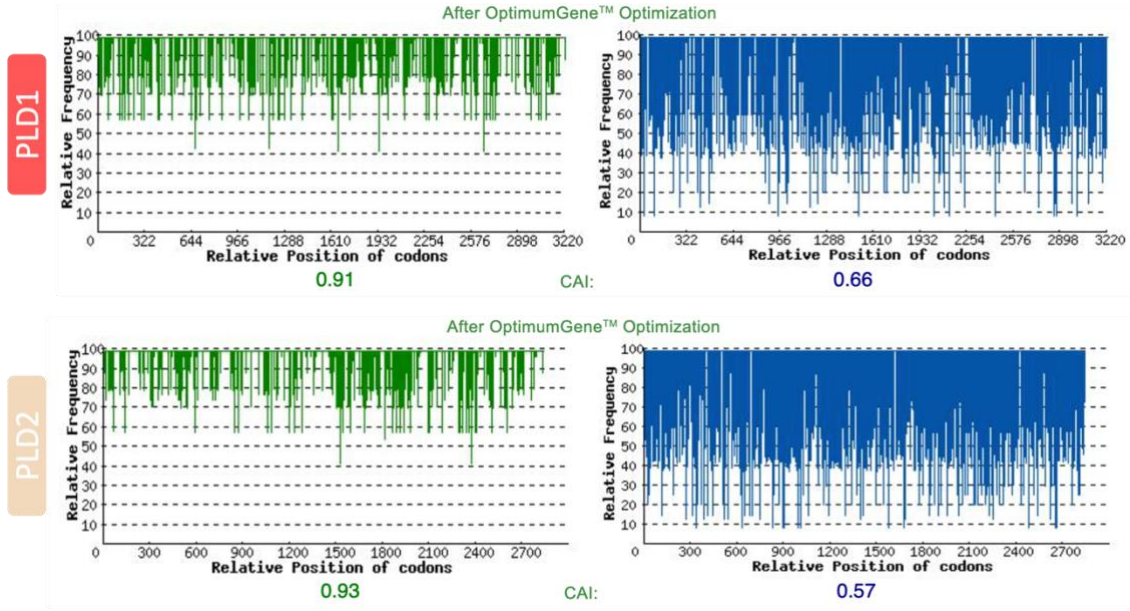

Figure 21. Distribution of codon usage frequency along the length of *PLD1* and *PLD2* to be expressed in *S. cerevisiae*

The predicted CAI of human *PLD1* was 0.66 before optimization and 0.91 after optimization.The predicted CAI of mouse *PLD2* was 0.57 before optimization and 0.93 after optimization. The CAI index predictions were performed using the Rare Codon Analysis Tool from GenScript.

VI.1.2. Plasmid maps and nucleotide sequence of optimized mammalian *PLD1* and *PLD2*

VI.1.2.1. Plasmid maps of hPLD1_pUC57 and mPLD2_PCCI-4K

The optimized *PLD1* and *PLD2* mammalian genes were synthesized by Genscript and cloned into the pUC57 and PCCI-4K vectors, respectively – Figure 22.

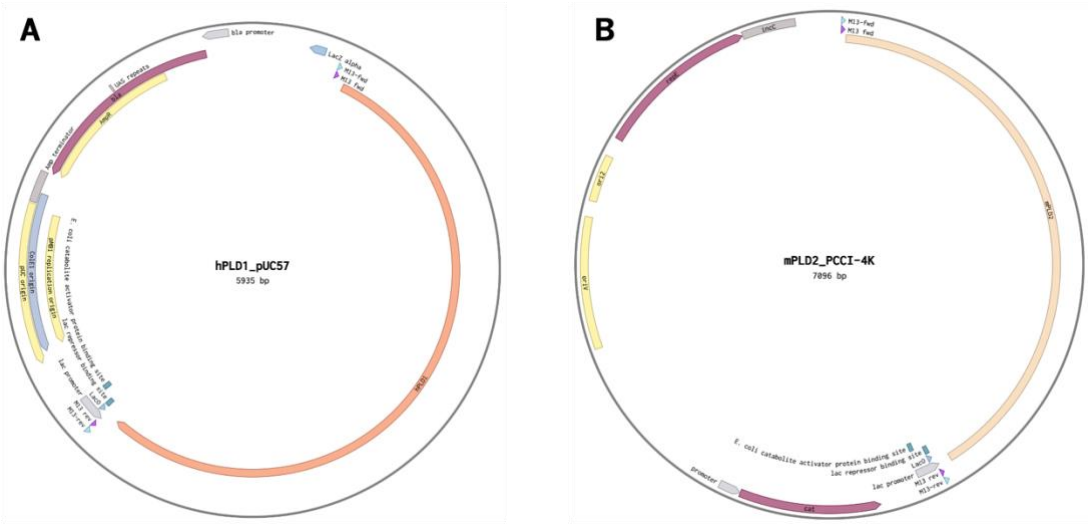

Figure 22. Plasmid maps for (A) hPLD1_pUC57 (5935 bp) and (B) mPLD2_PCCI-4K (7096 bp) containing the codon-optimized mammalian *PLD1* and *PLD2*, respectively.

Important features shown include: bla promoter and bla (confers resistance to ampicillin, carbenicillin, and related antibiotics); cat promoter and cat (confers resistance to the antibiotic chloramphenicol); ori (high-copy-number ColE1/pMB1/pBR322/pUC origin of replication); lac promoter (promoter for the E. coli lac operon);

Plasmid maps were constructed using Benchling [Biology Software]. (2021)

VI.1.3. Nucleotide sequence of codon-optimized mammalian *PLD1* and *PLD2*

VI.1.3.1. *coPLD1*

ATGTCATTGAAGAACGAACCAAGAGTTAACACTTCTGCTTTGCAAAAGATTGCTGCAGATATGTCAAACATCATCGAAAATTTGGATACA
AGAGAATTACATTTCGAAGGTGAAGAAGTTGATTATGATGTTTCTCCATCAGATCCAAAGATCCAAGAAGTTTACATCCCATTCTCAGCA
ATCTACAACACTCAAGGTTTCAAGGAACCAAACATCCAAACATACTTGTCTGGTTGTCCAATCAAGGCTCAAGTTTTAGAAGTTGAAAGA
TTCACTTCAACTACAAGAGTTCCATCTATCAACTTGTACACTATCGAATTAACACATGGTGAATTTAAGTGGCAAGTTAAGAGAAAGTTC
AAGCATTTCCAAGAATTTCATAGAGAATTGTTAAAATATAAAGCATTTATCAGAATACCAATCCCAACTAGAAGACATACATTCAGAAGAC
AAAACGTTAGAGAAGAACCAAGAGAAATGCCATCTTTGCCAAGATCATCTGAAAACATGATCAGAGAAGAACAATTCTTGGGTAGAAGA
AAGCAATTGGAAGATTACTTGACAAAAATTTTGAAAATGCCAATGTACAGAAACTACCATGCAACTACAGAATTTTTGGATATTTCTCAAT
TATCATTTATCCATGATTTGGGTCCAAAGGGTATCGAGGGTATGATCATGAAGAGATCAGGTGGTCATAGAATACCAGGTTTGAATTGTT

GTGGTCAAGGTAGAGCTTGTTACAGATGGTCTAAGAGATGGTTGATCGTTAAGGATTCATTTTTGTTGTACATGAAACCAGATTCTGGTG
CTATTGCATTTGTTTTGTTAGTTGATAAGGAATTTAAGATCAAAGTTGGTAAAAAAGAAACTGAAACAAAATATGGTATTAGAATTGATAAT
TTATCAAGAACTTTGATTTTAAAATGTAATTCTTACAGACATGCTAGATGGTGGGGTGGTGCAATTGAAGAATTTATCCAAAAGCATGGTA
CAAATTTCTTGAAGGATCATAGATTTGGTTCTTATGCTGCAATCCAAGAAAACGCTTTAGCAAAGTGGTATGTTAACGCAAAGGGTTACT
TCGAAGATGTTGCTAATGCAATGGAAGAAGCTAACGAAGAAATTTTTATCACTGATTGGTGGTTGTCTCCAGAAATTTTCTTGAAAAGAC
CAGTTGTTGAGGGTAACAGATGGAGATTAGATTGTATCTTGAAAAGAAAGGCACAACAAGGTGTTAGAATCTTCATCATGTTGTACAAAG
AAGTTGAATTGGCTTTGGGTATCAACTCTGAATACACTAAGAGAACATTGATGAGATTGCATCCAAACATCAAGGTTATGAGACATCCAG
ATCATGTTTCTTCAACAGTTTATTTGTGGGCTCATCATGAAAAATTGGTTATCATCGATCAATCAGTTGCTTTCGTTGGTGGTATTGATTT
GGCATACGGTAGATGGGATGATAACGAACATAGATTGACTGATGTTGGTTCTGTTAAGAGAGTTACATCTGGTCCATCATTGGGTTCTTT
ACCACCAGCTGCAATGGAATCAATGGAATCTTTGAGATTGAAGGATAAGAACGAACCAGTTCAAAACTTGCCAATCCAAAAGTCAATCG
ATGATGTTGATTCTAAATTGAAGGGTATCGGCAAGCCAAGAAAGTTCTCAAAGTTCTCTTTGTACAAACAATTGCATAGACATCATTTGC
ATGATGCAGATTCAATTTCTTCAATCGATTCTACTTCTTCATACTTCAATCATTACAGATCACATCATAATTTAATTCATGGTTTGAAGCC
ACATTTCAAATTGTTCCATCCATCTTCAGAATCTGAACAAGGTTTAACTAGACCACATGCTGATACAGGTTCAATTAGATCATTGCAAAC
TGGTGTTGGTGAATTACATGGTGAAACAAGATTCTGGCATGGCAAGGATTACTGTAACTTCGTTTTCAAGGATTGGGTTCAATTGGATAA
GCCATTCGCAGATTTCATCGATAGATACTCTACTCCAAGAATGCCTTGGCATGATATTGCTTCAGCAGTTCATGGTAAAGCTGCAAGAG
ATGTTGCTAGACATTTTATTCAAAGATGGAACTTCACAAAGATCATGAAGTCTAAGTACAGATCATTGTCATACCCATTTTTGTTACCAAA
ATCACAAACTACAGCTCATGAATTAAGATACCAAGTTCCAGGTTCTGTTCATGCAAATGTTCAATTGTTAAGATCAGCTGCAGATTGGTC
TGCTGGTATCAAGTACCATGAAGAATCTATCCATGCTGCATACGTTCATGTTATTGAAAATTCAAGACATTACATCTACATCGAAAACCA
ATTTTTCATTTCTTGTGCAGATGATAAGGTTGTTTTCAACAAGATTGGTGATGCTATTGCACAAAGAATTTTGAAAGCTCATAGAGAAAAC
CAAAAGTACAGAGTTTACGTTGTTATTCCATTGTTACCAGGTTTTGAAGGTGATATTTCTACTGGTGGTGGTAACGCTTTGCAAGCAATC
ATGCATTTCAATTACAGAACAATGTGTAGAGGTGAAAATTCAATCTTGGGTCAATTGAAAGCAGAATTGGGTAACCAATGGATCAACTAC
ATTTCTTTTTGTGGTTTAAGAACTCATGCTGAATTAGAAGGCAATTTGGTTACAGAATTAATCTACGTTCATTCAAAATTGTTGATCGCTG
ATGATAACACTGTTATCATCGGTTCAGCAAACATCAACGATAGATCAATGTTGGGTAAAAGAGATTCAGAAATGGCTGTTATTGTTCAAG
ATACTGAAACTGTTCCATCAGTTATGGATGGTAAAGAATATCAAGCTGGTAGATTTGCAAGAGGTTTGAGATTGCAATGTTTCAGAGTTG
TTTTGGGTTACTTAGATGATCCATCTGAAGATATTCAAGATCCAGTTTCTGATAAGTTTTTCAAAGAAGTTTGGGTTTCTACTGCTGCAAG
AAATGCTACAATCTACGATAAGGTTTTCAGATGTTTGCCAAACGATGAAGTTCATAACTTGATCCAATTGAGAGATTTCATCAATAAACCA
GTTTTAGCTAAAGAAGATCCAATCAGAGCAGAAGAAGAATTGAAGAAAATTAGAGGTTTCTTGGTTCAATTCCCATTCTACTTTTTATCAG
AAGAATCTTTGTTGCCATCAGTTGGTACTAAAGAAGCTATTGTTCCAATGGAAGTTTGGACATAA

VI.1.3.2. *coPLD2*

ATGACTGTTACACAAAAGAATTTGTTTCCATACGGTGATTACTTAAATTCTTCACAATTGCACATGGAACCAGATGAAGTTGATACTTTGA
GAGAAGGTGAAGATCCAGCAGATAGAATGCATCCATACTTGGCTATCTACGATTTGCAACCATTGAAAGCACATCCATTGGTTTTTGCT
CCAGGTGTTCCAGTTATTGCTCAAGTTGTTGGTACTGAAAGATATACATCTGGTTCAAAAGTTGGTACTTGTACATTATACTCTGTTAGAT
TGACTCATGGTGATTTTACATGGACTACTAAGAAAAAATTCAGACATTTCCAAGAATTACATAGAGATTTGCAAAGACATAAGGTTTTGAT
GTCATTGTTACCATTGGCAAGATTTGCTGTTACTCATTCTCCAGCTAGAGAAGCTGCAGCTGAAGATATTCCATCATTACCAAGAGGTG
GTTCTGAAGGTTCAGCAAGACATACAGCTTCTAAGCAAAAGTATTTAGAAAACTACTTGAATAGATTGTTAACTATGTCATTCTACAGAAA
CTACCATGCTATGACAGAATTTTTAGAAGTTTCTCAATTGTCATTTATCCCAGATTTAGGTTCAAAGGGTTTGGAAGGTGTTATTAGAAAA
AGATCAGGTGGTCATAGAGTTCCAGGTTTTACTTTTTGTGGTAGAGATCAAGTTTGTTACAGATGGTCAAAGAGATGGTTAGTTGTTAAG
GATTCATTTTTGTTGTACATGAGACCAGAAACAGGTGCTATTTCTTTTGTTCAATTGTTTGATCCAGGTTTTGAAGTTCAAGTTGGTAAAA
GATCAACTGAAACAAGATACGGTGTTAGAATCGATACTTCTCATAGATCATTAATCTTGAAATGTTCTTCATACAGACAAGCAAGATGGT
GGGGTCAAGAAATTACAGAATTGGCTCAAGGTTCTGGTAGAGATTTCTTGCAATTGCATCAACATGATTCTTATGCTCCACCAAGACCA
GGTACTTTAGCAAGATGGTTTGTTAATGGTGCTGGTTACTTTGCAGCTGTTGCAGATGCTATCTTGAGAGCACAAGAAGAAATTTTTATC
ACAGATTGGTGGTTGTCACCAGAAATTTATTTGAAGAGACCAGCACATTCTGATGATTGGAGATTAGATATTATGTTGAAGAGAAAAGCT
GAAGAAGGTGTTAGAGTTTCTATCTTGTTGTTCAAAGAAGTTGAATTAGCATTGGGTATCAACTCTGGTTACTCAAAGAGAACTTTGATGT
TGTTGCATCCAAACATCAAGGTTATGAGACATCCAGATTTAGTTACATTGTGGGCTCATCATGAAAAATTGTTAGTTGTTGATCAAGTTGT
TGCATTTTTGGGTGGTTTAGATTTGGCTTTTGGTAGATGGGATGATGTTCAATACAGATTGACTGATTTGGGTGATCCATCTGAACCAGT
TCATTTACAAACTCCAACATTGGGTTCAGATCCAGCAGCTACTCCAGATTTATCTCATAACCAATTTTTCTGGTTGGGCAAGGATTACTC
TAACTTGATCACAAAGGATTGGGTTCAATTGGATAGACCATTCGAAGATTTCATCGATAGAGAAACTACACCAAGAATGCCTTGGAGAGA
TGTTGGTGTTGTTGTTCATGGTGTTGCAGCTAGAGATTTAGCAAGACATTTCATCCAAAGATGGAACTTCACTAAGACTACAAAAGCTAG
ATACAAGACACCATTGTACCCATACTTGTTACCAAAATCTACTTCAACAGCAAACAACTTGCCATTCATGATTCCAGGTGGTCAATGTGC
TACTGTTCAAGTCTTAAGATCAGTTGATAGATGGTCAGCAGGTACTTTGGAAAATTCTATCTTGAACGCTTACTTGCATACAATCAGAGA
ATCACAACATTTCTTGTACATCGAAAACCAATTTTTCATCTCTTGTTCAGATGGTAGAACAGTTTTGAACAAGGTTGGTGATGAAATCGTT
GATAGAATTTTGAAAGCACATGAACAAGGTCAATGTTTCAGAGTTTATTTGTTATTGCCATTGTTGCCAGGTTTTGAAGGTGATATTTCTA
CTGGTGGTGGTAATTCTATCCAAGCTATCTTGCATTTCACATACTCATTGTGTTTGTTGCATCCATTTTTCTCTTTGAGAACTTTGTGTAG
AGGTGAACATTCTATCTTGCATAGATTGAAGGCAGCTATGGGTACTGCTTGGAGAGATTACATGTCTATTTGTGGTTTGAGAACACATGG
TGAATTGGGTGGTCATCCAATTTCTGAATTAATCTACATCCATTCAAAGATGTTGATCGCAGATGATAGAACTGTTATCATCGGTTCTGC
TAACATCAACGATAGATCATTATTGGGCAAGAGAGATTCTGAATTAGCTATCTTGATCAAGGATACAGAAATGGAACCATCTTTAATGGA
TGGTGTTGAATATCAAGCAGGTAGATTTGCTTTATCATTGAGAAAGCATTGTTTCTCTGTTATCTTGGGTGCTAACACTTGGCCAGATTTA
GATTTGAGAGATCCAGTTTGTGATGATTTCTTTCAATTGTGGCAAGAAACTGCAGAAAACAACGCTACAATCTACGAACAAATTTTTAGA
TGTTTGCCATCTAACGCAACTAGATCATTAAGAGCTTTGAGAGAATACGTTGCAGTTGAATCATTAGCTACAGTTTCTCCATCATTAGCA
CAATCTGAATTGGCTCATATTCAAGGTCATTTGGTTCATTTTCCATTGAAGTTTTTGGAAGATGAATCATTATTGCCACCATTAGGTTCTA
AAGAAGGTATGATTCCATTGGAAGTTTGGACATAA

VI.2. Plasmid maps and nucleotide sequences of p416_GPD-coPLD1-GFP and p416_GPD-coPLD2-GFP

VI.2.1. Plasmid maps of p416_GPD-coPLD1-GFP and p416_GPD-coPLD2-GFP

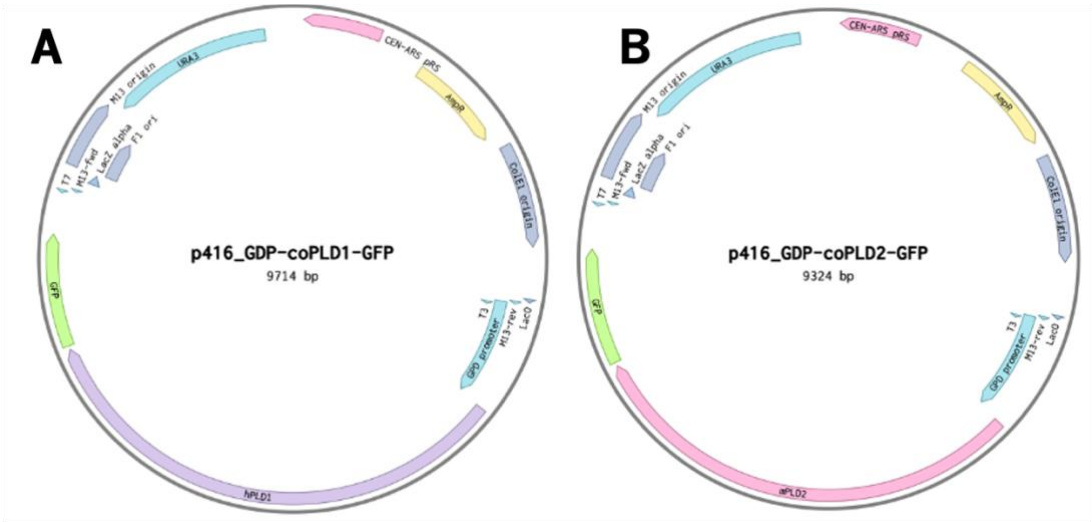

Figure 23. Plasmid maps for (A) p416_GPD-coPLD1-GFP (9714 bp) and (B) p416_GPD-coPLD2-GFP (9324 bp).

Important features shown include: CEN/ARS (*S. cerevisiae* CEN6 centromere fused to an autonomously replicating sequence); AmpR (confers resistance to ampicillin, carbenicillin, and related antibiotics); GPD promoter (promoter for glyceraldehyde-3-phosphate dehydrogenase); F1 ori (f1 bacteriophage origin of replication; arrow indicates direction of (+) strand synthesis); URA3 (yeast auxotrophic marker); Plasmid maps were constructed using Benchling [Biology Software]. (2021)

VI.2.2. Predicted nucleotide sequence for *PLD1-GFP* in p416_GPD-coPLD1-GFP

ATGTCATTGAAGAACGAACCAAGAGTTAACACTTCTGCTTTGCAAAAGATTGCTGCAGATATGTCAAACATCATCGAAAATTTGGAT
ACAAGAGAATTACATTTCGAAGGTGAAGAAGTTGATTATGATGTTTCTCCATCAGATCCAAAGATCCAAGAAGTTTACATCCCATTCTCA
GCAATCTACAACACTCAAGGTTTCAAGGAACCAAACATCCAAACATACTTGTCTGGTTGTCCAATCAAGGCTCAAGTTTTAGAAGTTGAA
AGATTCACTTCAACTACAAGAGTTCCATCTATCAACTTGTACACTATCGAATTAACACATGGTGAATTTAAGTGGCAAGTTAAGAGAAAG
TTCAAGCATTTCCAAGAATTTCATAGAGAATTGTTAAAATATAAAGCATTTATCAGAATACCAATCCCAACTAGAAGACATACATTCAGAA
GACAAAACGTTAGAGAAGAACCAAGAGAAATGCCATCTTTGCCAAGATCATCTGAAAACATGATCAGAGAAGAACAATTCTTGGGTAGA
AGAAAGCAATTGGAAGATTACTTGACAAAAATTTTGAAAATGCCAATGTACAGAAACTACCATGCAACTACAGAATTTTTGGATATTTCTC
AATTATCATTTATCCATGATTTGGGTCCAAAGGGTATCGAGGGTATGATCATGAAGAGATCAGGTGGTCATAGAATACCAGGTTTGAATT
GTTGTGGTCAAGGTAGAGCTTGTTACAGATGGTCTAAGAGATGGTTGATCGTTAAGGATTCATTTTTGTTGTACATGAAACCAGATTCTG
GTGCTATTGCATTTGTTTTGTTAGTTGATAAGGAATTTAAGATCAAAGTTGGTAAAAAAGAAACTGAAACAAAATATGGTATTAGAATTGAT
AATTTATCAAGAACTTTGATTTTAAAATGTAATTCTTACAGACATGCTAGATGGTGGGGTGGTGCAATTGAAGAATTTATCCAAAAGCATG
GTACAAATTTCTTGAAGGATCATAGATTTGGTTCTTATGCTGCAATCCAAGAAAACGCTTTAGCAAAGTGGTATGTTAACGCAAAGGGTT
ACTTCGAAGATGTTGCTAATGCAATGGAAGAAGCTAACGAAGAAATTTTTATCACTGATTGGTGGTTGTCTCCAGAAATTTTCTTGAAAA
GACCAGTTGTTGAGGGTAACAGATGGAGATTAGATTGTATCTTGAAAAGAAAGGCACAACAAGGTGTTAGAATCTTCATCATGTTGTACA
AAGAAGTTGAATTGGCTTTGGGTATCAACTCTGAATACACTAAGAGAACATTGATGAGATTGCATCCAAACATCAAGGTTATGAGACATC
CAGATCATGTTTCTTCAACAGTTTATTTGTGGGCTCATCATGAAAAATTGGTTATCATCGATCAATCAGTTGCTTTCGTTGGTGGTATTGA
TTTGGCATACGGTAGATGGGATGATAACGAACATAGATTGACTGATGTTGGTTCTGTTAAGAGAGTTACATCTGGTCCATCATTGGGTTC
TTTACCACCAGCTGCAATGGAATCAATGGAATCTTTGAGATTGAAGGATAAGAACGAACCAGTTCAAAACTTGCCAATCCAAAAGTCAAT
CGATGATGTTGATTCTAAATTGAAGGGTATCGGCAAGCCAAGAAAGTTCTCAAAGTTCTCTTTGTACAAACAATTGCATAGACATCATTT
GCATGATGCAGATTCAATTTCTTCAATCGATTCTACTTCTTCATACTTCAATCATTACAGATCACATCATAATTTAATTCATGGTTTGAAG
CCACATTTCAAATTGTTCCATCCATCTTCAGAATCTGAACAAGGTTTAACTAGACCACATGCTGATACAGGTTCAATTAGATCATTGCAA
ACTGGTGTTGGTGAATTACATGGTGAAACAAGATTCTGGCATGGCAAGGATTACTGTAACTTCGTTTTCAAGGATTGGGTTCAATTGGAT
AAGCCATTCGCAGATTTCATCGATAGATACTCTACTCCAAGAATGCCTTGGCATGATATTGCTTCAGCAGTTCATGGTAAAGCTGCAAG
AGATGTTGCTAGACATTTTATTCAAAGATGGAACTTCACAAAGATCATGAAGTCTAAGTACAGATCATTGTCATACCCATTTTTGTTACCA
AAATCACAAACTACAGCTCATGAATTAAGATACCAAGTTCCAGGTTCTGTTCATGCAAATGTTCAATTGTTAAGATCAGCTGCAGATTGG
TCTGCTGGTATCAAGTACCATGAAGAATCTATCCATGCTGCATACGTTCATGTTATTGAAAATTCAAGACATTACATCTACATCGAAAAC
CAATTTTTCATTTCTTGTGCAGATGATAAGGTTGTTTTCAACAAGATTGGTGATGCTATTGCACAAAGAATTTTGAAAGCTCATAGAGAAA
ACCAAAAGTACAGAGTTTACGTTGTTATTCCATTGTTACCAGGTTTTGAAGGTGATATTTCTACTGGTGGTGGTAACGCTTTGCAAGCAA
TCATGCATTTCAATTACAGAACAATGTGTAGAGGTGAAAATTCAATCTTGGGTCAATTGAAAGCAGAATTGGGTAACCAATGGATCAACT
ACATTTCTTTTTGTGGTTTAAGAACTCATGCTGAATTAGAAGGCAATTTGGTTACAGAATTAATCTACGTTCATTCAAAATTGTTGATCGC
TGATGATAACACTGTTATCATCGGTTCAGCAAACATCAACGATAGATCAATGTTGGGTAAAAGAGATTCAGAAATGGCTGTTATTGTTCA
AGATACTGAAACTGTTCCATCAGTTATGGATGGTAAAGAATATCAAGCTGGTAGATTTGCAAGAGGTTTGAGATTGCAATGTTTCAGAGT
TGTTTTGGGTTACTTAGATGATCCATCTGAAGATATTCAAGATCCAGTTTCTGATAAGTTTTTCAAAGAAGTTTGGGTTTCTACTGCTGCA
AGAAATGCTACAATCTACGATAAGGTTTTCAGATGTTTGCCAAACGATGAAGTTCATAACTTGATCCAATTGAGAGATTTCATCAATAAAC
CAGTTTTAGCTAAAGAAGATCCAATCAGAGCAGAAGAAGAATTGAAGAAAATTAGAGGTTTCTTGGTTCAATTCCCATTCTACTTTTTATC
AGAAGAATCTTTGTTGCCATCAGTTGGTACTAAAGAAGCTATTGTTCCAATGGAAGTTTGGACAGAATTCGATATCAAGCTTGTCGACAT

GAGTAAAGGAGAAGAACTTTTCACTGGAGTTGTCCCAATTCTTGTTGAATTAGATGGTGATGTTAATGGGCACAAATTTTCTGTCAGTGG
AGAGGGTGAAGGTGATGCAACATACGGAAAACTTACCCTTAAATTTATTTGCACTACTGGAAAACTACCTGTTCCATGGCCAACACTTG
TCACTACTTTCACTTATGGTGTTCAATGCTTTTCAAGATACCCAGATCATATGAAACGGCATGACTTTTTCAAGAGTGCCATGCCCGAAG
GTTATGTACAGGAAAGAACTATATTTTTCAAAGATGACGGGAACTACAAGACACGTGCTGAAGTCAAGTTTGAAGGTGATACCCTTGTTA
ATAGAATCGAGTTAAAAGGTATTGATTTTAAAGAAGATGGAAACATTCTTGGACACAAATTGGAATACAACTATAACTCACACAATGTATA
CATCATGGCAGACAAACAAAAGAATGGAATCAAAGTTAACTTCAAAATTAGACACAACATTGAAGATGGAAGCGTTCAACTAGCAGACC
ATTATCAACAAAATACTCCAATTGGCGATGGCCCTGTCCTTTTACCAGACAACCATTACCTGTCCACACAATCTGCCCTTTCGAAAGAT
CCCAACGAAAAGAGAGACCACATGGTCCTTCTTGAGTTTGTAACAGCTGCTGGGATTACACATGGCATGGATGAACTATACAAACACCA
TCACCATCACCATTAG

VI.2.3. Sequencing results for *PLD1-GFP* in p416_GPD-coPLD1-GFP

The p416_GPD-coPLD1-GFP construct was sequenced by Eurofins genomics using primers pGPD-co-hPLD1-GFP-fw and 1114_GFP-R. The plasmid was premixed with each primer individually according to Eurofins genomics directions.

VI.2.3.1. p416_GPD-coPLD1-GFP + pGPD-co-hPLD1-GFP-fw

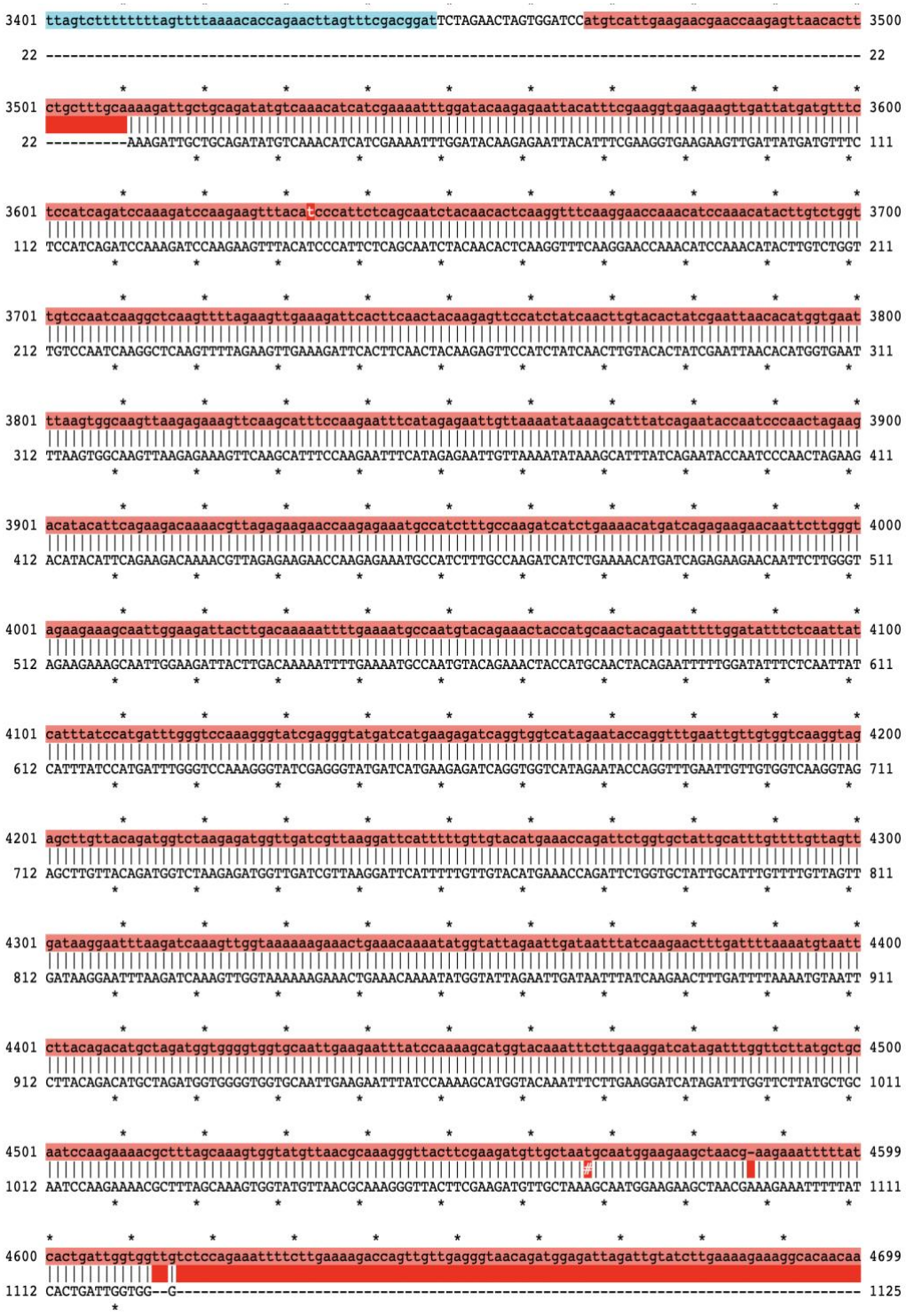

Figure 24. DNA Alignment of the p416_GPD-coPLD1-GFP predicted sequence with results obtained by sequencing the p416_GPD-coPLD1-GFP plasmid using primer pGPD-co-hPLD1-GFP-fw

Regions highlighted in red show the DNA sequence for *coPLD1* and regions highlighted in blue show DNA sequence for the GPD promoter. The alignment was performed using the ApE program (v 2.0.60).

VI.2.3.2. p416_GPD-coPLD1-GFP + 1114_GFP-R

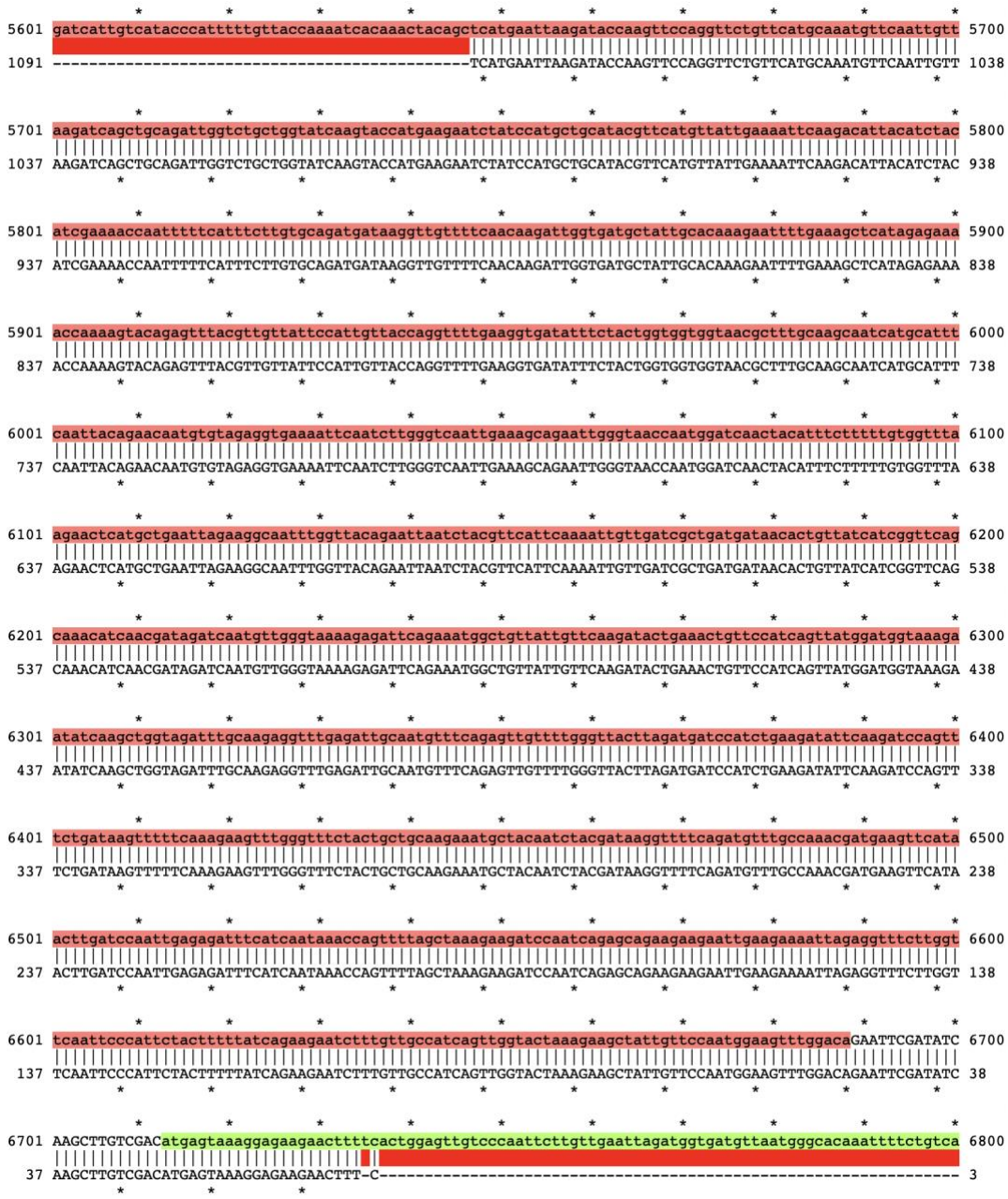

Figure 25. DNA Alignment of the p416_GPD-coPLD1-GFP predicted sequence with results obtained by sequencing the p416_GPD-coPLD1-GFP plasmid using primer 1114_GFP-R

Regions highlighted in red show the DNA sequence for *coPLD1* and regions highlighted in green show DNA sequence for *GFP*. The alignment was performed using the ApE program (v 2.0.60).

VI.2.4. Predicted nucleotide sequence for *PLD2-GFP* in p416_GPD-coPLD2-GFP

ATGACTGTTACACAAAAGAATTTGTTTCCATACGGTGATTACTTAAATTCTTCACAATTGCACATGGAACCAGATGAAGTTGATACTT
TGAGAGAAGGTGAAGATCCAGCAGATAGAATGCATCCATACTTGGCTATCTACGATTTGCAACCATTGAAAGCACATCCATTGGTTTTT
GCTCCAGGTGTTCCAGTTATTGCTCAAGTTGTTGGTACTGAAAGATATACATCTGGTTCAAAAGTTGGTACTTGTACATTATACTCTGTT
AGATTGACTCATGGTGATTTTACATGGACTACTAAGAAAAAATTCAGACATTTCCAAGAATTACATAGAGATTTGCAAAGACATAAGGTTT
TGATGTCATTGTTACCATTGGCAAGATTTGCTGTTACTCATTCTCCAGCTAGAGAAGCTGCAGCTGAAGATATTCCATCATTACCAAGAG
GTGGTTCTGAAGGTTCAGCAAGACATACAGCTTCTAAGCAAAAGTATTTAGAAAACTACTTGAATAGATTGTTAACTATGTCATTCTACA
GAAACTACCATGCTATGACAGAATTTTTAGAAGTTTCTCAATTGTCATTTATCCCAGATTTAGGTTCAAAGGGTTTGGAAGGTGTTATTAG
AAAAAGATCAGGTGGTCATAGAGTTCCAGGTTTTACTTTTTGTGGTAGAGATCAAGTTTGTTACAGATGGTCAAAGAGATGGTTAGTTGT
TAAGGATTCATTTTTGTTGTACATGAGACCAGAAACAGGTGCTATTTCTTTTGTTCAATTGTTTGATCCAGGTTTTGAAGTTCAAGTTGGT
AAAAGATCAACTGAAACAAGATACGGTGTTAGAATCGATACTTCTCATAGATCATTAATCTTGAAATGTTCTTCATACAGACAAGCAAGAT
GGTGGGGTCAAGAAATTACAGAATTGGCTCAAGGTTCTGGTAGAGATTTCTTGCAATTGCATCAACATGATTCTTATGCTCCACCAAGA
CCAGGTACTTTAGCAAGATGGTTTGTTAATGGTGCTGGTTACTTTGCAGCTGTTGCAGATGCTATCTTGAGAGCACAAGAAGAAATTTTT
ATCACAGATTGGTGGTTGTCACCAGAAATTTATTTGAAGAGACCAGCACATTCTGATGATTGGAGATTAGATATTATGTTGAAGAGAAAA
GCTGAAGAAGGTGTTAGAGTTTCTATCTTGTTGTTCAAAGAAGTTGAATTAGCATTGGGTATCAACTCTGGTTACTCAAAGAGAACTTTG
ATGTTGTTGCATCCAAACATCAAGGTTATGAGACATCCAGATTTAGTTACATTGTGGGCTCATCATGAAAAATTGTTAGTTGTTGATCAAG
TTGTTGCATTTTTGGGTGGTTTAGATTTGGCTTTTGGTAGATGGGATGATGTTCAATACAGATTGACTGATTTGGGTGATCCATCTGAAC
CAGTTCATTTACAAACTCCAACATTGGGTTCAGATCCAGCAGCTACTCCAGATTTATCTCATAACCAATTTTTCTGGTTGGGCAAGGATT
ACTCTAACTTGATCACAAAGGATTGGGTTCAATTGGATAGACCATTCGAAGATTTCATCGATAGAGAAACTACACCAAGAATGCCTTGGA
GAGATGTTGGTGTTGTTGTTCATGGTGTTGCAGCTAGAGATTTAGCAAGACATTTCATCCAAAGATGGAACTTCACTAAGACTACAAAAG
CTAGATACAAGACACCATTGTACCCATACTTGTTACCAAAATCTACTTCAACAGCAAACAACTTGCCATTCATGATTCCAGGTGGTCAAT
GTGCTACTGTTCAAGTCTTAAGATCAGTTGATAGATGGTCAGCAGGTACTTTGGAAAATTCTATCTTGAACGCTTACTTGCATACAATCA
GAGAATCACAACATTTCTTGTACATCGAAAACCAATTTTTCATCTCTTGTTCAGATGGTAGAACAGTTTTGAACAAGGTTGGTGATGAAAT
CGTTGATAGAATTTTGAAAGCACATGAACAAGGTCAATGTTTCAGAGTTTATTTGTTATTGCCATTGTTGCCAGGTTTTGAAGGTGATATT
TCTACTGGTGGTGGTAATTCTATCCAAGCTATCTTGCATTTCACATACTCATTGTGTTTGTTGCATCCATTTTTCTCTTTGAGAACTTTGT
GTAGAGGTGAACATTCTATCTTGCATAGATTGAAGGCAGCTATGGGTACTGCTTGGAGAGATTACATGTCTATTTGTGGTTTGAGAACAC
ATGGTGAATTGGGTGGTCATCCAATTTCTGAATTAATCTACATCCATTCAAAGATGTTGATCGCAGATGATAGAACTGTTATCATCGGTT
CTGCTAACATCAACGATAGATCATTATTGGGCAAGAGAGATTCTGAATTAGCTATCTTGATCAAGGATACAGAAATGGAACCATCTTTAA
TGGATGGTGTTGAATATCAAGCAGGTAGATTTGCTTTATCATTGAGAAAGCATTGTTTCTCTGTTATCTTGGGTGCTAACACTTGGCCAG
ATTTAGATTTGAGAGATCCAGTTTGTGATGATTTCTTTCAATTGTGGCAAGAAACTGCAGAAAACAACGCTACAATCTACGAACAAATTTT
TAGATGTTTGCCATCTAACGCAACTAGATCATTAAGAGCTTTGAGAGAATACGTTGCAGTTGAATCATTAGCTACAGTTTCTCCATCATT
AGCACAATCTGAATTGGCTCATATTCAAGGTCATTTGGTTCATTTTCCATTGAAGTTTTTGGAAGATGAATCATTATTGCCACCATTAGGT
TCTAAAGAAGGTATGATTCCATTGGAAGTTTGGACAGAATTCGATATCAAGCTTGTCGACATGAGTAAAGGAGAAGAACTTTTCACTGGA
GTTGTCCCAATTCTTGTTGAATTAGATGGTGATGTTAATGGGCACAAATTTTCTGTCAGTGGAGAGGGTGAAGGTGATGCAACATACGG
AAAACTTACCCTTAAATTTATTTGCACTACTGGAAAACTACCTGTTCCATGGCCAACACTTGTCACTACTTTCACTTATGGTGTTCAATG
CTTTTCAAGATACCCAGATCATATGAAACGGCATGACTTTTTCAAGAGTGCCATGCCCGAAGGTTATGTACAGGAAAGAACTATATTTTT
CAAAGATGACGGGAACTACAAGACACGTGCTGAAGTCAAGTTTGAAGGTGATACCCTTGTTAATAGAATCGAGTTAAAAGGTATTGATTT

TAAAGAAGATGGAAACATTCTTGGACACAAATTGGAATACAACTATAACTCACACAATGTATACATCATGGCAGACAAACAAAAGAATGG
AATCAAAGTTAACTTCAAAATTAGACACAACATTGAAGATGGAAGCGTTCAACTAGCAGACCATTATCAACAAAATACTCCAATTGGCGA
TGGCCCTGTCCTTTTACCAGACAACCATTACCTGTCCACACAATCTGCCCTTTCGAAAGATCCCAACGAAAAGAGAGACCACATGGTC
CTTCTTGAGTTTGTAACAGCTGCTGGGATTACACATGGCATGGATGAACTATACAAACACCATCACCATCACCATTAG

VI.2.5. Sequencing results for *PLD2-GFP* in p416_GPD-coPLD2-GFP

The p416_GPD-coPLD2-GFP construct was sequenced by Eurofins genomics using primers pGPD-co-mPLD2-GFP-fw and 1114_GFP-R. The plasmid was premixed with each primer individually according to Eurofins genomics directions

VI.2.5.1. p416_GPD-coPLD2-GFP + pGPD-co-mPLD2-GFP-fw

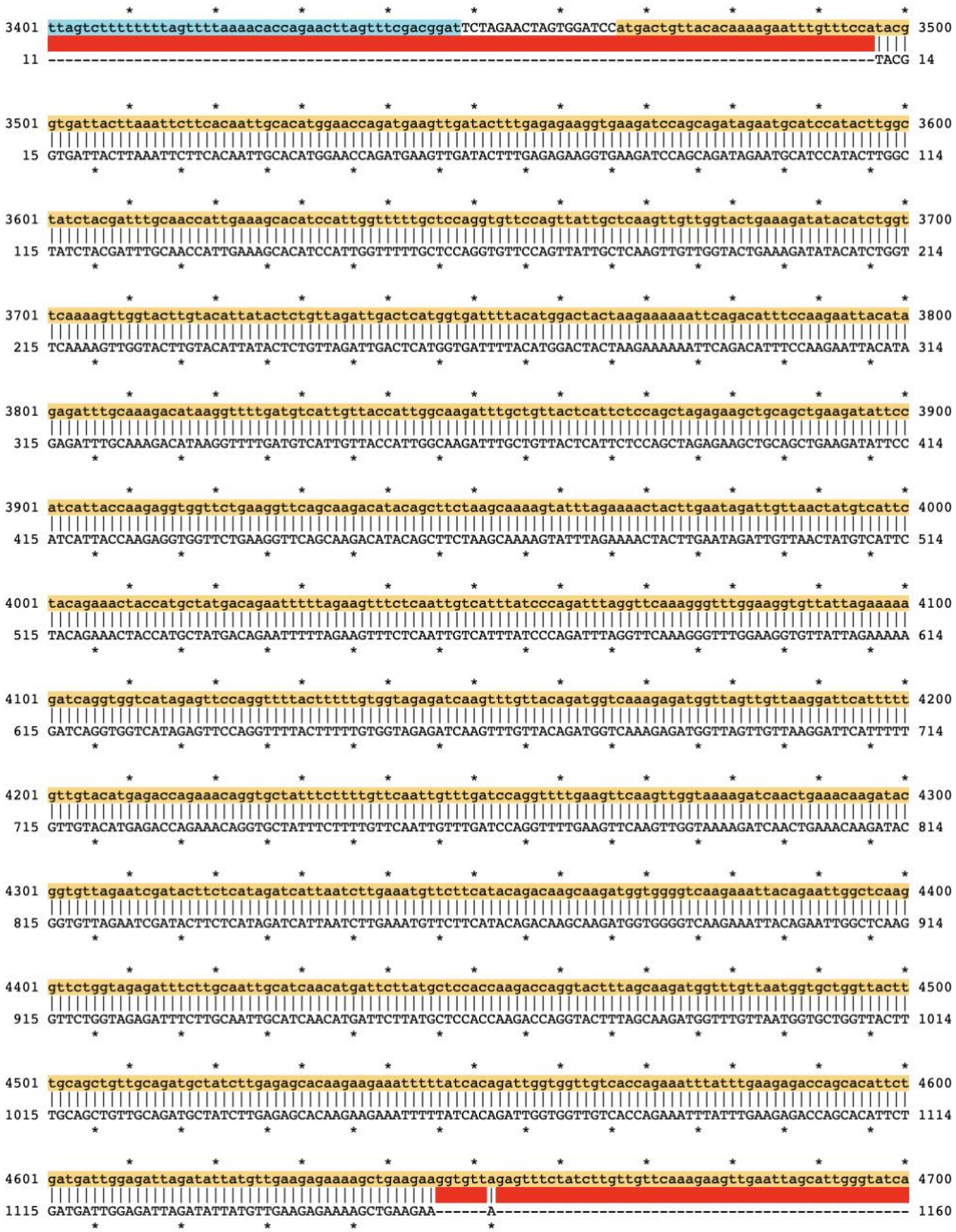

Figure 26. DNA Alignment of the p416_GPD-coPLD2-GFP predicted sequence with results obtained by sequencing the p416_GPD-coPLD2-GFP plasmid using primer pGPD-co-mPLD2-GFP-fw

Regions highlighted in yellow show the DNA sequence for *coPLD2* and regions highlighted in blue show DNA sequence for the GPD promoter. The alignment was performed using the ApE program (v 2.0.60).

VI.2.5.1. p416_GPD-coPLD2-GFP + 1114_GFP-R

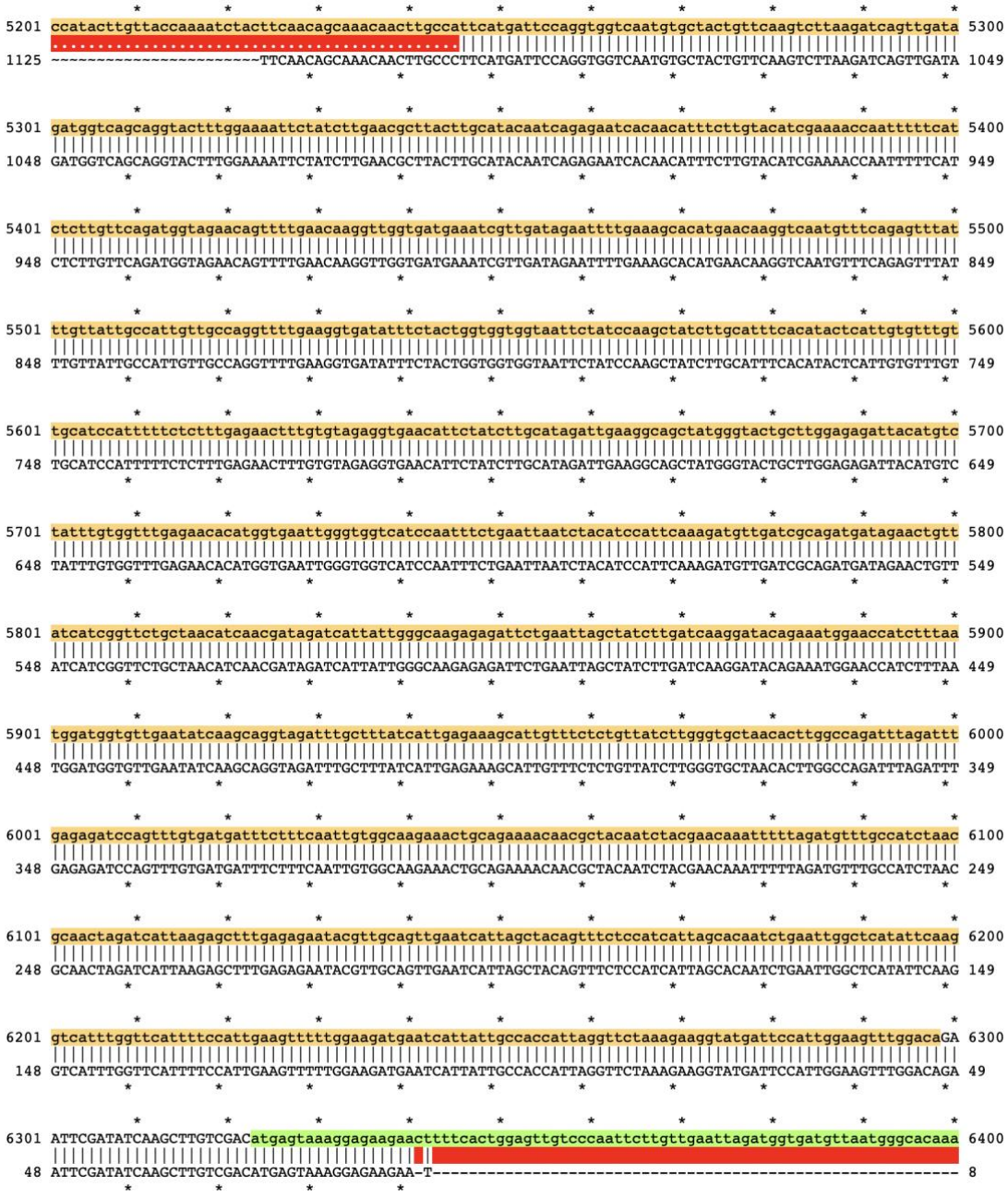

Figure 27. DNA Alignment of the p416_GPD-coPLD2-GFP predicted sequence with results obtained by sequencing the p416_GPD-coPLD2-GFP plasmid using primer 1114_GFP-R

Regions highlighted in yellow show the DNA sequence for *coPLD2* and regions highlighted in green show DNA sequence for the *GFP*. The alignment was performed using the ApE program (v 2.0.60).

VI.3. PCR cycling conditions

VI.3.1. Construction of *SPO14* deletion

The KanMX cassette was amplified by PCR from strain IR04 (see Table 2 in Chapter II-Materials and methods) using primers primerA-spo14-del and primerD-spo14-del (see Table 3 in Chapter II-Materials and methods). Reagents were prepared according to the manufacturers' suggested protocol for Phusion™ High–Fidelity DNA Polymerase (Thermo Scientific). The cycling conditions were chosen according to the WebPCR online software (http://bjornfjohansson.pythonanywhere.com/pcr) and the enzyme manufacturers' protocol - Table 5.

Table 5. Cycling conditions for amplification of KanMX cassette from IR04 using Phusion™ High–Fidelity DNA Polymerase (Thermo Scientific)

Initial denaturation	98 °C for 30 seconds	1 x
Denaturation	98 °C for 10 seconds	30 x
Annealing	60 °C for 30 seconds	
Extension	72 °C for 30 seconds	
Final extension	72 °C for 10 minutes	1 x

For the colony PCR for integration of the KanMX in the *SPO14* locus primers K3 and primerD-spo14-del were used (see Table 3 in Chapter II-Materials and methods). Reagents were prepared according to the protocol described in Chapter II-Materials and methods (see II.5 Colony PCR). The cycling conditions were chosen according to the WebPCR online software (http://bjornfjohansson.pythonanywhere.com/pcr), with the exception of the initial denaturation step where a longer incubation period was used - Table 6.

Table 6. Cycling conditions for colony PCR of integration of KanMX in the *SPO14* locus

Initial denaturation	94 °C for 10 minutes	1 x
Denaturation	94 °C for 30 seconds	30 x
Annealing	55 °C for 30 seconds	
Extension	72 °C for 2 minutes	
Final extension	72 °C for 10 minutes	1 x

The HygMX cassette was amplified by PCR from pAG32 (Table 4 in Chapter II-Material and methods) using 150_MX4fwd and 149_MX4rev (see Table 3 in Materials and methods). Reagents were prepared according to the manufacturers' suggested protocol for Phusion™ High–Fidelity DNA Polymerase (Thermo Scientific). The cycling conditions were chosen according to the WebPCR online software (http://bjornfjohansson.pythonanywhere.com/pcr) and the enzyme manufacturers' protocol - Table 7.

Table 7. Cycling conditions for amplification of HygMX cassette from pAG32 using Phusion™ High–Fidelity DNA Polymerase (Thermo Scientific)

Initial denaturation	98 °C for 30 seconds	1 x
Denaturation	98 °C for 10 seconds	30 x
Annealing	59 °C for 30 seconds	
Extension	72 °C for 30 seconds	
Final extension	72 °C for 10 minutes	1 x

For the colony PCR for integration of the HygMX in the *SPO14* locus primers 256_KanB and primerA-spo14-del were used (see Table 3 in Chapter II-Materials and methods). Reagents were prepared according to the protocol described in Chapter II-Materials and methods (see II.5 Colony PCR). The cycling conditions were chosen according to the WebPCR online software (http://bjornfjohansson.pythonanywhere.com/pcr), with the exception of the initial denaturation step where a longer incubation period was used - Table 8.

Table 8. Cycling conditions for colony PCR of integration of HygMX in the SPO14 locus

Initial denaturation	94 °C for 10 minutes	1 x
Denaturation	94 °C for 30 seconds	30 x
Annealing	50 °C for 30 seconds	
Extension	72 °C for 1 minutes	
Final extension	72 °C for 10 minutes	1 x

VI.3.2. Construction of p416_GPD-coPLD1-GFP and p416_GPD-coPLD2-GFP

The codon-optimized *PLD1* and *PLD2* genes were amplified by PCR from hPLD1_pUC57 and mPLD2_PCCI-4K, respectively. *PLD1* was amplified using primers pGPD-co-hPLD1-GFP-fw plus pGPD-co-hPLD1-GFP-rv (see Table 3 in Chapter II-Materials and methods) and *PLD2* was amplified with primers pGPD-co-mPLD2-GFP-fw plus pGPD-co-mPLD2-GFP-rv (see Table 3 in Chapter II-Materials and methods). Reagents were prepared according to the manufacturers' suggested protocol for Phusion™ High–Fidelity DNA Polymerase (Thermo Scientific). The cycling conditions were chosen according to the WebPCR online software (http://bjornfjohansson.pythonanywhere.com/pcr) and the enzyme manufacturers' protocol - Table 9.

Table 9. Cycling conditions for amplification of *PLD1* and *PLD2* from hPLD1_pUC57 and mPLD2_PCCI-4K, respectively using Phusion™ High–Fidelity DNA Polymerase (Thermo Scientific).

Initial denaturation	98 °C for 30 seconds	1 x
Denaturation	98 °C for 10 seconds	30 x
Annealing	70.5 °C for 30 seconds	
Extension	72 °C for 48 seconds	
Final extension	72 °C for 10 minutes	1 x

For the colony PCR for correct assembly of the desired genetic constructs primers pGPD-co-hPLD1-GFP-fw and screening-hPLD1-rv for p416-coPLD1-GFP and pGPD-co-mPLD2-GFP-fw screening-mPLD2-rv for p416-coPLD2-GFP (see Table 3 in Chapter II-Materials and methods). Reagents were prepared according to the protocol described in Chapter II-Materials and methods (see II.5 Colony PCR). The cycling conditions were chosen according to the WebPCR online software (http://bjornfjohansson.pythonanywhere.com/pcr), with the exception of the initial denaturation step where a longer incubation period was used - Table 10.

Table 10. Cycling conditions for colony PCR for correct assembly of p416_GDP-coPLD1-GFP and p416_GPD-coPLD2-GFP

Initial denaturation	94 °C for 10 minutes	1 x
Denaturation	94 °C for 30 seconds	30 x
Annealing	54 °C for 30 seconds	
Extension	72 °C for 32 seconds	
Final extension	72 °C for 10 minutes	1 x

VI.3.3. Genomic integration of codon-optimized *PLD1* and *PLD2* in the *SPO14* locus of a mutant strain

The pRCC-K plasmid was amplified in three parts: the first fragment was amplified with primers gRNA_HygMX4-FW and 253_KanC3 (see Table 3 in Chapter II-Materials and methods). The second fragment was amplified with primers 473_MSW_rev and 576_pBR322_2 (see Table 3 in Chapter II-Materials and methods). The third fragment was amplified with primers 196_pMEC_MX4_fwd and gRNA_HygMX4-RV (see Table 3 in Chapter II-Materials and methods). Reagents were prepared according to the manufacturers' suggested protocol for Phusion™ High–Fidelity DNA Polymerase (Thermo Scientific). The cycling conditions were chosen according to the WebPCR online software (http://bjornfjohansson.pythonanywhere.com/pcr) and the enzyme manufacturers' protocol – Table 11, Table 12 and Table 13.

Table 11. Cycling conditions for amplification of fragment 1 from pRCC-K using Phusion™ High–Fidelity DNA Polymerase (Thermo Scientific)

Initial denaturation	98 °C for 30 seconds	1 x
Denaturation	98 °C for 10 seconds	35 x
Annealing	58.9 °C for 30 seconds	
Extension	72 °C for 2 minutes	
Final extension	72 °C for 10 minutes	1 x

Table 12. Cycling conditions for amplification of fragment 2 from pRCC-K using Phusion™ High–Fidelity DNA Polymerase (Thermo Scientific)

Initial denaturation	98 °C for 30 seconds	1 x
Denaturation	98 °C for 10 seconds	30 x
Annealing	68 °C for 10 seconds	
Extension	72 °C for 1 minute and 19 seconds	
Final extension	72 °C for 10 minutes	1 x

Table 13. Cycling conditions for amplification of fragment 3 from pRCC-K using Phusion™ High–Fidelity DNA Polymerase (Thermo Scientific)

Initial denaturation	98 °C for 30 seconds	1 x
Denaturation	98 °C for 10 seconds	30 x
Annealing	58.5 °C for 10 seconds	
Extension	72 °C for 31 seconds	
Final extension	72 °C for 10 minutes	1 x

The codon-optimized *PLD1* and *PLD2* genes were amplifed by PCR from hPLD1_pUC57 and mPLD2_PCCI-4K, respectively. *PLD1* was amplfied using primers primers Long-up-SPO14-hPLD1-FW and Long-down-SPO14-hPLD1-RV (see Table 3 in Chapter II-Materials and methods). *PLD2* was amplified with primers Long-up-SPO14-mPLD2-FW and Long-down-SPO14-mPLD2-RV (see Table 3 in Chapter II-Materials and methods). Reagents were prepared according to the manufacturers' suggested protocol for Platinum™ II Hot-Start DNA Polymerase (Thermo Scientific). The cycling conditions were chosen according to the WebPCR online software (http://bjornfjohansson.pythonanywhere.com/pcr) and the enzyme manufacturers' protocol - Table 14 and Table 15.

Table 14. Cycling conditions for amplification of *PLD1* from hPLD1_pUC57 using Platinum™ II Hot-Start DNA Polymerase (Thermo Scientific)

Initial denaturation	94 °C for 2 minutes	1 x
Denaturation	94 °C for 15 seconds	30 x
Annealing	55 °C for 30 seconds	
Extension	68 °C for 1 minute	
Hold	4 °C for 10 minutes	1 x

Table 15. Cycling conditions for amplification of *PLD2* from mPLD2_PCCI-4K using Platinum™ II Hot-Start DNA Polymerase (Thermo Scientific)

Initial denaturation	94 °C for 2 minutes	1 x
Denaturation	94 °C for 15 seconds	30 x
Annealing	60 °C for 30 seconds	
Extension	68 °C for 1 minute	
Hold	4 °C for 10 minutes	1 x

For the colony PCR for integration of P*LD1* or *PLD2* in the *SPO14* locus primers screening-down-SPO14-rv and screening-hPLD1-fw (see Table 3 in Chapter II-Materials and methods) for *PLD1* and screening-down-SPO14-rv and screening-mPLD2-fw (see Table 3 in Chapter II-Materials and methods). for *PLD2* were used (see Table 3 in Chapter II-Materials and methods). Reagents were prepared according to the protocol described in Chapter II-Materials and methods (see II.5 Colony PCR). The cycling conditions were chosen according to the WebPCR online software (http://bjornfjohansson.pythonanywhere.com/pcr), with the exception of the initial denaturation step where a longer incubation period was used - Table 16.

Table 16. Cycling conditions for colony PCR of integration of *PLD1* or *PLD2* in the *SPO14* locus

Initial denaturation	94 °C for 10 minutes	1 x
Denaturation	94 °C for 30 seconds	30 x
Annealing	53 °C for 30 seconds	
Extension	72 °C for 32 seconds	
Final extension	72 °C for 10 minutes	1 x